RARE EARTH DOPED GALLIUM NITRIDE POWDERS: SYNTHESIS, PURIFICATION, LUMINESCENCE ENHANCEMENT, NANOSIZING, LUMINESCENCE MECHANISM INVESTIGATION AND LARGE AREA DEPOSITION

A Dissertation

Presented to the Faculty of the Graduate School

of Cornell University

in Partial Fulfillment of the Requirements for the Degree of

Doctor of Philosophy

by

Tiju Thomas

January 2011

RARE EARTH DOPED GALLIUM NITRIDE POWDERS: SYNTHESIS, PURIFICATION, LUMINESCENCE ENHANCEMENT, NANOSIZING, LUMINESCENCE QUENCHING STUDIES AND LARGE AREA DEPOSITION

Tiju Thomas, Ph.D.

Cornell University 2011

Gallium Nitride is a III-V compound semiconductor that has attracted a lot of interest among both applied and basic researchers because of its potential applications in optoelectronic, high power and high frequency devices. However, many questions about the material remain unanswered. In this thesis, we will present our investigation of GaN. We will first describe an ammonothermal method for the synthesis of un-doped and rare earth doped GaN powders. Using careful observations and calculations, we show that the powder growth is primarily a liquid phase phenomenon.

We also present a chemical method to achieve luminescence enhancement in ammonothermally grown Eu:GaN powders. Based on arguments drawn from the surface chemistry and XRD of these samples, we conclude that elimination of dark mixed oxides from the powder results in the observed luminescence enhancement. We also demonstrate a nano Eu:GaN synthesis process using a simple mechanical top-down method. The optical properties of nano Eu:GaN prepared in this manner is comparable to that of the bulk material. Based on a similar mechanical process we synthesized nano Er:GaN powders that emit in the C band (1.55 μm).

The mechanism involved in the luminescence of rare earth doped GaN is investigated using thermal quenching and high pressure studies. Our results suggest

that an exciton bound to rare earth structured isovalent impurity (RESI) is responsible for luminescence in these materials. Luminescence quenching and pressure dependent photoluminescence enhancement in RE:GaN can be explained based on this model. Our results clearly suggest that thermal quenching can be undone by application of pressure. These powders are discovered to be fairly radiation hard as well.

In the last section of this thesis, we will present an electrophoretic technique to deposit nano GaN on a fluorine doped tin oxide coated glass substrate. The technique can be easily adapted to grow layered structures that can find application in optical fibers and as a laser gain medium. Preliminary results for highly densified GaN ceramic obtained using a hot-press process are discussed. These results suggest that further densification is necessary for achieving a completely transparent GaN ceramic made out of ammonothermally synthesized GaN powders.

BIOGRAPHICAL SKETCH

Tiju Thomas was born in Kottayam, Kerala in India on July 10, 1983. Soon after that his parents moved to Hyderabad. In 1988, Tiju and his mother moved to Bangalore to join his dad. Very soon it was evident that he was excited by the causal patterns that nature seemed to constantly obey. Questions to do with how, when and why came naturally to him. He started doing gardening when he was 8 years old because he was fascinated by the phenomenon of germination. The fact that life could remain dormant in the form a seed had captivated his imagination. He quickly learnt how water and sunlight had to be optimized for healthy plant growth. Soon he started growing hybrid sunflower plants. He also collected simple building materials to learn the art of constructing buildings when he was just 12 years old. The nature of the universe was fascinating to him, but he was also amazed at the engineering marvels that surrounded him. Recognizing his gift for science, he was awarded the Kishore Vaigyanik Protsahana Yojana by the Indian Institute of Science when he was 14 years old. He was among the 50 students selected nationwide for this program. It was that very same year that he started taking keen interest in Indian philosophy as well.

At about this time, his great passion for vocal music intensified. His chronic asthma did not prevent him from participating in the many musical events within Karnataka throughout his middle school. He won many interschool music awards, including a state award. Unfortunately, his physical and emotional health started becoming frail during his high school years. This poor health was to haunt him for several years to come.

Given the demand for engineering jobs in early 2000s, Tiju was advised by his dad to pursue engineering. He joined an engineering program in MS Ramaiah Institute of Technology (MSRIT) where he specialized in Electronics and Communication

Engineering. The presence of National Institute of Advanced Studies (NIAS) in the vicinity of his college provided him with a constant reminder about the holistic nature of academic research. Several times during his engineering education he saw himself as a "bridge-builder" – someone who could work across disciplines, helping in the unification of subjects that had diverged due to historical reasons. He enjoyed learning the various sciences, and frequently used principles of one discipline to enrich his understanding of some other area. Cross disciplinary studies were the way for him.

While learning electrical engineering, he realized that even simple, everyday electrical phenomena have very rich physical explanations. He taught himself all the core physics courses that were part of the B.S. (physics) curriculum within the Indian scheme. Hence, he taught himself fluid mechanics, classical mechanics, quantum and statistical mechanics, thermodynamics and optics. He also read several chapters of Morrison and Boyd; and was thrilled to see that one could predict products of organic reactions using a few simple concepts. He used all this knowledge of physics and chemistry to enrich his understanding of electrical systems.

By the end of his Bachelors, he realized that he needed to work on his basic science skills so that he could understand the physical world better. He passed a national level exam, and went through a highly selective process to gain admission to the prestigious Jawaharlal Nehru Centre for Advanced Scientific Research (JNCASR) in Bangalore. In the interview he was asked questions on quantum mechanics and statistical mechanics, all of which he answered. He could do so because he had self-educated himself in these areas when he was in the engineering school.

Ironically, at that stage in his life he also felt like returning to one of his first loves: biology. That same year, he also cleared a biology interview and exam to get admitted to one of the very few evolutionary biology graduate programs in India. He attributes his success in that exam and interview to his sustained interest in biology.

However, that year he made the difficult choice of forgoing biology in favor of physical sciences. He still thinks about the biological world and marvels at the splendor of the animate world.

In JNCASR he received an environment where multidisciplinary research was highly encouraged. Unlike most universities in India and around the world, JNCASR has no disciplinary boundaries. People from several disciplines openly collaborate with one another in this tiny campus. Here he got a taste for graduate level quantum mechanics, statistical mechanics, solid state physics, mathematical and computational methods. He also participated in an International Chemistry of Materials conference during his stay there.

At JNCASR, Tiju was fortunate to work under Prof. Umesh Waghmare. Prof. Waghmare is easily one of the best advisors that he could have hoped for. Throughout his work with the professor, he was constantly inspired by the brilliance his advisor possessed. For his masters, he started out trying to explain stacking fault expansion in Silicon Carbide (SiC). His work involved the use of Density Functional Theory based calculations. He proved that at high temperatures, stacking faults are preferred in 4H- and 6H-SiC primarily due to frozen phonons associated with these faults. He discovered that these frozen phonons stabilize the stacking faults in 4H- and 6H-SiC by minimizing the free energy of the faulted structures. During his masters he also got to work with Mr. Shubhrodeep Pathak, an integrated PhD student at S. N. Bose National Center for Basic Sciences. It was around the time of their work together that graphene was taking off as a material of importance. Along with Shubro, Tiju investigated MoS_2 as a surface to stabilize graphene. They discovered that the interface of graphene and MoS_2 was such that the 2D sheet was expected to have no folding. They thought that this had applications in areas such as 2D electronics. It is interesting to note that the 2010 Nobel Prize for physics went to Prof. Geim and Dr.

Novoselov for their discovery of graphene, just four years after Tiju and Shubhro dabbled with graphene.

During his masters, Tiju also met Prof. Prashant Shevgaonkar, a visitor to Prof. Umesh's group. Prof. Prashant was a keen learner, and encouraged Tiju to be like that too. Together they investigated if stacking fault expansion in 4H- and 6H-SiC could be arrested using transition metal dopants. They discovered that in addition to arresting stacking fault expansion in hexagonal polytypes of SiC, transition metal doping made the material a dilute magnetic semiconductor (DMS) as well. This result was verified experimentally shortly after they arrived at their theoretical result. Together they wanted to refine Prof. Ohno and Prof. Coey's explanation of dilute magnetic semiconductors. However, before they could work on it, Tiju's time in JNC had come to an end. In August 2007, he was awarded a master's degree for his dissertation entitled "Polytypes and Stacking Faults in C, Si, Ge and SiC".

After his stay in JNC, the world of science seemed too big and daunting to Tiju. He realized that having exposure to experimental science would help him appreciate the various aspects of physical sciences better. He reasoned that, science was after all fundamentally empirical. He was very fortunate to learn about Cornell University through Prof. Chandrabhas Narayana with whom he studied solid state physics during his JNC stay. Prof. Narayana was a postdoc with the Cornell legend, Prof. Arthur Ruoff. Their combined work had led to a conclusive demonstration that applying high pressure to hydrogen does not make it an alkali metal.

Tiju applied to Cornell's graduate program and was soon accepted for the Fall 2007 session. This was very welcome news for Tiju. There was a hidden realization within him that he was leaving the country for more than academics – he needed a change in his environment to investigate his own identity; something that was to take him through a deep internal journey.

Even before he had arrived on Cornell campus, he had established contact with Prof. Michael G. Spencer. He soon realized that he was destined to do his doctoral work under the professor. Prof. Spencer led a team that worked on SiC, GaN, AlN, nanosensors and bio-filtration at the time when Tiju joined him. Now the professor's group works mostly on graphene growth and ultra-fast devices.

In his very first meeting with Prof. Spencer, he talked about his work with Prof. Shevgaonkar that suggested that transition metal doping could be used to arrest stacking faults in hexagonal polytypes of SiC. Prof. Spencer was thrilled at the idea. Unfortunately, the concept never got tested for reasons to do with limited funding. Instead Tiju ended up working on a project that was started by Huaqiang Wu, a former group member. Prof. Spencer's group had already developed a technique to grow GaN powders; but several questions remained unsolved. This thesis presents answers to some of those questions. The abstract and conclusion sections of this thesis present all major results that have emerged as a result of Tiju's doctoral work.

Prof. Francis J. DiSalvo and Prof. Lester F. Eastman agreed to be on Tiju's graduate committee. His committee gave him the academic freedom that only few graduate students can dream of. Besides doing his doctoral work, Tiju read voraciously in several disciplines and educated himself in areas that he had not ventured into before. The diverse talents and specialties on Cornell campus provided him with the motivation to learn something new every day. In addition to the science he did, Tiju also dabbled with poetry and spiritual writing during his Cornell stay. His reading list reflected his eclectic interests. He read anthropology, chemistry, planetary sciences, materials physics, sociology, psychology, philosophy, religious history and theology. In late 2008, he met George Kandathil, who is currently a professor at the Indian Institute of Management (Ahmedabad). In George, he found a sociologist par

excellence. With him he learnt the art and thought of sociology in a one-on-one setting.

While Tiju's academic journey was taking all these multi-dimensional paths, a nagging question that had been suppressed for too long emerged; this time in the most disabling manner. He was too afraid to address this question. In fact his failing physical and emotional health was probably due to this secret he was harboring in his heart for too long. He had hidden it from himself and from everyone else. He thought that a veiled existence would be a panacea. He knew as he was growing up that the social signs that he received about gender roles and identities did not match his own human experience. There was a gradually loudening voice within him that was convincing him that this world was for people different from him. The traditional gender roles were not natural to him, nor were the traditional notions of gender identity. His gender had always been elusive to him. He constantly tried to live up to the expectations of being a man. As he was growing up, he experienced real fear that he was very different. Perhaps, his multi-faceted academic pursuits were a way for him to avoid thinking about himself. Earlier in this biography, it was alluded to that Tiju's physical and emotional health had been deteriorating. It was very clear that harboring a secret fear since his early days had lately had its consequences on his health. He doubted acceptance by his family, friends and co-workers. He did not even entrust his best kept secret with those who told him that they were his best friends. Social integration and acceptance had now become the central question of his life. He had been chronically depressed for several years now, and had masterfully hidden it from everyone. But now it had become very severe. By June 2009 he had become so sick that he decided to rush to his home in India. That did not help, and the secret kept taking its toll on him every moment. He came back to Ithaca, only to realize that he had almost become dysfunctional. A sense of duty propelled him to go to the lab every

day, but soon it became clear that he had come to a dead end. Unfortunately, his religious social circle and their attitudes towards lgbt people only heightened his loneliness. In many parts of the world broaching a topic such as this, is reason enough to receive a long prison sentence or an execution. He was aware of the highly marginalized Hijra community in India, and that only made it harder for him to come to terms with himself. Self-rejection is the closest one comes to death in this life. It was clear that he needed psychological assistance. Social constructions and social pressures had taken their toll on him; and he was already bruised to the point that defies easy description. Historically mankind has chosen to adhere to a binary when it comes to gender and gender roles. Many like Tiju struggle to live in a world where their very existence questions this social consciousness; and yet societal norms do not evolve to involve people like him. Such societal strictures cost a lot. Sometimes, as in his case pressures can come very close to costing one's sanity and one's life. It was then that he met Lynn Podhaski, a counselor at Family and Children's, one of the kindest people he has ever met. Lynn helped Tiju through the very challenging process of accepting himself by fighting against ingrained social and religious biases. It is a long process, which still continues. To be in a foreign land is hard enough, to have a community that misunderstands and uses words of rejection is reason enough to think that goodness and meaning in life is overrated. It was Lynn who helped him through the rehabilitation process, which continues to this day.

On a cold winter day in December 2009, Tiju met a gentle film-maker, author and hymn-writer; Edward Moran. Ed was soon to become another of his pillars of strength. For about a year, Lynn and Ed were his only confidantes. Soon he found a compassionate listener in Fr. Daniel McMullin, the Catholic chaplain at Cornell. Later in 2010, he found a devoted friend in Elliot Bassman, a renowned artist, film-maker and poet. Currently Tiju's universe is upheld by Lynn, Fr. Dan, Edward and Elliot –

his “fantastic four”. He now realizes that only supportive environments can help him lead a complete human life. The confident tone one hears in this biography should be entirely attributed to his fantastic four.

Lynn and Edward encouraged him to dream, and did not dismiss his dreams that transgressed the norms of his own society and his own people. To dream is after all one of man’s most basic freedoms. It was through the valuable companionship and advice of these people that he gathered the strength to write this dissertation. Today Tiju looks towards a future wherein he can be a father, mother, brother, sister, uncle, aunt, friend, spouse, neighbor, priest, teacher and researcher all at once. He does not consider himself to be a prisoner of his circumstances. He wishes to live in constant wonder, asking child-like questions about the world that he finds himself in; while reminding himself that no learning is sufficient. He also looks forward to a future where he experiences his own humanity in the fullest measure. In the future he expects to participate in the lives of those who are as lost as he once was.

To all my friends and family

ACKNOWLEDGMENTS

Every doctoral work has many people behind it; people from every walk of life. I hesitate to claim that I can acknowledge every person who has contributed in one way or the other to this work. In fact, I could never write an acknowledgement that does justice to all who ought to be credited. Even if my memory does not fail me in remembering every person involved, I am sure that my vocabulary will fail me in expressing my gratitude. First and foremost, I must mention my infinite debt to Prof. Michael Spencer and Prof. Francis J. DiSalvo. Prof. Spencer has been the most supportive supervisor I could hope for. In him I found a mentor, a role model and a friend. Not only is he a fountain of ideas, but he also has a heart of gold. He stood beside me through thick and thin, and played a very special role in my return to school after the medical leave. When I had to return from leave, neither Prof. Spencer nor I had the funding to help me get back on the graduate student roster. In such a gridlock situation, Prof. DiSalvo stepped in with moral support and financial assistance. I can never repay his kindness. This dissertation would not have been possible without the generosity and moral support of Prof. Spencer and Prof. DiSalvo. I shall be indebted to them forever.

Dr. Lori Lepak deserves a very special mention at this point. She has been one of my closest companions during the doctorate. If you ever meet her, you will know that you have met one of brightest chemists in the world. My scientific discussions with Lori have always helped me think out of the box. Her breadth of knowledge is second to none in the world. Chemistry has become second nature to me, thanks to Lori. Because of her and my committee, I consider myself a chemist, physicist, and engineer all at the same time. She is also one of the editors of this dissertation. In the preparation of the manuscript of this dissertation, Lori has played a very special role.

She proofread my manuscript, suggesting both scientific and literary stylistic corrections. If you think that this thesis is well organized and a pleasure to read, you must thank Lori for that. I extend my heartfelt gratitude to my friend, Lori.

Prof. MVS Chandrashekhar has been a co-author with me on several papers. He belongs to the category of scientists who never ran out of ideas. I would also like to mention the contributions of Dr. Chris Ian Thomas, Jie Lu and Virgil B. Shields, all of whom gave me valuable advice on experimental science. I would also like to remember the many teachers whom I have come to admire over the years. At Cornell, I have had the honor of listening to lectures by Professors Lara Estroff, Michael Thompson, Edwin Kan, J. Richard Shealy, Clifford Pollock and Francis DiSalvo. Through each of them I learnt that the only criteria for scholarship are humility and perseverance.

I would like to thank Prof. Eastman for his trust in my sincerity. He agreed to be on my committee, and guided me through the science of gallium nitride. I still remember the first meeting I had with Prof. Eastman. That day, in a single sitting, he explained to me the history of compound semiconductors, and gave me a set of unsolved issues in compound semiconductor physics. I have come to know Prof. Eastman as a person who believed that every student's mind is waiting to be ignited.

I also remember my teachers at JNCASR and MSRIT with gratitude. I would like to recall Professors Umesh Waghmare, Chandrabhas Narayana, Swapan Pati, Meheboob Alam, Shobhana Narasimhan, S. Ranganathan, V. Venkataraman (IISc), Narendra, M. Madhusudan Rao and M. S. Sudhi all whom have contributed to my doctorate in ways that are tangible and intangible.

Cathleen Donovan has been a friend who taught me the importance of accepting oneself. We met one another at St. Catherine's at a time when there were uncertainties looming all over me. In the months that followed, we had several

conversations that have shaped me in ways I cannot entirely describe. In her, I have found a role model. She has taught me the value of listening to one's own heart. At this point I very fondly remember Edith Johnson, Cathleen Donovan, Faik Bouhrik and Peter Lundquist. I had the good fortune of being Peter's roommate for a good two and a half years. During this time, I have grown to respect and admire Peter's rectitude and humility. He has much to offer, perhaps more than he can imagine. Edith has been a source of strength for not just me, but many other international students. She is one of those kindliest people who becomes the family to all those who knock at her doors. Faik Bouhrik showed me that one can live without adhering to boundaries. He is at once a physicist, philosopher, historian, script-writer and a mathematician. Through him I learnt that life is colorful, and a constant journey. To impose a black and white description on what is inherently colorful is denying the richness of reality. At this point I must also thank some very special young people in my life: Shea Hasenauer, Brendan Barrett and Dominic Rozzario. I have looked at each of these precious people as my own kin. If I am ever blessed with a child, I would pray for him/her/hir to be like these beautiful people.

I would like to thank my dad (C.T. Thomas), my mom (Elsie Kutty Thomas) and my beloved brother (Seby Thomas) for being with me through the rough and smooth rides of my life. I know that I have wronged them several times, especially when I was sick. When I wronged against them, I knew nothing better than blaming and turning away from those whom I could take for granted. My ignorance, my ambiguous existence, and my inner struggles have all taken a toll on my family. I sincerely thank them for being the rock on which I have been able to lean. May God bless my family!

It was on an occasion of exceptional weakness that I met Lynn Podhaski. He has been my counselor, philosopher and friend. Without Lynn's wise counsel I would

have never made it to the end of this thesis. I will continue to remain obligated to Lynn Podhavski. I wonder if he knows how great he is. This thesis is dedicated to Lynn, and people like him who make our world a more beautiful and loving place. Speaking of people who make the world a more beautiful place, I would like to specially acknowledge the beauty that Edward Moran and Elliot Bassman have brought into my life. Few friends do as much as these two have done for me in such a short time.

This work is supported primarily by the Nanoscale Science and Engineering Initiative of the National Science Foundation under NSF Award #EEC-0117770, 0646547 and in part by NSF grant number DMR-0602526.

TABLE OF CONTENTS

LIST OF FIGURES

LIST OF TABLE

CHAPTER 1

INTRODUCTION

1.1 Nitride based solid state optical technologies

Lighting currently consumes roughly 20% of the electricity used in the United States. It is predicted that solid state lighting based on efficient light emitting diodes (LEDs), if used widely, has the potential to reduce this share of energy consumption by 30% by 2025. In particular, considerable effort is being directed towards enhancing the efficiency of near UV and blue LEDs to promote solid state lighting as a viable alternate to incandescent technologies.[1,2] Currently, most LED materials are made from a variety of inorganic compound semiconductor materials, including gallium nitride (GaN). Gallium nitride is a binary III/V direct bandgap semiconductor. The first blue LEDs based on GaN were made in 1971 by Jacques Pankove at RCA Laboratories. These devices had very little light output and hence did not have much practical use. However, LEDs were eventually used in some low-light applications, such as the indicator lamps in devices.[3]

In the late 1980s, key breakthroughs in GaN epitaxial growth and p-type doping ushered in the modern era of GaN-based optoelectronic devices.[3] The first GaN-based high-brightness LEDs used a thin film of GaN deposited via MOCVD on sapphire. Other substrates useful for GaN crystal growth include zinc oxide, with a lattice constant mismatch of only 2%, and silicon carbide (SiC).[4] Mixing GaN with In (InGaN) or Al (AlGaN) creates a band gap dependent on the ratio of In or Al to GaN, allowing the production of LEDs with any color on the red to blue spectrum.[4]

Building upon this foundation, in 1993 high brightness blue LEDs were demonstrated.[5] Since the mid-1990s GaN and InGaN based blue LEDs have been very

successful in the market. These blue LEDs can be added to existing red and green LEDs to produce white light that mimics natural sunlight (although white LEDs today rarely use this method of white light production). Today, group III nitride based semiconductors are recognized as some of the most promising materials for fabricating optical devices in the short-wavelength visible and UV region.

1.2 Emission spectrum characterization of phosphor materials

A phosphor is a substance that exhibits the phenomenon of phosphorescence. Phosphorescence is the sustained glow of a material, following excitation by energized particles such as electrons or ultraviolet photons. In order to understand phosphor technologies, it is important to remember that all materials have a characteristic emission spectrum. The light emitted from a certain material governs the response of the human eye. The response of the human eye is such that some combinations of colors can be combined to produce white light. Combinations of colors that yield white light are usually mentioned in the form of 3-tuples, which is basically a set of coordinates in a color space. This is so because human beings have trichromatic eyes, with cones that respond primarily to red, blue and green light respectively.

The coordinates in the color space defines the intensities; while the color space defines the basic color functions that we operate on. Figure 1.1 shows the 1931 Chromaticity diagram, which was published by the International Commission of Illumination (CIE). The CIE is the global scientific community that determines the standards on color space representations. The figure shown is one of the first chromaticity diagrams published that allows us to calculate the colors that have to mixed to yield white light as perceived by a standard human observer. A standard human observer is defined for a given chromaticity diagram. The definition of the observer includes specification on distribution of color detector cells called cones in

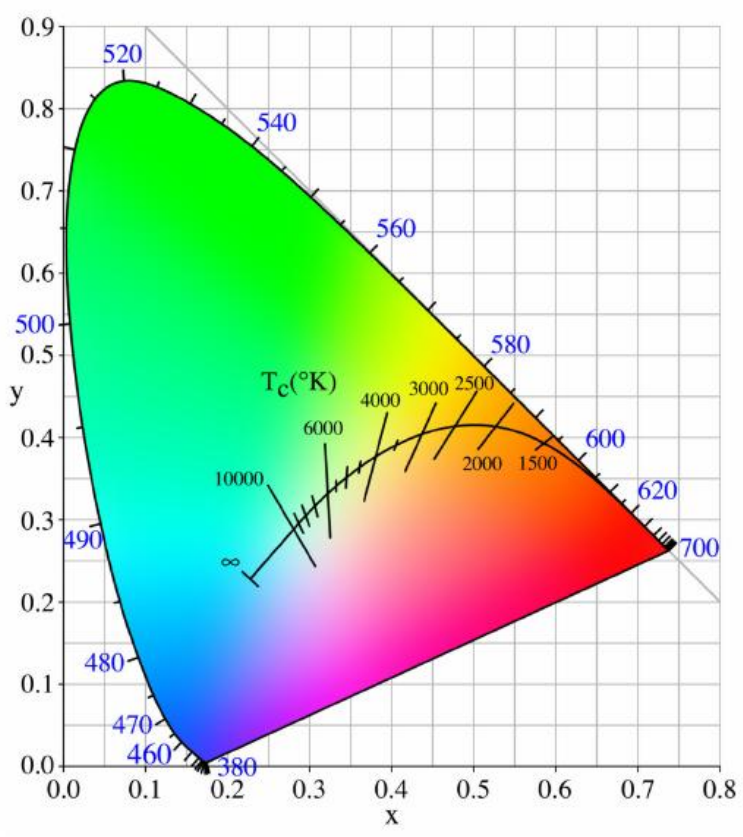

Figure 1.1 CIE 1931, Chromaticity diagram. The cross-sectional locus is the color of the black body radiator at the given temperature. [6,7,8]

the fovea of the eye. Currently it is believed that most color perception happens within a 10^{o} arc in a region of the human retina called the fovea. The chromaticity diagram in Fig 1.1 assumed all cone cells to be within a 2^{o} arc on the fovea. Practical applications of phosphor materials are explored based on the coordinates of emitted wavelength within this chromaticity diagram. The chromaticity diagram is used widely by technologists to determine the colors that should be combined to obtain white light. [9]

As mentioned before red, green, and blue light can be mixed to yield white light with a high color rendering index (CRI) (see Figure 1.1). The color rendering index is a quantitative measurement of a light source's ability to reproduce the colors of objects faithfully, relative to natural light. It is typically reported on a scale of 100, where the numerical value 100 is associated with the appearance of colors under ideal lighting. If the rendering index of the white light is too low, then certain colors will appear washed out; for example, red may appear brown. Alternately, white light can also be produced by a combination of blue and yellow light. The CRI of this combination can be improved by mixing in a small portion of orange or red into the spectrum.

To generate the full palette of colors, materials with an appropriate combination of emission and absorption spectra must be used. Hence, developing a near UV or blue emitting LED, combined with the ability to down convert the high energy photons emitted by the LED to other colors, is a significant area of interest. The desired absorption and emission characteristics are typical of a class of materials known as phosphors. The most common uses of phosphors are in CRT displays and fluorescent lights. When applied to LEDs, a phosphor would absorb the emitted photons from the LED and down convert their energy by re-emitting them at a longer wavelength.

It is possible to allow a portion of the LED emission to stimulate a phosphor, while some of the blue light is passed unaltered. Mixing these two emissions would then produce white light. Similarly, if a near UV or blue emitting LED is paired with several appropriate down converting phosphors in the red, green, and blue (in the case of the UV LED), an even higher quality white light may be produced. As it turns out, this is the crux of the materials problem facing white LED systems.

Several practical difficulties with the phosphor based approach of making white light LEDs should be noted. It is often difficult to appropriately match the excitation to the desired output. Furthermore, both red and green emissions result from low energy transitions that are difficult to produce with a commercially viable efficiency.

Therefore, one of the major endeavors in materials research today is to invent efficient phosphors for solid state lighting applications. Group III nitrides and related materials have proved to be promising optical materials. Transition metals incorporated in a lattice tend to exhibit crystal field splitting which results in compounds that are optically active in the visible region. Compounds which have rare earth incorporation tend to show sharp transitions (even in the visible region) because of the *f* shell electrons. Hence most phosphor compounds contain transition metal or rare earth atoms; thus, transition metal or rare earth doping of the nitride may prove beneficial.

1.3 GaN technologies: history and commercial success so far

Over the last two decades, GaN-based blue/UV-LEDs[1] have undergone significant developments, which have led to the commercialization of highly efficient blue LEDs and reliable violet-laser diodes. High-brightness GaN light-emitting diodes

(LEDs) emitting primary colors have been used for applications such as daylight visible full-color LED displays, white LEDs, and blue laser devices.

However, the current interest in GaN encompasses a literature devoted not only to LED's, but to many other specialized applications.[4] These include high-power/high-frequency devices such as microwave radio-frequency power amplifiers (including those used in high-speed wireless data transmission) and high-voltage switching devices for power grids. GaN-based RF transistors may someday find mass-market application as the microwave source for microwave ovens, replacing the magnetrons currently used. Nitride-based materials have also been developed for use in devices such as UV detectors and high-speed field-effect transistors. In particular, the low sensitivity of GaN to ionizing radiation (like other group III nitrides), may make it a suitable material for solar cell arrays for satellites.

GaN is also very promising as a transistor material, since its relatively large band gap allows higher operating temperatures than silicon based transistors. For devices, high quality monocrystalline GaN is necessary. To grow high quality GaN crystal, a technology employing a low temperature deposited buffer layer was developed in 1986.[10] The advent of high quality GaN crystals enabled the fabrication of p-type GaN[1], which in turn led to the development of GaN based p-n junction devices. The first gallium nitride metal/oxide semiconductor field-effect transistors (GaN MOSFETs) were experimentally demonstrated in 1993[4] and are currently being actively developed.

Interestingly, GaN has also found a place in the emerging area of spintronics. When doped with a suitable transition metal such as manganese, GaN is a promising spintronic material (a magnetic semiconductor). GaN high electron mobility transistors (HEMTs) have been available commercially since 2006, and have found an immediate home in various wireless infrastructure applications due to their high

efficiency and high voltage operation.

Finally, room-temperature stimulated emission has been observed in GaN heterojunctions.[11,12] This is expected to make GaN a laser material of choice in the near future.

1.4 Nature of chemical bond in nitride materials

A nitride is a solid state compound that contains monatomic nitrogen in the form of N^{3-} as the lone anion. Hence, only materials such as Mg_3N_2 or GaN are classified as nitrides. GaN occurs most frequently in the wurtzite crystal structure (see Figure 1.2). In this crystal structure GaN has a bandgap of 3.4 eV, which renders it special properties which enables its use in optoelectronic, high power and high frequency applications.

The electronic structure of doped GaN is dictated by the chemical environment surrounding the dopant. In GaN, nitrogen tends to form covalent bonds with its surroundings. This results in the expansion of the electron clouds on the dopant atom that is bonded to N^{3-}. This is called the nephelauxetic effect. In addition, because the activator is expected to be coordinated to the N^{3-} anions, which have a large formal charge, there will be a great degree of crystal field splitting. A combination of these two factors implies that there is a reasonable probability for low energy optical transitions in doped GaN. When rare earth ions are used as dopants the inner *f* shell electrons remains almost unperturbed by the local bonding. Hence the *f-f* transitions remain almost unaffected by the local chemical environment surrounding the RE ion. This makes RE:GaN a very promising material for phosphor and LED applications, especially because sharply defined *f-f* transitions could be obtained from such materials.

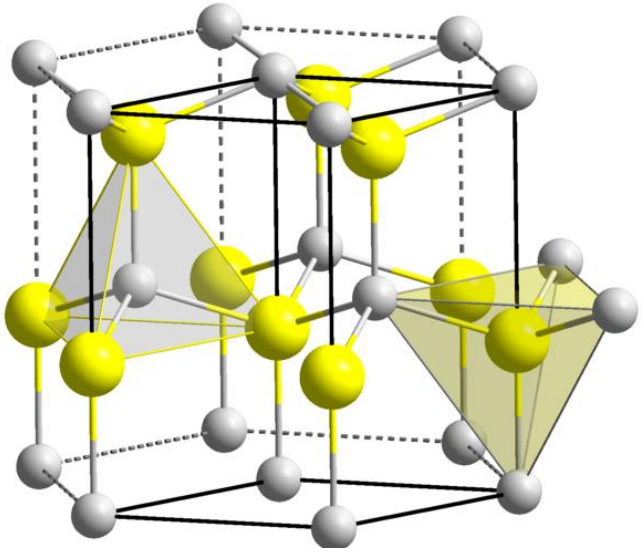

Figure 1.2. Gallium Nitride has a wurtzite crystal structure, with each N atom (gray sphere) attached to four Ga atoms (yellow spheres). Notice that the Ga atom is much larger (covalent radius: 122pm) than the N atom (covalent radius: 72pm). [13]

Mixed nitrides such as oxynitrides and halonitrides are known; however, the family of solid state materials containing the nitrogen anion is quite small. On the

other hand, many oxides exist. While many naturally occurring materials contain oxygen, only one nitride (TiN) occurs in Nature. At first glance, this may seem quite surprising, since nitrogen is far more abundant in the atmosphere (78%) than oxygen (21%). However, the rarity of nitride phases in comparison to oxides is readily explained by the thermodynamics of formation of nitride materials. [6]

1.5 Synthesis criteria for GaN

We have seen that nitrides very rarely occur in nature. Understanding the reason for this can also give us insight into the synthesis of nitrides in a lab.

The Gibbs-Helmholz free energy of a reaction is given by:

$$\Delta G = \Delta H - T\Delta S$$

The free energy of formation (ΔG) is dependent upon the change in enthalpy of formation (ΔH) and the change in entropy of the reaction (ΔS). There is a negative change in entropy during the formation of an oxide or nitride from its constituent elements, since there is a net consumption of gas in these reactions. This implies that the feasibility of formation of the oxide or nitride will depend significantly on the enthalpy of formation.

The change in enthalpy is the difference in energy between the bonds being formed and the energy of the bonds being broken. In the case of nitride formation, one has to overcome the energy barrier of breaking the very strong triple bond of diatomic nitrogen at 945 $kJ*(mol)^{-1}$, which is second in strength only to the carbon-oxygen triple bond in carbon monoxide.[6] The oxygen molecule double bond is far weaker, at a mere 498 $kJ*(mol)^{-1}$. This is the key reason for the ΔH of formation of nitrides being fairly low when compared to their corresponding oxides.

From the Gibbs-Helmholtz equation, it follows that the ΔH of formation of nitride or oxide must be as negative as possible so that the entropic factor is overcome at the temperatures of synthesis. If the enthalpy of formation is low (as it is in the case of GaN, which is about -165±16 kJ/mol), then for the enthalpy to have a chance to overcome the negative entropy change during the reaction, the synthesis must be carried out at low temperatures. However, the very slow reaction rates at these temperatures make this approach inadvisable. Hence, low temperature synthesis would not be a feasible method for the rapid, high throughput production of nitrides.

The thermodynamic analysis above suggests that many nitrides will have limited air or water stability. At typical synthesis temperatures, GaN should rapidly decompose into oxides or hydroxides in the presence of air or water. Therefore, oxygen and water must be strictly avoided from the GaN synthesis chamber. At room temperature, however, the kinetics of the reaction prevents nitrides such as AlN and TiN from converting to their corresponding oxides when exposed to air.

This "air stability" of GaN is believed to result from the formation of a thin surface oxide layer, which protects the bulk against further oxidation. This phenomenon is associated with the air stability of nitrides that are currently used in devices (such as AlN and InN). The air and water stability of these nitrides and related materials (such as rare earth doped GaN) is a kinetic, and not a thermodynamic, phenomenon. These issues are discussed in great detail in the dissertation of Mark Bailey, of the DiSalvo group at Cornell.[14]

1.6 GaN as a phosphor and LED material: Stokes loss based analysis

Phosphor materials may be excited by several different mechanisms: photons (photoluminescence), electrons (cathodoluminescence), sound waves (sonoluminescence), or even mechanical agitation (mechanoluminescence). In

semiconductor LEDs, the energy of the emitted photon is dependent upon the band gap of the material. In GaN based LEDs, the band gap may be engineered via alloying with InN.[9] In this thesis, photoexcited rare-earth doped GaN is studied as a luminescent material. The host material (GaN) contains an activator (a rare-earth element such as Eu^{3+}, Er^{3+}, Ce^{3+}, and Tb^{3+}) which generates the luminescence. The energy of the emission is dependent primarily upon the activator, but is also affected by the host.

The observed luminescence in these rare earth activator ions is due to transitions occurring within the 4*f* shell, so they tend to behave similarly in different host materials. Perhaps the most well characterized electronic transitions among the lanthanides are the inner shell transitions of Eu^{3+}, Gd^{3+}, Tb^{3+} and Er^{3+}. These species are extensively used in technology today. For example, Eu^{3+} activators are used as the source of red in cathode ray tubes in TVs and computers. Similarly, Tb^{3+} activators are used to generate green in tricolor lamps.

The basic steps involved in luminescence in the RE:GaN system are (a) absorption of a photon and excitation of the rare-earth ion (b) non-radiative relaxation of the excited electronic state of the activator to a low-vibrational level (c) relaxation of the activator ion to its ground state resulting in spontaneous emission of a photon. Figure 1.3 illustrates each of these three steps involved in luminescence.

Figure 1.3, as drawn, implies that the bond-lengths in the excited level are slightly longer than the ground state RE^{n+}-N^{3-} bond. This need not be the case. In fact $R_0 = R'_0$ for the inner shell transitions of many trivalent rare earth activators. In such

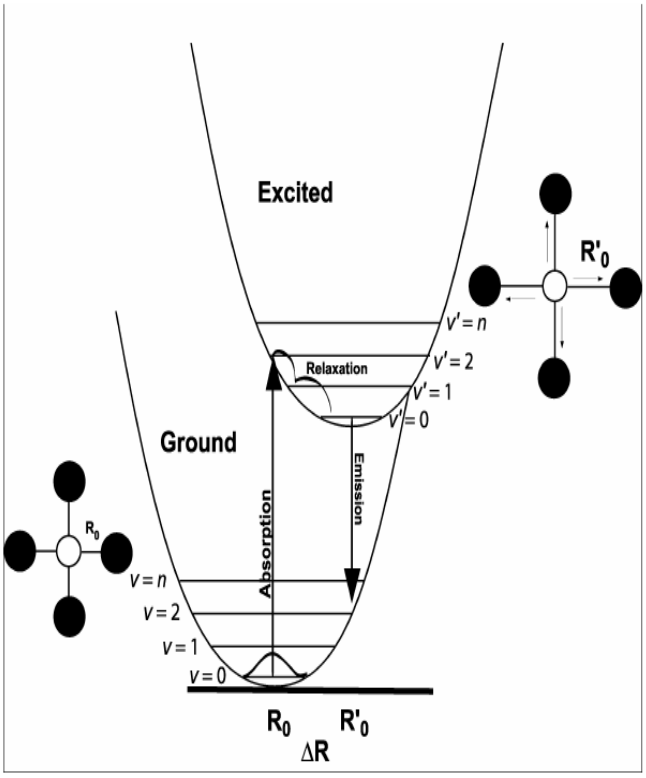

Figure 1.3. Configurational coordinate diagram showing the ground and first excited electronic states. The vibrational levels are represented using the symbols ν and ν'. R_0 and R'_0 represent the equilibrium bond lengths of the ground and excited electronic states, respectively. [6,15]

cases, the absorption bandwidth vanishes. However, it must be noted that temperature dependent line widths are possible in both absorption and emission spectra, because of the many possible excitation and relaxation transitions of the activator ion.[15]

Relaxation of the ion occurs when, upon reaching the lowest possible vibrational level in the excited state, the activator system spontaneously transitions back down to an excited vibrational level within the electronic ground state (see Figure 1.3). The spontaneous transition leads to the release of a photon, with an energy equal to the energy difference between these two states. Finally, nonradiative relaxation restores the system to the vibrational ground state, and the activator-ligand distance returns to the equilibrium bond length (R_0).

The above description of the mechanism of luminescence also explains why the emitted photons will always have a lower energy than the photons used to excite the material (absorbed photons). This difference in energy (ΔR) is known as the Stokes shift. Essentially, the larger ΔR is, the larger the Stokes shift will be, and the broader the observed optical transitions will be. Whenever ΔR is large, there is a large Stokes shift, and thus a low efficiency. The loss in emission efficiency with increasing Stokes shift is often called Stokes loss. The Stokes shift is equal to $2\Sigma h\nu$, where Σ is the electron-lattice coupling constant, which is proportional to $(\Delta R)^2$.

In the case of the inner shell transitions observed in trivalent rare earths, $\Delta R = 0$ due to the heavy shielding of the *f* orbitals, and as a result the observed transitions are sharp lines instead of broad bands. Viewed another way, the *f*-shell electrons in RE^{n+} ions are inner shell electrons, and thus do not interact significantly with the host lattice. Hence the observed transitions (both absorption and emission) are sharp, which in turn minimizes Stokes losses. This is why rare-earth metals are preferred the dopants in GaN. However, if the lattice vibrations have a high enough energy, they

can effectively quench some or all of the expected luminescence. Thus, the choice of a host lattice free of these high energy vibrations (in this case GaN) is critical as well. Optical transitions are also governed by quantum mechanical selection rules for parity and spin. In solid systems, these rules serve as general guidelines, rather than rigid restrictions. There are several ways around the selection rules, such as uneven crystal field terms or spin-orbit coupling, which provide the basis for several current widespread technologies.[16] For example, many phosphors used in current display technologies such as $Y_2O_2S:Eu^{3+}$ exploit these so-called 'forbidden' transitions.[6]

Spin-forbidden relaxations ($\Delta S > 0$) occur slowly and result in phosphorescence, while spin-allowed transitions ($\Delta S = 0$) occur rapidly and result in fluorescence. Lifetimes for spin-forbidden transitions can vary from a few microseconds to a few days, while relaxation times in fluorescent materials can be as short as a few nanoseconds. In some materials, the incoming energy is first absorbed elsewhere, and then transferred to the activating center. In some cases it is possible to transfer energy from the host lattice (which could absorb incoming energy) to the activating center.

The concentration of activator ions in doped phosphors is typically <10 at% to prevent quenching. As more activators are placed in the lattice, the average distance between activating centers becomes smaller. This increases the opportunity for energy sharing between activating sites, which in turn will lead to excitation energy migrating far from the initial absorption site. This energy may eventually migrate to a defect or quenching site, where it may be dissipated through a nonradiative transition. This is known as concentration quenching. At some critical concentration, this process usually results in the total elimination of emission.[17]

For the present, we will look at Eu^{3+} as the activator species. Since inner 4*f* electron-transitions are involved, $\Delta R = 0$ and sharp emission lines can be expected.

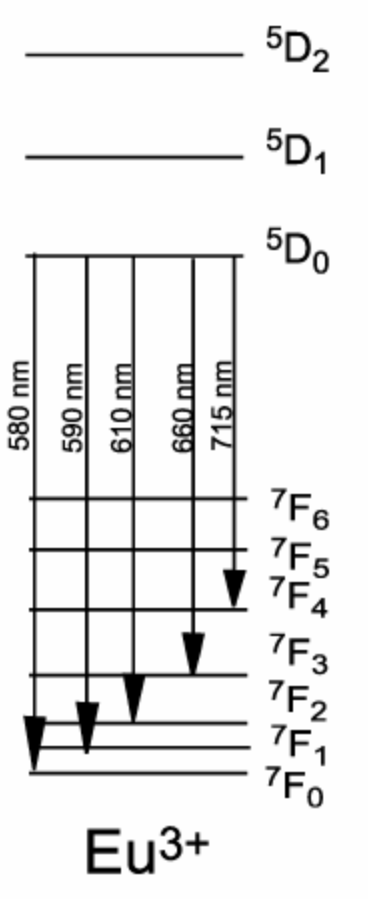

Figure 1.4 Electronic energy diagram of the Eu^{3+} activator ion.[6,18]

The ground state electronic configuration of Eu^{3+} is $4f^6$. Due to L-S coupling, the $4f$ level is split into several sublevels. The ground electronic state of the system is $^7F_0$ (L=3, S=3, J=0) (refer Figure 1.4). Given that the spin-orbit interactions in rare earth ions is in the strong coupling regime, it is probably more appropriate to say that the $4f$ level splits into sublevels due to *j-j* coupling.

Emission from the Eu^{3+} activator is typically observed in the red spectral region (max around 610 nm), originating from transitions between the excited $^5D_0$ state (L=2, S=2, J=0) and the various ^7F_J (J = 0-6) levels. Depending on the host lattice, it is sometimes possible to observe additional emissions from the higher energy levels of $^5D_3$, $^5D_2$, and $^5D_1$ to ^7F_J. If present, the higher energy transitions will appear in the green ($^5D_1$) and the blue ($^5D_2$), but their intensity is heavily dependent on the vibrational levels within the host lattice. If the vibrational energy is high enough, the difference in energy between the various ^5D_J states can be exchanged against the vibrational levels, leading to quenching of the higher energy emission. In a similar manner, the relative intensity of the transitions from $^5D_0$ to ^7F_J is also heavily host dependent. For example, if the Eu is coordinated in a site with inversion symmetry, the transition of $^5D_0 \rightarrow {}^7F_1$ (around ~590 nm) will dominate. Conversely, if Eu is located in a site without inversion symmetry, the transition of $^5D_0 \rightarrow {}^7F_2$ (~610 nm) will dominate.[16]

In the case of Eu:GaN, the Eu occupies a site with no inversion symmetry; therefore, this system has a maximum emission intensity at about ~620 nm. It is of interest to note that the $^5D_0 \rightarrow {}^7F_2$ (~610 nm) transition involves a spin flip and a $\Delta L = 1$. Hence this transition is doubly forbidden and thus can be expected to be very slow. In fact, this transition has been shown to have a lifetime of about 170 μs. This indicates that the $^5D_0$ level in Eu^{3+} is a metastable state, which may be useful to achieve population inversion for laser applications.[19]

If the luminescent events of interest involve transitions between 5*d* and 4*f* orbitals, there is a greater dependence on the host lattice. The 5*d* orbitals are not as heavily shielded as the 4*f* orbitals, and thus will interact more with the lattice-dependent local crystal field environment. This interaction influences the 5*d* energy levels, which will in turn influence both the transition probabilities and the energies associated with the 5*d*-4*f* transitions. Hence the same activator can have very different optical characteristics, depending on the host lattice.[16]

We have seen several ways in which the host lattice plays a very important role. The host lattice can be responsible for quenching effects (either partial or total quenching), and may be critical in determining the observed luminescence. The first consideration is known as the "nephelauxetic effect". This effect arises due to the coordination of RE^{n+} to the surrounding anions. This can cause a mixing of anion orbitals with activator orbitals, leading to orbital expansion and a decrease in interelectronic repulsion. In general, the more covalent bonds there are in the coordination sphere of an activator, the greater the nephelauxetic effect will be. Increasing covalency lowers the energies of the 5*d* orbitals with respect to the 4*f* orbitals, resulting in lower energy emissions.

The second, and probably more obvious, influence of the host lattice involves the local symmetry and crystal field splitting. The symmetry of a specific dopant site can be extremely important in determining the observed luminescence. We have seen that the lack of inversion symmetry of the Eu site in Eu:GaN determines the predominant emission line (~620 nm). Additionally, the local coordination number of the RE^{n+} ion influences the crystal field splitting, and therefore the emission spectrum. We can expect RE^{n+} with tetrahedral coordination to exhibit longer wavelength emissions when compared to the corresponding octahedral coordination, since the

energy level splitting associated with the latter coordination geometry is usually larger.

The host lattice has an impact on the Stokes shift as well. Since the Stokes shift is strongly correlated to the degree of energy loss in a system, this is an important factor to consider. There are two primary ways in which the host lattice environment can directly affect the Stokes shift. A more confined activator ion is usually more tightly coupled to the lattice, which in turn leads to a bigger Stokes loss. For example, for RE^{2+} on a Mg^{2+} site, due the huge size difference between the RE^{2+} ion and the Mg^{2+} ion, the Stokes shift will tend to be large. Also, the more rigid the lattice, the smaller the Stokes shift will generally be.[20] If a potential host displays a significant amount of three dimensional cross linking (as is found in silicates, silicon nitrides, and borates, for example), then there will be a tendency towards a smaller Stokes shift, and thus greater emission efficiency. The GaN structure is particularly rigid, making it a good host for RE^{n+}-doped optical applications.

1.7 Conclusions

In this chapter, I have tried to locate our research on GaN based phosphors in the context of the technological developments that have happened in the last four decades. I have also presented detailed discussions on excitation and de-excitation mechanisms in phosphor materials, and the various physico-chemical criteria that are taken into consideration while inventing new phosphor materials. A Stokes loss based analysis justifies the reason to look among rare earth doped nitride materials for new phosphor and laser gain materials. We also developed a thermodynamics based chemical picture for the formation of nitride materials. This thermodynamic analysis provides insight into methods used in this thesis for nitride synthesis. An exposition of the importance of the chromaticity diagram in phosphor research emphasized the need

to optically characterize every material using its emission spectrum and locating its coordinates in the color space. A combination of all these physico-chemical and technological considerations is used to understand and develop commercially viable phosphors and laser gain materials. We believe that this thesis will be a step towards developing rare earth doped GaN particle which will find applications in large and small area lighting applications, light emitting diodes and laser gain media respectively.

REFERENCES

1. H. Amano, M. Kito, K. Hiramatsu and I. Akasaki, Jpn. J. Appl. Phys. **28**, L2112 (1989).

2. I. Akasaki and H. Amano, Jpn. J. Appl. Phys. **45**, 9001 (2006).

3. Takeda Foundation. Takeda Award 2002 achievement fact sheet. http://www.takeda-foundation.jp/en/award/takeda/2002/fact/pdf/fact01.pdf (accessed Nov 3, 2010).

4. H. Morkoç, S. Strite, G. B. Gao, M. E. Lin, B. Sverdlov, and M. Burns, J. Appl. Phys. **76**, 1363 (1994).

5. S. Nakamura, T. Mukai, N. Iwasa. U.S. Patent 5,578,839, 1996.

6. J. C. Reiherzer. Synthesis and luminescent properties of rare earth activated phosphors. Ph.D Dissertation, Cornell University, Ithaca, 2009.

7. U.S Department of Energy. Basic research needs for solid state lighting. http://www.er.doe.gov/bes/reports/files/SSL_rpt.pdf (accessed Nov 3, 2010).

8. T. Smith and J. Guild, Transactions of the Optical Society, **33**, 73 (1931).

9. A. Kitai. Solid State Luminescence: Theory, Materials, and devices; Chapman and Hall, 1993.

10. H. Amano, N. Sawaki, I. Akasaki and Y. Toyoda, Appl. Phys. Lett. **48**, 353 (1986).

11. I. Akasaki, H. Amano, S. Sota, H. Sakai, T. Tanaka and M. Koike, Jpn. J. Appl. Phys. **34**, L1517 (1995).

12. H. Amano, T. Asahi and I.Akasaki, Jpn. J. Appl. Phys. **29**, L205 (1990).

13. M. S. Bailey. Synthesis and Characterization of Nitrides and other Non-oxides Materials. Ph.D Dissertation, Cornell University, Ithaca, 2005.

14. B. Cordero, V. Gómez, A. E. Platero-Prats, M. Revés, J. Echeverría, E. Cremades, F. Barragán and S. Alvarez, Dalton Trans., 2832 (2008).

15. P. Atkins and J. de Paula. Physical Chemistry, 7th ed.; W. H. Freeman and Co.: New York, 2002.

16. G. Blasse and B. C. Grabmier. Luminescent Materials; Springer Verlag: Berlin, 1994.

17. Y. Q. Li, J. E. J. van Steen, J. W. H. van Krevel, G. Botty, A. C. A.Delsing, F. J. DiSalvo, G. deWith, H. T. Hintzen, J. Alloys Compd. **417**, 273 (2006).

18. W. T. Carnall, G. L. Goodman, K. Rajnak and R. S. Rana, J. Chem. Phys. **90**, 3443 (1989).

19. C. B. Poitras, M. Lipson, H. Wu and M. G. Spencer, Mater. Res. Soc. Symp. Proc. **866**, V.3.2.1 (2005).

20. A. Meijerink and G. Blasse, J. Luminescence **43**, 283 **(**1989).

CHAPTER 2

GaN POWDER SYNTHESIS

2.1 Introduction

Significant interest exists in using high purity, crystalline GaN powder to grow bulk GaN substrates using either sublimation or high-pressure methods.[1] GaN powder also has potential applications as an electroluminescent phosphor. Quantum confinement effects in nano-scale GaN particles could be of significant interest as well.[2] Thus, there are many reasons to explore the efficient production of GaN powder (both RE-doped and intentionally undoped) of various particle sizes.

2.2 Overview of GaN powder synthesis methods

Johnson et al. reported the first successful effort to synthesize GaN powder by flowing NH_3 over molten gallium at temperatures of 900-1000^{o}C.[3] Since then the reactions of Ga_2O_3,[4] Ga_2O,[5] GaP, or GaAs [6] with NH_3 have been reported to produce GaN powder as well. Other methods of synthesizing GaN powder involve the decomposition of organometallic compounds containing Ga and N,[7] plasma synthesis,[8] and microwave-assisted combustion methods.[9] However, all of these alternative methods suffer from either very low yields or high impurity concentrations. To my knowledge, prior to Huaqiang Wu's work, only one report exists in literature of the efficient conversion of Ga metal to GaN using flowing NH_3 in a horizontal furnace.[5]

While undoped GaN powder in itself has optical applications, red luminescence can be obtained from doping GaN with Eu. Several techniques have been developed to grow red phosphorescent Eu:GaN powder. These synthetic methods include combustion using $Ga(NO_3)_3$. $6H_2O$, $Eu(NO_3)_3$.$6H_2O$ and N_2H_4 as starting

materials;[10] and ammonolysis of $Ga(NO_3)_3$.$6H_2O$, $Eu(NO_3)_3$.$5H_2O$, $GaCl_3$, $EuCl_3$, GaF_3,+HF, EuF_3 mixtures as starting materials.[11] Another successful method demonstrated to synthesis Eu:GaN was a two-stage vapor-phase method where Ga, Eu, $GaCl_3$ and NH_3 are used to produce Eu:GaN powders. $GaCl_3$ is used as a carrier of the rare earth dopant.[12]

In this work, we use a novel GaN, Eu:GaN, Er:GaN powder synthesis process developed in the Spencer Group by Wu et. al. [13-16]

2.3 Ammononthermal GaN and Eu:GaN powder synthesis

A solid solution of Eu, Bi, and Ga was prepared prior to the synthesis of the GaN:Eu powder. For the preparation of intentionally undoped GaN powder, Eu is omitted from the alloy synthesis process. The initial precursors were 99.9999% gallium, 99.999% bismuth, and 99.9% europium. About 25 g of Ga were mixed with 1.25 mol% of Eu and 3 mol% Bi in a glove box under purified Ar. The mixture was then sealed in a quartz tube under vacuum and heated to 850^{o}C for 24 hours. The temperature was ramped up at the rate of 100^{o}C per hour and maintained at 850^{o}C.

Afterwards the quartz tube was removed from the furnace, and was quenched in cold water to reduce the amount of inter-metallic formation in the melt. Such alloy synthesis results in a homogeneous alloy suitable as a starting material for RE:GaN synthesis. The alloy was stored under N_2 to prevent oxidation. Longer term storage was done at about 5^{o}C to prevent both oxidation and melting of the alloy.

The solid alloy was transferred to a thick quartz tube to make the GaN:Eu powder (see Figure 2.1 and Figure 2.2). After purging the tube with flowing Ar for 20 min, the temperature was brought up to 950^{o}C and the gas switched to 99.9999% NH_3 to begin the reaction. After 5 hours of reaction, the product (which is mostly in the

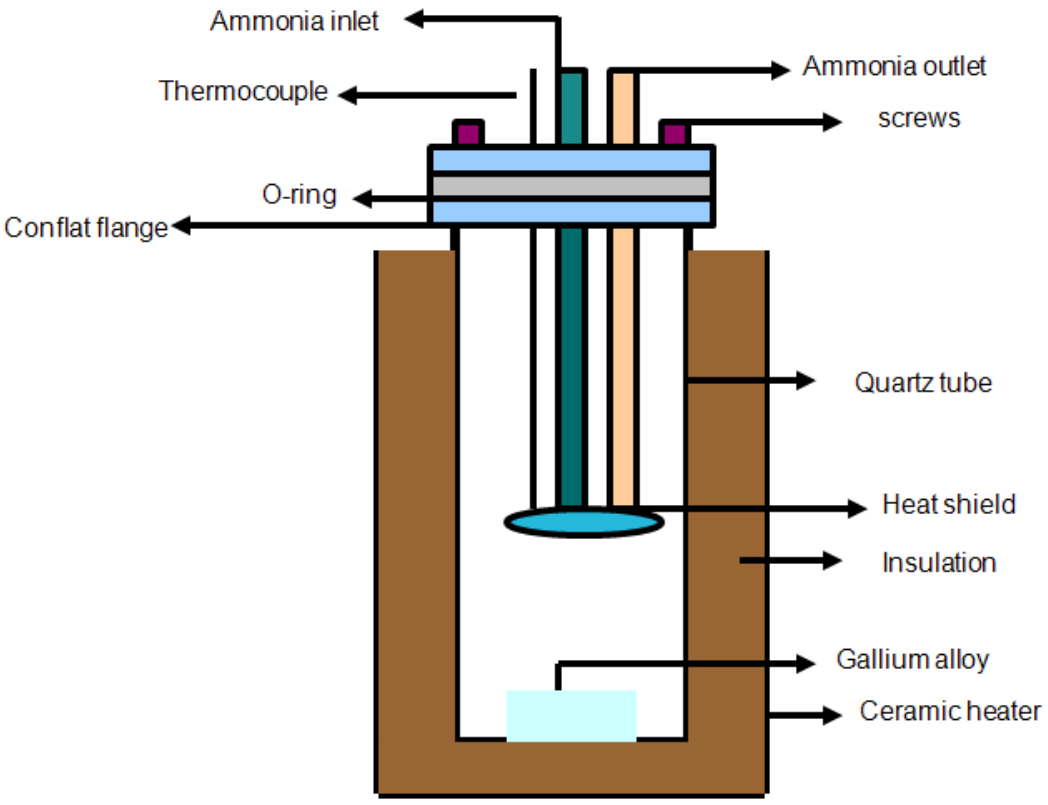

Figure 2.1 Schematic diagram of the ammonothermal reactor used for GaN powder synthesis. The ammonia inlet is used to let in high purity ammonia at 0.8 litres/minute. The O-ring is used to get an airtight seal with a leak rate less than 10^{-9} cm^3/s. The conflat flange is made of a heat resistant stainless-steel. A 3 cm diameter Boron nitride (BN) circular disc is employed as a heat shield. The insulation is made of silica glass fiber. Anywhere between 5-25 grams of Ga alloy can be used. The ceramic heater (manufacturer: Watlow) can be used to heat the reaction chamber up to $1050^{o}C$.

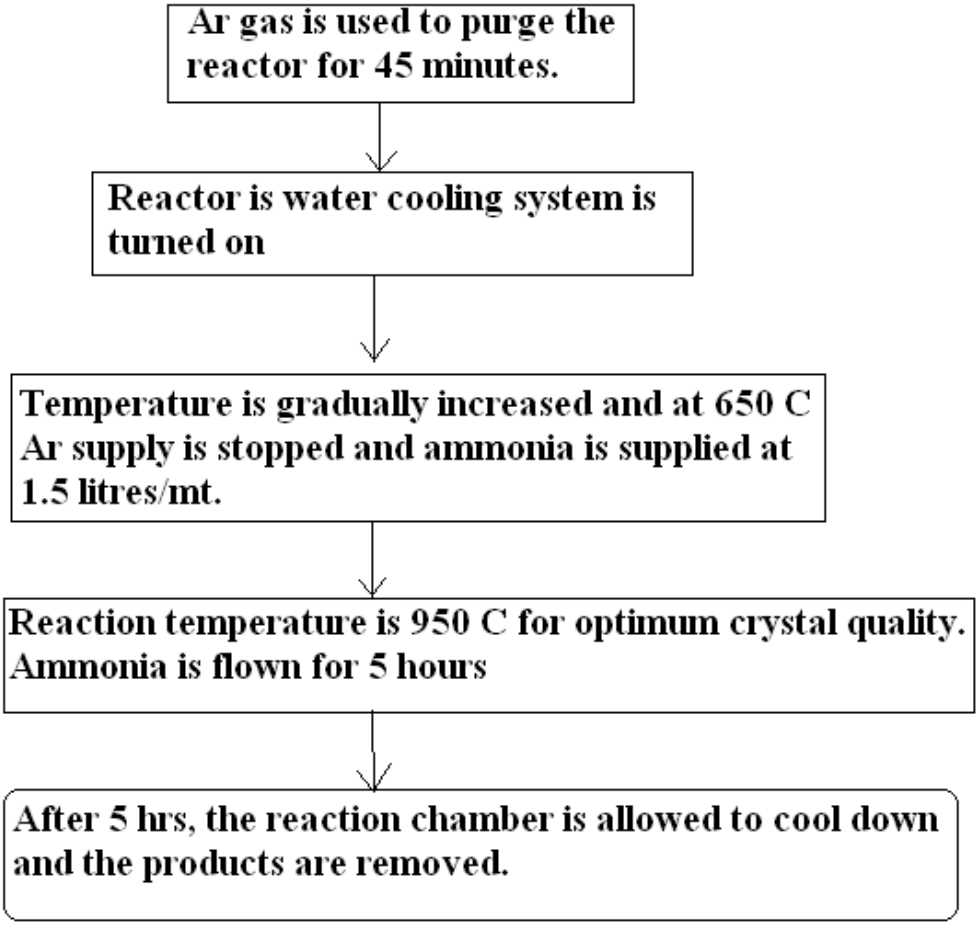

Figure 2.2 Steps involved in the synthesis of Eu:GaN starting from Eu-Bi-Ga alloy as the starting material.

form of chunks/aggregates of powder) was taken out and ground into a fine powder with typical particle sizes of 3-5 μm, as observed by SEM.

Any residual Bi can be removed by annealing the powder at 1020^{o}C for a few hours under flowing NH_3. At this temperature, the Bi equilibrium vapor pressure is ~10^3 and ~10^6 times higher than that of Ga and Eu respectively.[15]

2.4 Role of bismuth in ammonothermal GaN powder synthesis

Bismuth is used as a wetting agent for the complete conversion of Ga to GaN powder. This is because the reaction of pure Ga with NH_3 at high temperatures only results in a partial conversion of Ga, resulting in very low yields. When 3 at% of Bi is used in the starting material all of the gallium reacts completely with NH_3 at 900–1050 °C within 5 hours.

We observed that high percentage of Bi (> 3 at.%) in the alloy resulted in complete conversion of Ga to GaN in the temperature range 900–1050 °C, within 3 hours. However we also noticed that most of the Ga (about 95%) was converted to GaN in just 1 hour after reaching 900 °C. When Bi added exceeds 3 at% the powder obtained is found to be dark gray because of the remaining Bi. The powder color became progressively lighter as the Bi concentration was decreased.[14] Needle-like crystals were common at high Bi concentrations, while plate-like particles predominated at low Bi concentrations (<3 at.%). We employed 3 at% Bi in the alloy used in this thesis. This composition enabled us to get relatively clean, gray-colored GaN powder at the end of 5 hours of reaction time at 950^{0}C.[13]

Cahn first introduced the idea of interfacial wetting in 1977 (see Figure 2.3). He suggested that one component in a binary liquid mixture might segregate to the liquid surface.[17] Interfacial wetting has been observed in fused alkali metal–alkali halide systems, and in liquid gallium-based binary alloys such as Ga–Bi and and Ga–

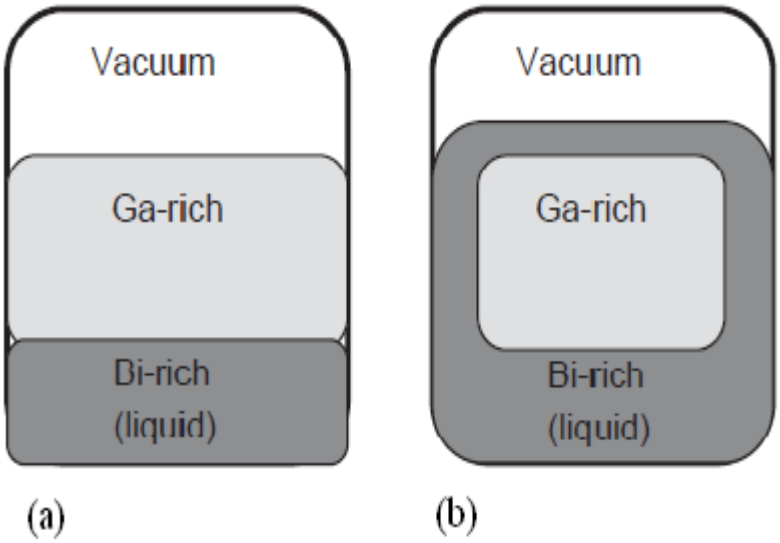

Figure 2.3 Ga-Bi binary solution. The wetting behavior of Bi above 262^{o}C is shown in (b) and below 262^{0} is shown in (a). This suggests that at the reaction temperature (~950^{0}C), Bi is the predominant species at the reaction mixture-gas interface. (Courtesy: Tosmann) [13,14, 18]

T_{crit}=262^{o}C.[14] Above this critical temperature, the low surface tension component, Bi, is present at the interface of the binary mixture. The high density phase completely wets the exposed surface by intruding between the low density phase and the gas Pb. For the Ga–Bi system, the high density phase (Bi) is confined to the bottom of the container when the temperature is lower than the characteristic wetting temperature phase (see Figure 2.3b). Even in Ga-rich alloys of Ga–Bi, Bi is highly concentrated on the surface of the Ga-rich liquid, to form a film at least 30 Å thick at temperatures higher than 262 °C. This Bi layer apparently prevents GaN crust formation and facilitates the full, rapid conversion from Ga to GaN.[14]

2.5 GaN powder growth mechanism

2.5a. Experimental results

To determine the powder growth mechanism, a sapphire [0001] substrate was loaded on the Boron nitride heat shield held 4 cm above the Ga-alloy (see Figure 2.4). The substrate used for epitaxial growth had a root mean square surface roughness of less than 1nm and was purchased from Meller optics. We first observed that a few large particles had accumulated on the boron nitride heat shields. These particles were confirmed to be GaN using Raman spectroscopy.

On the upper end of the reactor tube, black soot was present. The soot was composed primarily of Bi, although some GaN particulates were observed as well (see Figure 2.5). The particles collected from the heat shield were analyzed using backscattered electron (BSE) images from the electron microprobe JEOL 8900. This technique is particularly sensitive in detecting elements with atomic number greater than 11. Hence, Ga and Bi composition was obtained for these particles using

quantitative analysis based on the BSE images obtained. We noticed that some particulates (see particulate shown in Figure 2.5b) are almost entirely made of Bi,

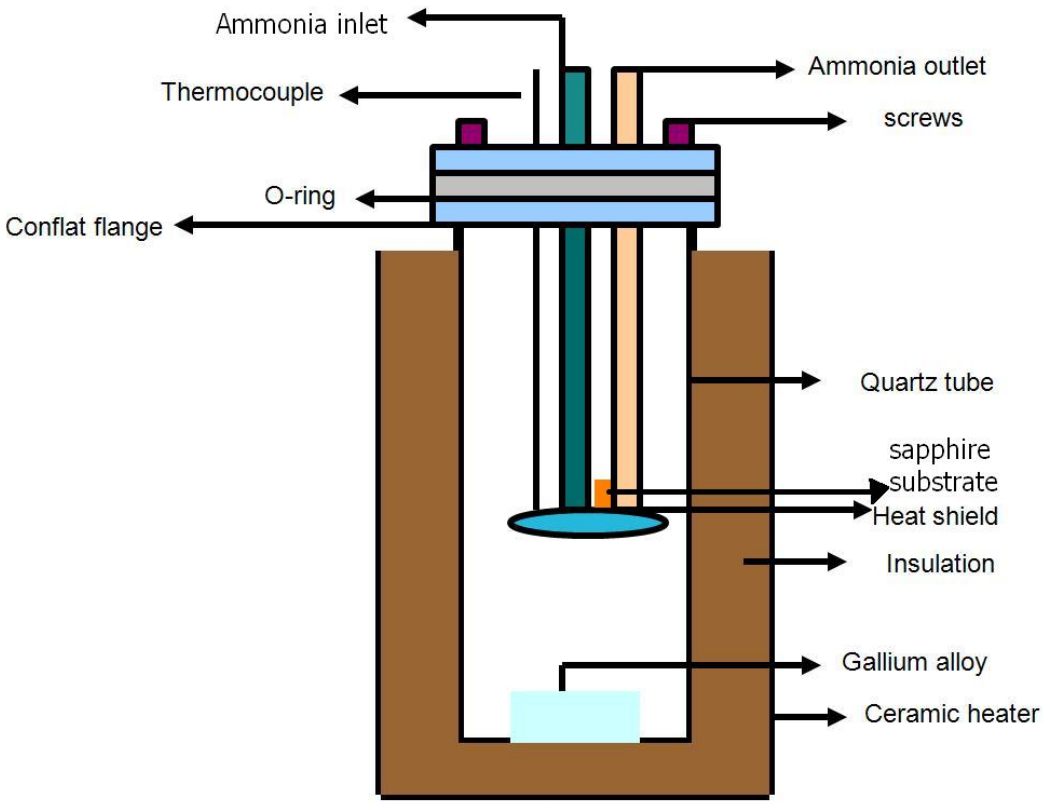

Figure 2.4 GaN ammonothermal reactor. A sapphire substrate is placed on the boron nitride heat shield to investigate the amount of vapor phase growth occurring in the chamber. The substrate was held 4 cm above the Ga alloy melt.

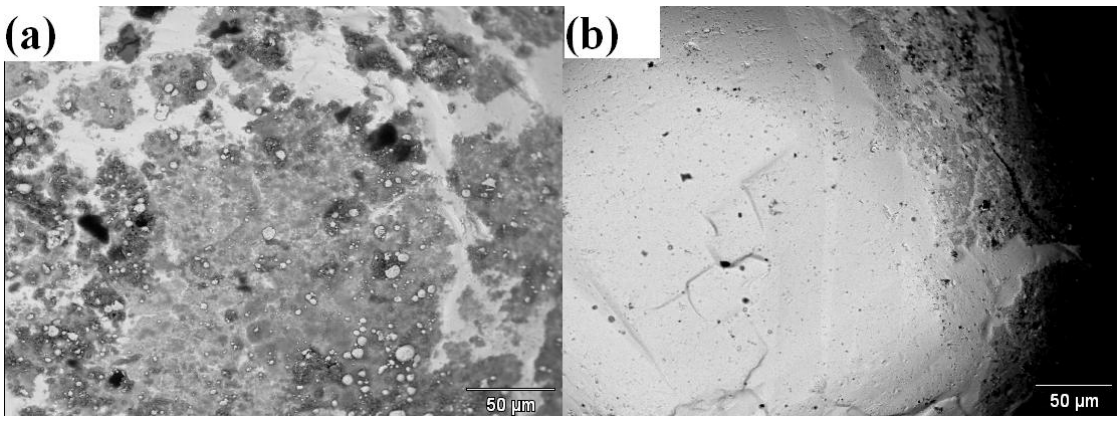

Figure 2.5 Backscattered electron image of (a) a particle collected from the heat shield. The darker regions are Ga rich, while the lighter regions are Bi rich. This particle was found to be 54 at% Bi and about 21 at% Ga. (b) a second particle collected from the heat shield. This particle was almost entirely Bi (~100 at.%).

while some particles have significant amount of Ga (see Figure 2.5a). This coupled with the results from Raman spectroscopy helped us to conclude that GaN powders obtained about 4 cms above the melt zone is grown primarily by vapor growth phenomena. However it must be noted that most of the powder is limited to 2 cms below the heat shield.

In order to determine the dominant phenomenon involved in GaN powder synthesis, we decided to perform a Knudsen equation based analysis. This analysis can be used to determine the relative contributions of vapor phase and liquid phase mechanisms to the observed particle growth.

2.5b Knudsen's analysis

The Knudsen's equations can be used to analyze the flux of particles (measured in number of particles/cm^2*sec) as a function of temperature. The fundamental underlying assumption is that the gas pressures are sufficiently low for ideal gas assumptions to be valid. The particle flux is usually designated as z, and the number of particles that escape a given cross sectional area is designated as N. Hence, N = zAt, where A is the area of the cross section across which the particles escape, and t is the time over which the mass flow is measured. In the given case, N is the number of Ga particles that will be consumed. The plots for Figure 2.6 assume an initial Ga sample of 25 grams. The equations employed are:

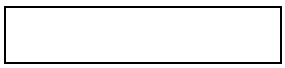

(1.1)

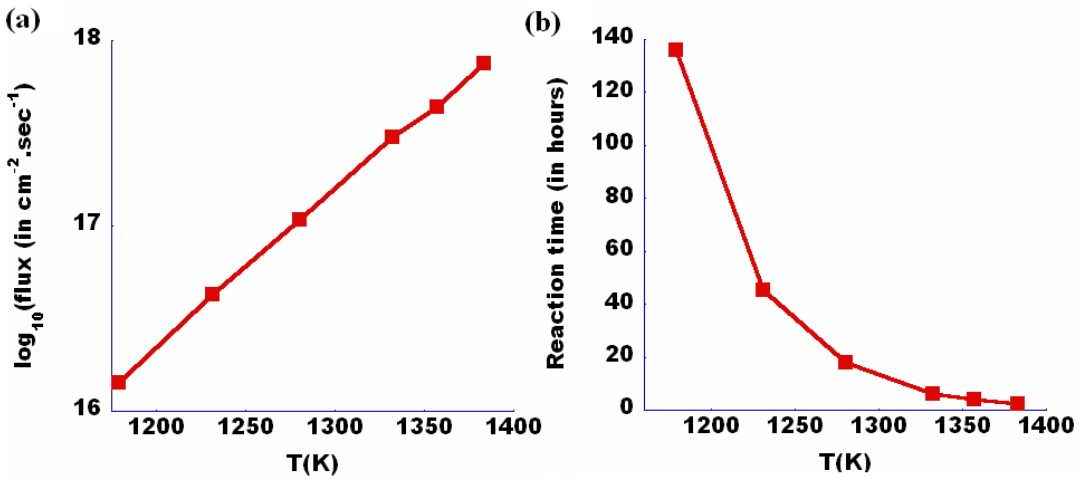

Figure 2.6 (a) Ga flux with respect to temperature (b) The reaction time assuming 25 grams of Ga metal initially, in a reaction chamber 4.5 cm in diameter. Note that the predicted reaction time is several orders of magnitude higher than observed reaction rate, suggesting that a vapor phase phenomenon alone is insufficient to account for the rapid synthesis.

where <v> is the average thermal speed of the gas particles.

The thermal speed of the gas particles is dependent upon their mass and the temperature; and given by the expression:

$$\langle v \rangle = \sqrt{8kT/\pi m} \tag{1.2}$$

Also, since we assume the pressure to be low enough and the temperature to be high enough for the ideal gas equation to apply, we can write

$$\frac{N}{V} = \frac{p}{kT} \tag{1.3}$$

Therefore using eqn.1.1 and 1.2 we get

$$N = \frac{1}{4}\frac{p}{kT}\sqrt{8kT/\pi m}\ A\ t \tag{1.4}$$

$$\text{Mass loss} = mN = \sqrt{m/2\pi kT}\ pA\ t \tag{1.5}$$

2.6 Results and Discussion

We observed that a 5 hour GaN growth run resulted in the deposition of about 65 nm of nitride material on the [0001] sapphire substrate, with a measurement error of less than 2.5 nm. The thickness of GaN was obtained by contact profilometry using a Tencor contact profiler. Knudsen's analysis (see equations 1.1-1.5) based data was used to plot the Ga flux (number of Ga atoms per cm^2 per second) with respect to the temperature (see Figure 2.6a). In order to perform the analysis we assumed that the Ga vapor in our reactor behaves like an ideal gas. This is a reasonable assumption, since at the operating temperatures (850^{o}C and above), the vapor pressure of Ga is fairly low.

For partial pressures of Ga as a function of temperature, we used data from Cochran et al.[19] We chose their data since the values in their paper is consistent with the accepted value for the enthalpy of vaporization of Ga (ΔHvap = -254 kJ*mol^{-1}).[20] Data based on the above equations were used to plot the Ga flux (number of Ga atoms per cm^2 per second) with respect to the temperature (see Figure 2.6a). Since NH_3 is flown into the reactor at a rate of 1.5 litres/min, the reaction rate was assumed to be limited by the availability of Ga atoms alone. Also it has been demonstrated that beyond 650^{o}C, NH_3 cracks to give reactive nitrogenous radical species, which rapidly combine with Ga to give GaN.[21] Therefore, an instantaneous reaction between the Ga and activated nitrogen species to form GaN was assumed, to get data for Figure 2.6b. With this assumption, we can then use the Ga flux obtained (from the above analysis) to calculate the maximum thickness of epitaxial GaN on the sapphire substrate. For the given reaction temperature (950^{o}C), we can hence determine the mass of GaN that would be deposited on the sapphire substrate. This mass can be used to calculate the expected thickness of epitaxial GaN on the substrate. The thickness was found to be 10 μm, which is much larger than the observed thickness (~65 nm). This indicates that the Ga vapor is mostly confined to the first 2 inches of the vertical reaction chamber. This is in keeping with the observation that most of the GaN powder is found at the bottom of the chamber. Very little powder is seen on the reactor walls above 2 inches from the reactor-base. The growth on the vertical walls can be attributed to vapor phase growth. However, this is only a tiny fraction when compared to the powder found at the bottom of the chamber. If the powder at the bottom of the reaction tube were a purely vapor phase phenomenon, the time to completion of the reaction would be ~160 hours (see Figure 2.6b), which is two orders of magnitude higher than the observed reaction time (5 hours). Hence we may infer that although there is vapor phase growth occurring in the upper part of the chamber, most of the powder growth

happens through liquid phase processes. At a distance of 2.5 inches or more above the reaction mixture, growth occurs primarily via vapor phase phenomena. This is further confirmed by the Bi rich particles discovered on the heat shield (refer to Fig. 2.5).

It must be noted here that there is no evidence that Bi enters the GaN matrix, in powders synthesized by the ammonothermal technique. Due to the high vapor pressure of Bi almost all of it escapes from the reaction mixture during the reaction. Hence mixing with Bi was not found to be a problem in growth of pure GaN.[13,14]

We also know that at the synthesis temperature we used, about ~0.5 at% of Eu is incorporated into GaN matrix.[22] The enthalpy of vaporization of Eu is known to be 177.9±2.5 $kJ^{*}mol^{-1}$ and its vapor pressure at 822^{o}C is known to be 144 Pa.[23,24] Knudsen's analysis based on this data suggests that at the reaction temperature the vapor flux of Eu is about 1.8 $millimol^{*}cm^{-2}{*}sec^{-1}$, which is sufficient to achieve 0.5 at% of Eu. It must be noted here that this dopant concentration could be achieved through a liquid phase process as well. Hence, Eu incorporation in GaN could occur through either vapor phase or liquid phase processes. Our analysis does not give conclusive evidence in favor of either liquid or vapor phase dopant incorporation process.

Our observations and Knudsen's analysis strongly suggest that although there is some vapor phase phenomenon occurring, the GaN growth process is most likely a liquid phase phenomenon. However, the rare earth dopant incorporation in the GaN matrix could proceed via either liquid or vapor phase mechanism.

2.6 Conclusions

We have examined the details of the ammonothermal reaction employed to synthesize the GaN powder used in this thesis. The crucial role of bismuth in this process is understood based on the wetting properties of the element and the interfacial

properties of the alloy mixture at the operating temperatures. The powder growth processes are understood to be primarily liquid phase phenomena, although some vapor phase process is also occurring. Eu incorporation into the GaN matrix could be either a liquid phase or vapor phase phenomenon.

REFERENCES

1. B. Raghothamachar, J. Bai, M. Dudley, R. Dalmau, D. Zhuang, Z. Herro, R. Schlesser, Z. Sitar, B. Wang, M. Callahan, K. Rakes, P. Konkapaka and M. Spencer, J. Crystal Growth, **287**, 349 (2006).

2. T. J. Goodwin, V. J. Leppert, S. H. Risbud, I. M. Kennedy and H. W. H. Lee, Appl. Phys. Lett. **70**, 3122 (1997).

3. W. C. Johnson and J. B. Parsons, J. Phys. Chem. **36**, 2588 (1932).

4. M. R. Lorenz and B. B. Binkowski, J. Electrochem. Soc. **109**, 24 (1962).

5. C. M. Balkas and R. F. Davis, J. Am. Ceram. Soc. **79**, 2309 (1996).

6. A. Addamino, J. Electrochem. Soc. **108**, 1072 (1961).

7. K. H. Kim, C. H. Ho, H. Doerr, C. Deshpandey, and R. F. Bunshah, J. Mater. Sci. **27**, 2580 (1992).

8. K. Baba, N. Shokata, and M. Tonezawa, Appl. Phys. Lett. **54**, 2309 (1989).

9. B. Vaidyanathan, D. K. Agrawal and J. Roy, J. Mater. Res. **15**, 974 (2000).

10. G. A. Hirata, F. Ramos, R. Garcia, E.J. Bosze, J. Mckittrick, O. Contreras and F. A. Ponce, Phys. Stat. Sol. A **188**, 179 (2001).

11. A. El-Himri, D. Perez-Coll, P. Nunez, I. R. Martin, V. Lavin and V. D. Rodriguez, J. Solid State Chem. **177**, 4213 (2004).

12. K. Hara, E. Okuyama, A. Yonemura, T. Uchida and N. Okamoto, Phys. Stat. Sol. A **203**, 2694 (2006).

13. H. Wu, J. Hunting, F. J. DiSalvo and M. G. Spencer, Phys. Stat. Sol. C **2**, 2074 (2005).

14. H. Wu, J. Hunting, K. Uheda, L. Lepak, P. Konkapaka, F. J. DiSalvo and M. G. Spencer, J. Crystal Growth **279**, 303 (2005).

15. H. Wu, C. B. Poitras, M. Lipson, M. G. Spencer, J. Hunting and F. J. DiSalvo, Appl. Phys. Lett. **88**, 011921 (2006).

16. H. Wu, C. B. Poitras, M. Lipson, M. G. Spencer, J. Hunting and F. J. DiSalvo, Appl. Phys. Lett. **86**, 191918 (2005).

17. J. W. Cahn, J. Chem. Phys. **66**, 3667 (1977).

18. H. Tosmann, E. DiMasi, O. G. Shpyrko, P. S. Pershan, B. M. Ocko, and M. Deutssh, Phys. Rev. Lett. **84**, 4385 (2000).

19. C. N. Cochran and L. M. Foster, J. Electrochem. Soc 109, 144 (1962).

20. CRC Handbook of Chemistry and Physics, 86th ed. D. R. Lide, Ed.; CRC Press: Boca Raton, FL, 2005; Chapter 6, p 96.

21. M. Kamp, M. Mayer, A. Pelzmann, A. Thies, H. Y. Chung, H. Sternschulte, O. Marti and K. J. Ebeling, Mat. Res. Symp. Proc. **395**, 135 (1996).

22. J. Shi, MVS Chandrashekhar, J. Reiherzer, W. J. Schaff, J. Lu, F. J. DiSalvo and M. G. Spencer, J. Crystal Growth, **310**, 452 (2008).

23. J. A. Rard, Chem. Rev. 85, 555 (1985).

24. F. H. Spedding, J. J. Hanak, and A. H. Daane, Trans. Metall. Soc. AIME 212, 379 (1958).

CHAPTER 3

PHOTOLUMINESCENCE ENHANCEMENT IN Eu DOPED GaN POWDER

3.1 Introduction

In this chapter, we solve a critical problem with Eu:GaN powder. It is reasonable to expect that the visual appearance of Eu:GaN should be similar to that of pure GaN, because of the relatively dilute concentration of Eu (~0.5 at.%).[1] However, the Eu:GaN produced using a high temperature ammonothermal process is observed to have a much darker appearance than pure GaN (see Figure 3.1).[2,3] As is explained below, this dark color poses an obvious impediment to the practical application of Eu:GaN as a laser material or as a phosphor, since it contributes to reduced luminescence.

We demonstrate a chemical process which removes the impurities in the Eu:GaN particles that contribute to this dark appearance, thereby improving the photoluminescence (PL) of these particles by 300 % compared to the powder previously reported.[1] The light color of the processed powder approaches that of pure GaN (Figure 3.1). The mechanism of the improvement in photoluminescence intensity is investigated using X-ray photoelectron spectroscopy (XPS), X-ray diffraction (XRD) and PL measurements.

3.2 Experimental procedure

The powder was synthesized using a Ga-Eu-Bi alloy (composition: 95.75, 1.25, 3 atomic % respectively) as the starting material. This alloy was initially heated in a quartz tube reactor in an argon atmosphere to a temperature of 650°C. The heating was continued beyond 650°C in ammonia ambient to the reaction temperature of

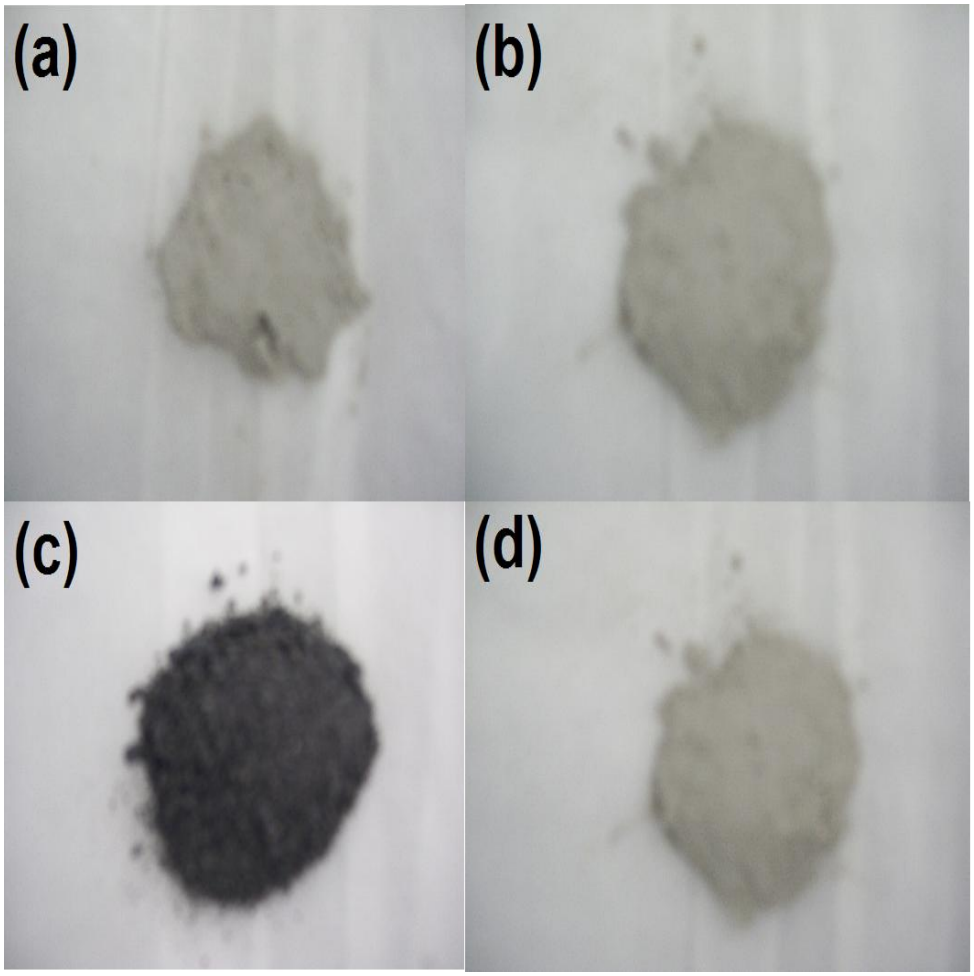

Figure 3.1 (a) & (b) is pure GaN; (c) & (d) is Eu:GaN powder, before and after the acid-rinse respectively. The acid-rinse does not change the visual appearance of pure GaN powder, but renders the dark as-prepared Eu:GaN powder almost as visually light-colored as pure-GaN powder. [4]

950°C, which was kept constant for 5 hours while maintaining a constant partial pressure of ammonia in the reaction chamber. High purity Eu:GaN with an approximately 0.5 atomic % Eu doping was obtained. The details of the mechanisms of the reaction were previously discussed in Chapter 2. In this study, we used powder samples formed via this method.[1,3]

Powder prepared in this manner is known to have a strong emission in the red.[3] Despite its strong luminescence, this powder appears dark due to the presence of several impurities. These dark impurities contribute to a reduced efficiency of PL in the material, as can be concluded from the results below.

3.3 Optical characterization using photoluminescence

The removal of the impurities from the powder was investigated by rinsing in dilute acid solutions. 1M HNO_3 and 1M HCl were used for chemical rinsing over varying durations (0-16 hours) and temperatures (room temperature and 100 ^oC). The effect of each rinse on the luminescence was quantified using PL (see Figures 3.2a and b). The PL measurements were performed using a HeCd laser (325 nm).

The best purification was achieved with a room temperature rinse for 4 hours using 1M HNO_3. This chemical rinse clears the powder of all dark impurities, as verified by XRD. Furthermore, PL measurements show that the acid rinsed powder has 300 % higher luminescence intensity than the as-prepared powder. A comparable luminescence enhancement was obtained by HNO_3 rinsing at 100^oC. However, this last process tends to be more aggressive, as longer rinse times lead to an irrecoverable quenching of luminescence. We believe that this is due to the cannibalistic oxidation of entire GaN particles.[5] This is discussed in greater detail later in this chapter. In short, a room temperature rinse for 4 hours using 1M HNO_3 was determined to be the

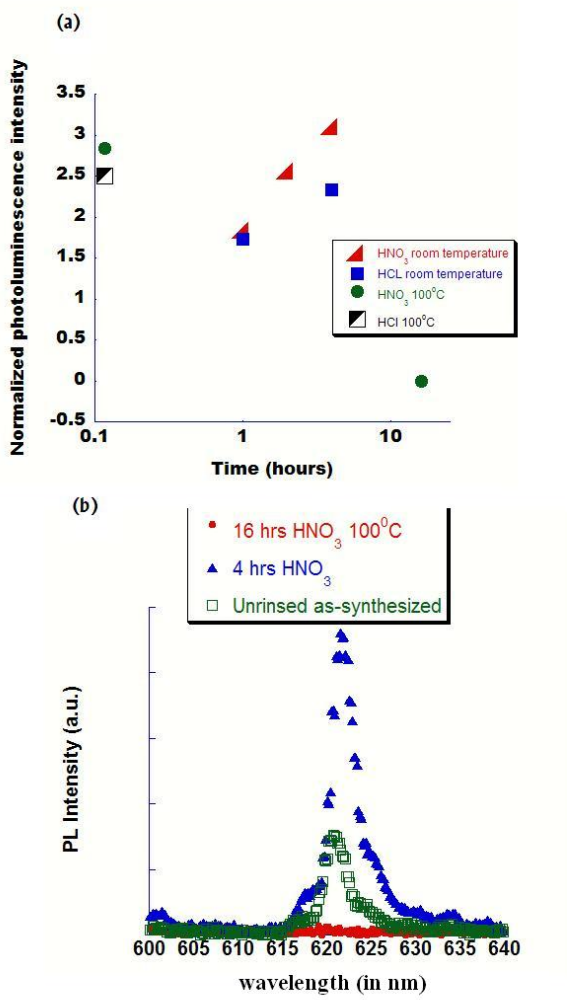

Figure 3.2 (a) PL intensity as a function of rinse time, for various rinse solutions. The graph shows that the HNO_3 rinses result in greater improvements in PL intensity than HCl rinses. Results for 15 minute rinses in boiling HNO_3 and HCl are also shown. All luminescence intensities are normalized to the peak intensity of the as-prepared powder. (b) PL spectra for unrinsed, 4 hour and 16 hour HNO_3 rinse at 100 °C samples. All of the samples came from the same initial batch. Boiling in HNO_3 for 16 hours quenches the PL completely. Optimized rinsing substantially increases the photoluminescence intensity, accompanied by an improved decoloration of the powder.[4]

optimal way to achieve the maximum luminescence enhancement in a controllable fashion.

3.4 Mechanism of luminescence enhancement

In order to further understand the surface chemistry of GaN particles subject to an acid rinse, XPS studies were undertaken. XPS measurements were performed using Al Kα X-rays with energy of 1486 eV, and a spot size of 1 mm. The spectral resolution of the XPS system is ~0.1 eV. As revealed by the XPS measurements, two peaks corresponding to the Ga 3*d* level, at ~20.7 eV and ~19.7 eV, were observed in all of the samples. These two peaks were attributed to Ga-N and Ga-O bonds, respectively.[5] The oxide peak corresponding to Ga_2O_3 also shows a shift from the GaN peak, attributed to band bending at the Ga_2O_3-GaN interface. This Ga_2O_3-Ga 3*d* level shifted continuously with respect to the duration of the chemical rinse before reverting back to its nominal position for longer, more aggressive rinses (see Fig.3.3a).

This observation indicates that the acid rinse process continuously oxidizes the GaN surface, forming a cleaner GaN-oxide interface with progressive rinsing. This consistently increasing shift is attributed to electrostatic potentials at the interface, arising from the valence band discontinuity between the GaN and the Ga_2O_3, in analogy with GaN-AlN interfaces.[6]

The oxide formed on the surface is also expected to be responsible for the yellowish-green coloration of the Eu:GaN powder after the acid-rinse. It must also be noted that because the rinsing is done at room temperature and for short durations (~4 hours), O or Cl contamination of the GaN matrix due to diffusion is not expected.

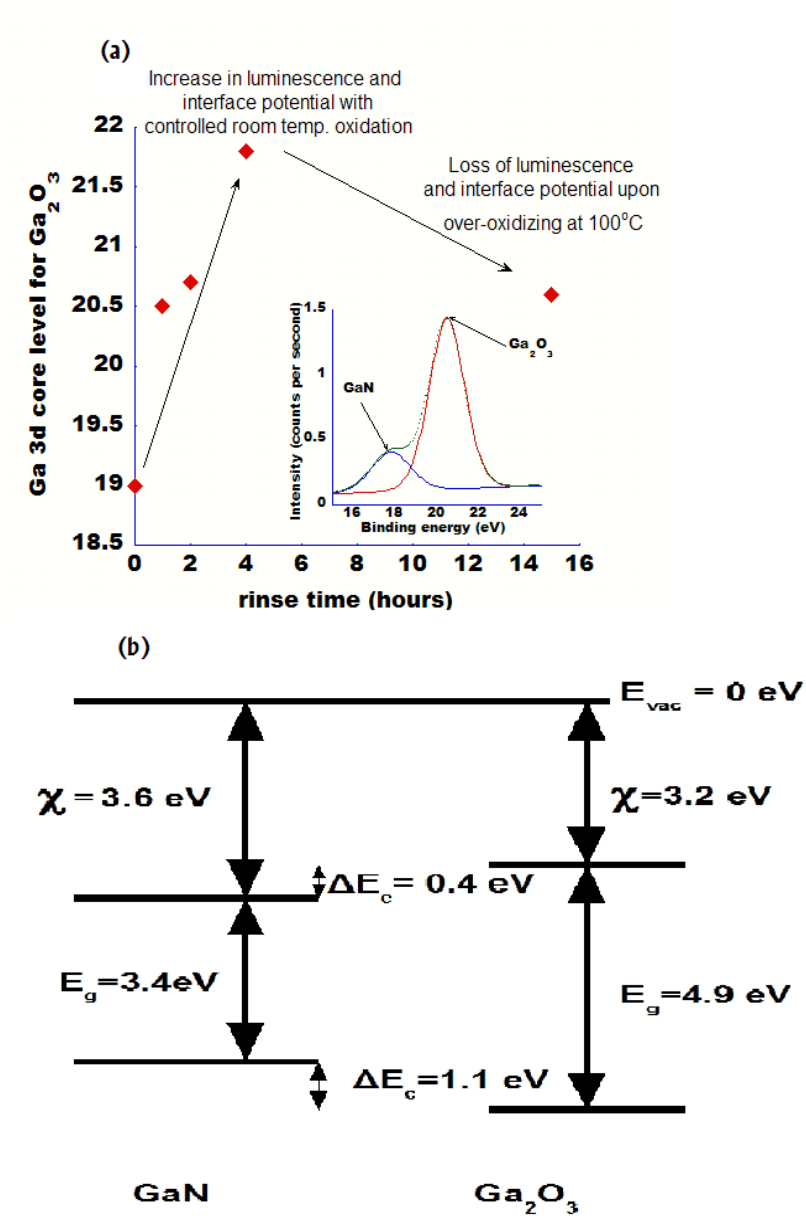

Figure 3.3 (a) Evolution of the Ga 3*d* core energy levels (with the Fermi level as a reference) in Ga_2O_3. The inset shows the XPS spectra for the Ga 3*d* core levels in Eu:GaN after 1 hour HNO_3 rinse. (b) The band diagram of GaN and Ga_2O_3 with experimentally determined values of electron affinities (χ), valence band and conduction band offsets, and bandgaps.[4]

The valence band offset was determined by using the following expression:[6]

$$\Delta E_v = (E_v - E_{CL})_{GaN} - (E_v - E_{CL})_{Ga_2O_3} - \Delta E_{CL}, \quad (3.1)$$

where $(E_v\text{-}E_{CL})$ is the difference between the valence band maximum and a conveniently identifiable core level (in this case, the 3*d* level), and ΔE_{CL} is the difference between the characteristic core levels in GaN and Ga_2O_3 in the case where a heterojunction is formed, i.e. in the brightest sample. $(E_v\text{-}E_{CL})_{GaN}$ was measured on the as-prepared powder, which did not undergo any rinsing. $(E_v\text{-}E_{CL})_{Ga2O3}$ was obtained from the over-oxidized sample, with quenched luminescence, which was attributed to Ga_2O_3 as discussed above. We obtain values for $(E_{CL})_{GaN}$ and $(E_{CL})_{Ga2O3}$ of -17.1 eV and -20.6 eV respectively, and ΔE_{CL} is 4.5 eV. Therefore, a valence band offset of 1.0 eV was extracted. This value agrees well with the experimentally measured values of the various band parameters. Furthermore, experimentally determined values of the electron affinities of GaN and Ga_2O_3 are ~3.6 eV and 3.2 eV respectively, which leads to a conduction band offset ΔE_c of ~0.4 eV, assuming bandgaps of 3.4 eV and 4.9 eV for GaN and Ga_2O_3 respectively.[6-8] This implies a valence band offset of 1.1 eV, which agrees very well with our measurements. This is illustrated in Fig. 3.3 b.

XPS data also shows increasing nitride-oxide interface potentials with longer rinse times. We found that a well-defined GaN-Ga_2O_3 interface was formed by rinsing in 1M HNO_3 for 4 hours at room temperature (Figure 3.3 b). This is because longer rinse times result in better and uniform oxide layer around the GaN particles. In these particles, the valence band offset attains the ideal GaN/Ga_2O_3 value when the PL intensity of the powder is greatest. For the optimized room temperature rinse, a Ga_2O_3 thickness of ~3 nm is obtained, as measured by XPS (comparing the Ga_2O_3 and GaN 3*d* peaks). This is in agreement with the limiting thickness in thermally oxidized planar GaN, measured by Wolter et al.[5] An oxidation using a more aggressive etch

(e.g., boiling in HNO_3, or higher temperature thermal oxidation) is not self-limiting, and can completely oxidize the GaN particles to Ga_2O_3, leading to the loss of luminescence (Figure 3.2).

To determine if the PL enhancement in acid-rinsed Eu:GaN is due to the cleaning of the GaN/Ga_2O_3 interface, we performed similar acid-rinse experiments on undoped-GaN. We observed no increase in PL enhancement in the acid-rinsed GaN, when compared to as-prepared GaN. Hence a clean GaN/Ga_2O_3 interface cannot account for the PL enhancement in acid-rinsed Eu:GaN. This implies that Eu containing compounds, which are expected to be dark in appearance, are responsible for the sub-optimal luminescence in as-prepared Eu:GaN. The likely candidates are acid-soluble mixed nitrides/oxides of Ga and Eu in the as-prepared Eu:GaN powders.[9] Hence we conclude that the removal of Eu-containing absorbing impurities in the as-prepared powder is the primary reason for the observed increase in photoluminescence in acid rinsed Eu:GaN. If the rinse time is too short, the luminescence is not maximized due to incomplete impurity removal. However, if the chemical rinse is too long, all of the GaN is consumed due to cannibalistic oxidation, quenching the luminescence completely (Figure 3.2 a). This quenching is accompanied by a corresponding loss of interface potential, as observed by XPS (inset of Figure 3.3a), indicating that all of the GaN has been consumed.

3.5 Conclusions

We have demonstrated a significant enhancement of the PL intensity of Eu:GaN using acid rinses to obtain visually lighter-colored powders. We have shown that the improvement of the PL is primarily due to the removal of dark Eu-containing compounds from the powder, through a 1 M HNO_3 rinse.

REFERENCES

1. J. Shi, M. V. S Chandrashekhar, J. Reiherzer, W. J. Schaff, J. Lu, F. J. Di Salvo and M. G. Spencer, J. Crystal Growth **310**, 452 (2008).

2. C. B. Poitras, M. Lipson, H. Wu and M. G. Spencer, Mater. Res. Soc. Symp. Proc., **866**, V3.2.1 (2005).

3. H. Wu, C. B. Poitras, M. Lipson, M. G. Spencer, J. Hunting and F. J. Di Salvo, Appl. Phys. Lett. **88**, 011921 (2006).

4. T. Thomas, X. Guo, MVS Chandrashekhar, C. B. Poitras, W. Schaff, M. Dreibelbis, H. Reiherzer, K. Li, F. J. DiSalvo, M. Lipson and M. G. Spencer, J. of Crystal Growth **311**, 4402 (2009).

5. S. D. Wolter, J. M. DeLucca, S. E. Mohney, R. S. Kern and C. P. Kuo, Thin Solid Films **371**, 153 (2000).

6. G. Martin, S. Strite, A. Botchkarev, A. Agarwal, A. Rockett, H. Morkoc, W. R. L. Lambrecht and B. Segall, Appl. Phys. Lett. **65**, 610 (1994).

7. G. Koley and M. G. Spencer, J. Appl. Phys. **90**, 337 (2001).

8. E. F. Archibong and E. N. Mvula, Chem. Phys. Lett. **408**, 371 (2005).

9. CRC Handbook of Chemistry and Physics, 76th Edition; CRC Press: Florida (1995-96).

CHAPTER 4

NANOSIZING AND RARE EARTH DOPING OF GaN POWDERS THROUGH BALL MILLING

4.1 Introduction

One of the major issues encountered with high power lasers is the management of the heat generated during lasing. Gallium nitride (GaN) possesses a high heat conductivity (1.3 W cm^{-1} $^{o}C^{-1}$), making it a promising candidate for high power applications. However, it is extremely difficult to produce single crystal GaN with a sufficient size and optical quality to serve as a laser material. Moreover, the specialized equipment and personnel needed to produce a single crystal GaN laser gain medium makes the process extremely expensive. Polycrystalline laser hosts offer several noteworthy advantages over conventional single crystals: higher active ion doping concentrations, larger host sizes, and more complex shapes. In addition, the cost of fabricating polycrystalline laser hosts is much lower than single crystal, due to shorter fabrication processes, and large size, high volume production capability.[1] Therefore, the fabrication of GaN ceramic laser hosts has been a very attractive topic for research in recent years.

The key for achieving desirable optical transparency in GaN ceramics is an appropriate, uniform particle size in the initial powder. Typically when the average crystallite size falls into the submicron range, the properties of the resulting polycrystals become isotropic.[2] However, the synthesis of monodisperse GaN nanoparticles has remained a challenge. The difficulties confronted by researchers include impurity removal, yield, size uniformity and crystallinity. Wu et al. have produced GaN powders with high yield and high purity using an ammonothermal

process.[3] However, such powders typically have an average particle size on the order of microns, with a broad size distribution. This typically leads to a wide pore size distribution within the medium upon pressing into a ceramic. Sintering at high temperatures and long durations becomes necessary to eliminate the porosity during the ceramic consolidation process. Consequently, using micron-sized powders as the starting material hinders the process of obtaining a high-quality transparent sintered ceramic. To improve the potential of using ammonothermally synthesized GaN powder as a starting material for producing GaN based laser gain media, we successfully reduced the average particle size in the powder via ball milling. In addition, a ball milling assisted solid state reaction process was performed to dope commercial GaN powders with rare earth ions. This process is a low cost, scalable, effective, and generalizable method for the rare earth doping of GaN powders. Finally, the luminescence properties of the doped GaN powders were investigated.

4.2 Experimental Procedure

The starting powders for ball milling were synthesized using the ammonothermal method described in Chapter 2. The as-synthesized powders were dark in color, probably due to the presence of mixed nitrides. These nitrides can be dissolved away using nitric acid[4] (refer to Chapter 3). A roll milling machine (U.S. Stoneware Company, model: 784) was utilized for the ball milling process. Yttria-stabilized zirconia balls of assorted sizes were used, with a total ball-to-powder weight ratio of ~ 20:1. The ball milling was performed in ethanol. The crystalline structures of the as-received and ball milled powders were compared using a Rigaku X-ray diffraction spectrometer, Malvern Zetasizer (Nano-ZS), and LEO 1550 Field Emission scanning electron microscope (SEM).

For the luminescence measurements, mixtures of GaN powder and rare earth acetates were ball milled in ethanol for 12 hours. The resulting powders were dried in air, pressed into pellets. One sample was made by annealing in NH_3 at 650^oC. Other samples were similarly prepared by annealing in air, and NH_3 + air at 650^oC. Photoluminescence was performed on Erbium and ytterbium doped GaN samples. The powders were pumped by a 970 nm continuous wave laser (Boston laser, Inc.) with a maximum power of 3 Watts (working power of 1 Watt) and a power density of ~2.0 Watt/cm^2. A NanoLog spectrometer from Horiba Jobin Yvon with a FL-1073 detector working at 950 V was used to measure the luminescence emission spectra. A diode laser with its emission wavelength centered at 798 nm (LD1-820) was used to pump thulium doped GaN samples. A PbS detector working at 1400 nm to 2200 nm and a Hamamatsu R1387 photomultiplier with a McPherson Model 2051 scanning monochromator were used to investigate the luminescence properties. All photoluminescence measurements were performed at room temperature. Raman spectropscopy was performed to determine the crystalline quality, induced stress, and electron concentration of the ball milled powders. These measurements were performed using a Renishaw reflection configuration, with an excitation wavelength of 488 nm and with spectral resolution of 0.1 cm^{-1} and spatial resolution of 1 μm.

4.3 Results and Discussion

4.3.a Size reduction through ball milling

The as-synthesized GaN powders were rinsed with nitric acid[4] prior to ball milling. The as-rinsed powders are brownish gray in color, and are much lighter than the as-synthesized powder, indicating the removal of mixed-nitride impurities. For ball-milling, the abrasive of choice is zirconia balls in a 'stabilized' state. Stabilization is necessary because zirconia can exist in a metastable tetragonal phase. If a sufficient

quantity of the tetragonal phase is present, then an applied stress can cause the tetragonal phase to convert to a monoclinic phase. This process is expedited by the concentration of stresses at the tip of a crack. A volume expansion associated with this phase transformation puts the crack into compression, retarding its growth, and enhancing the fracture toughness. This mechanism, known as transformation toughening, significantly extends the reliability and lifetime of products made with stabilized zirconia.[5,6] Several different oxides may be added to zirconia to stabilize the tetragonal and/or cubic phases: magnesium oxide (MgO), yttrium oxide, (Y_2O_3), calcium oxide (CaO), and cerium(III) oxide (Ce_2O_3), amongst others.[5]

After ball milling, the powders displayed noticeably brighter colors and improved dispersibility in the solvent (ethanol), possibly indicating reduced levels of agglomeration. XRD was performed on the powder with a Scintag theta-theta X-ray diffractometer. An obvious broadening of the XRD peaks was observed in the milled powders as shown in Figure 4.1. The peak broadening was attributed to either a reduction in average particle size, lattice strain possibly induced by the milling action, or both.

A significant particle size reduction was confirmed by SEM observations, as shown in Figure 4.2. The SEM images show that the as-prepared particles have fairly regular faces and platelet-like shapes. The image also indicates the presence of particles in the 1-10 μm size range. In the SEM images of the ball-milled samples, the average particle size has decreased to about 40 nm, with a few larger particles remaining.

The SEM images also confirm the tendency of GaN nanoparticles to agglomerate. We attribute this to the large surface-area-to-volume ratio of the particles. Unfortunately, such agglomeration limits the usefulness of GaN nanoparticles in many practical applications. Therefore, methods to prevent particle

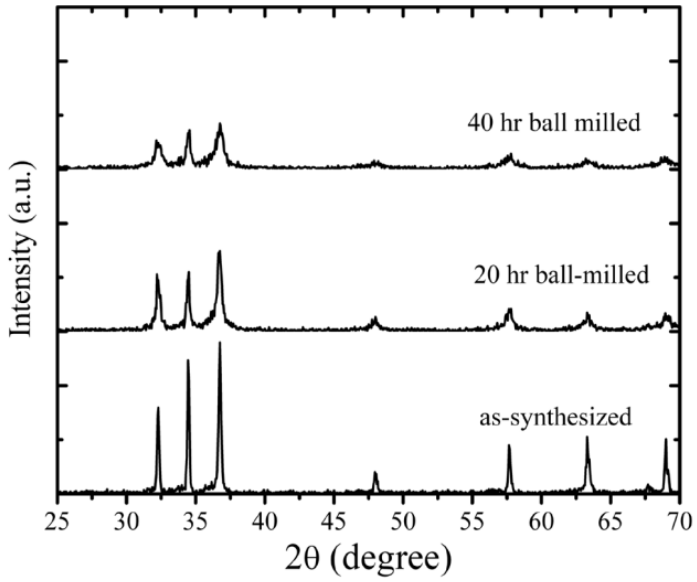

Figure 4.1 XRD patterns of GaN powders, before and after ball milling. The powders were dispersed in ethanol. An increased duration of ball-milling was accompanied by a better dispersability of the powder in ethanol, attributable to the size-reduction of the particles. A longer duration of ball-milling corresponds to smaller particle-sizes, as is evident from the patterns above.

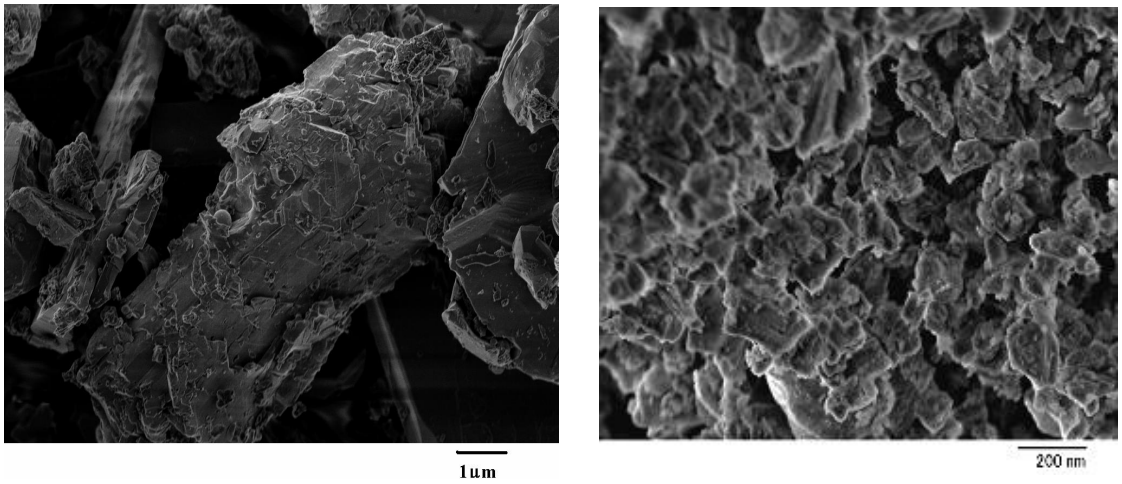

Figure 4.2 SEM images of ammonothermally synthesized GaN powder before (left) and after (right) 40 hours of ball milling.

agglomeration are currently being investigated. We predict that adding a suitable surfactant such as methyl cellulose at the ball-milling stage could substantially reduce the agglomeration of the GaN particles. Measurements of particle size made using a Dynamic Light Scattering (DLS) based Malvern Zetasizer agree well with a Scherrer formula based analysis using XRD and SEM data.

As expected, the factors that affect the particle size of ball-milled powder include the initial particle size, duration, media, and liquid used in the ball milling process. In the present work, ball milling was performed using a roll milling machine under relatively mild conditions. The ball milling process is said to be 'mild' or 'soft', when a solvent is used to control the intensity of the internal cascade effect that causes particle size reduction. Using a low-energy, soft nano-sizing process minimizes the introduction of contamination from the milling media or the container, and thus is practically useful for obtaining high purity samples. Ball-mill assisted nano-sizing also allows control over the particle surface areas within a wide range. This is particularly important for realizing GaN powder based transparent ceramics.[1] Small, monodisperse average particle sizes permit sintering at lower temperatures and shorter times. This in turn restrains pore growth and increases the average grain size during the final consolidation stage.

4.3.b Rare Earth doping via ball-mill assisted solid state reaction

Due to the larger ionic radius of Er^{3+} (1.75 Å) relative to Ga^{3+} (1.30 Å), one might expect that the concentration of erbium that can be doped into the GaN lattice would be rather small. However, research has shown that in situ doping can be achieved up to 3-5 at. % with MBE while preserving the optical activation of erbium.[7] Green emission has also been observed from GaN:Er created by in situ ammonothermal doping of erbium into GaN powder.[8] An alternative way to realize the

doping is by solid state reactions. Ball milling could be used to agitate the reactants in the reaction chamber, thereby accelerating mixing. This should in turn promote solid state diffusion, and may even activate the powder surface,[9,10] thus facilitating the rare earth doping into GaN.

Unfortunately, ball milling can cause significant surface and crystal damage. Hence, annealing (thermal treatment) is an important post-reaction step which allows the relaxation of the crystal, through atomic rearrangements in the crystal lattice and surfaces. The exact effects of thermal treatment on the crystal depend on the temperature, duration, and chemical environment chosen for annealing. For example, there is evidence that when Yb^{3+} is co-doped with Er^{3+}, it enhances the PL emission of the Er^{3+} ion.[11]

Er^{3+} emits in the 1.54 μm IR regime. This falls within the C-band (1.525-1.560 μm) used in fibre optic communication, making Er^{3+} of significant great interest. Samples containing either Er or Er/Yb doping were prepared. $Er(CH_3COO)_3.xH_2O$ and $Yb(CH_3COO)_3.xH_2O$ are used for achieving Er and Yb doping. Stoichiometric amounts of the acetate salts were mixed based on the amount of RE doping desired (refer Figure 4.3).

One sample of Er/Yb doped GaN sample was annealed at 600ºC for 4 hours in an NH_3 atmosphere. A 1 at% Er doped sample was annealed in presence of NH_3 for 4 hours and then annealed in the presence of air for 5 hours. This was done to evaluate the effect of the presence of oxygen during the annealing process. There is some evidence that oxygen co-doping could be beneficial for Er^{3+} emission. It has been suggested that the increased ionic nature of Er^{3+} local environment due to oxygen co-doping results in better emission.[11]

The room temperature photoluminescence (PL) properties of the annealed samples were measured at infrared wavelengths. A 970 nm centered diode laser with a

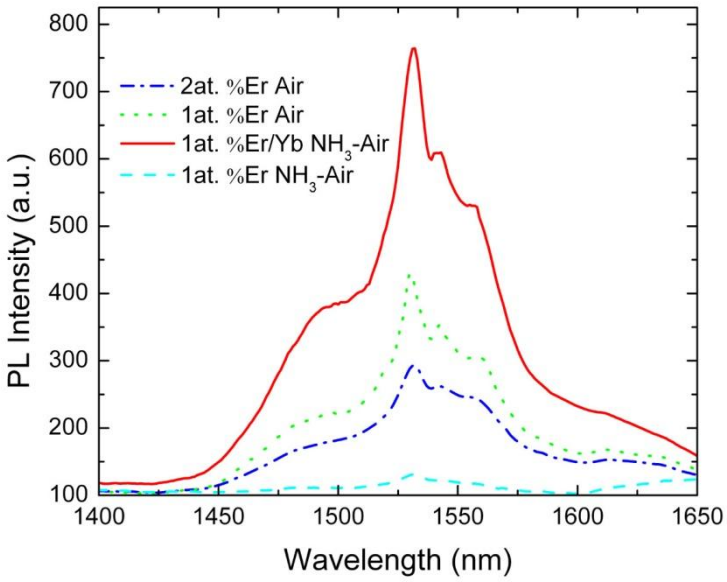

Figure 4.3 Photoluminescence spectra of doped GaN powders annealed under different conditions.

power density of 2 Watts/cm^2 was used to excite the samples. Figure 4.3 shows the PL spectrum of a 1 at.% Er doped GaN sample in the near infrared wavelength range.

The photoluminescence spectrum of the sample indicates that the Er^{3+} ions have been successfully doped into GaN through the ball mill assisted solid state reaction process.[12] Additional samples were produced with 1 at. % and 2 at. % Er^{3+} doping. The PL spectra of these samples are shown in Figure 4.3. We see that the strongest emission peak among the four samples is exhibited by the air re-annealed Er^{3+}/Yb^{3+} co-doped sample. This probably indicates that the oxygen-containing annealing atmosphere enhances the PL of the Er^{3+}/Yb^{3+} co-doped GaN, as has been reported in an earlier experiment.[11]

If we were to focus only on the air annealed samples, we may conclude that the Er^{3+} doped GaN shows decreasing PL intensity with increasing dopant concentration, suggesting a possible concentration quenching effect. In general we also observe that the samples annealed in air show broadened peaks, that is, a higher full-width-at-half-maximum (FWHM) when compared to samples annealed in pure NH_3. However, as mentioned before the air annealing does seem to improve luminescence in agreement with an earlier report.[11] FWHM decreases and PL intensity increases with the use of Yb as a codopant in GaN:Er. Decreased FWHM suggests an increased quality factor associated with the emission process, suggesting a higher quantum yield associated with Er^{3+} emission in Yb co-doped samples.

Thulium doped GaN samples were also produced, through a similar ball mill assisted solid state reaction process. It is suspected, though unproven, that Tm exists in the Tm^{3+} state in GaN. The ionic radius of Tm has never been reported, but Tm is a larger atom (covalent radius: 1.90 A^o) than Er. When incorporated into the GaN lattice, Tm is therefore likely to have higher compressive stresses in its local environment. To relieve these presumed stresses, a higher annealing temperature was

chosen for Tm:GaN (800^{o}C) than for Er:GaN (600^{o}C). Samples with 0.5 at%, 1 at%, and 2 at% Tm^{3+} were pressed into pellets and annealed at 800^{o}C in an oxygen atmosphere. The photoluminescence properties of Tm:GaN were then measured.

A low power (~ milliwatts) diode laser with an emission wavelength centered at 798 nm was used to pump the samples. PbS was chosen as the detector, because of its high sensitivity near the peak Tm emission wavelength range (1600 nm to 2000 nm). Unfortunately, no Tm emission lines were detected. Hence, it is uncertain whether we succeeded in incorporating Tm into GaN. Currently, the use of ball-milling assisted methods to incorporate other rare earth dopants – Tm, Pr, Tb, Dy, and Nd – into GaN, remains an active area of investigation.

4.3.c Strain analysis in nanosized Eu:GaN

Raman spectroscopy was performed to determine the crystalline quality, induced stresses, and electron concentration of the ball milled powders. The results of these measurements are given in Figure 4.4. We observe that 20 and 40 hours of ball-milling introduces a red-shift in the E2 peak of approximately 12.1 cm^{-1} and 13.9 cm^{-1} respectively (Table 4.1) which implies internal stresses in these samples. The presence of internal stresses is confirmed by the XRD data as well which shows that with respect to as-prepared Eu:GaN, (100) XRD peak of the ball-milled powders is shifted to smaller angles ($2\Delta\theta$ = -0.12, -0.14 after 20, 40 hrs ball-milling), while the (002) peak is shifted to a higher angle ($2\Delta\theta$ = 0.05, 0.1 after 20, 40 hrs ball-milling). The relative shifts in the angles may be used to calculate the strains in a and c directions respectively. These strains were calculated for both the as-prepared and ball-milled powders, using the Kisielowski's model.[13] This model can be stated using the following mathematical statements:

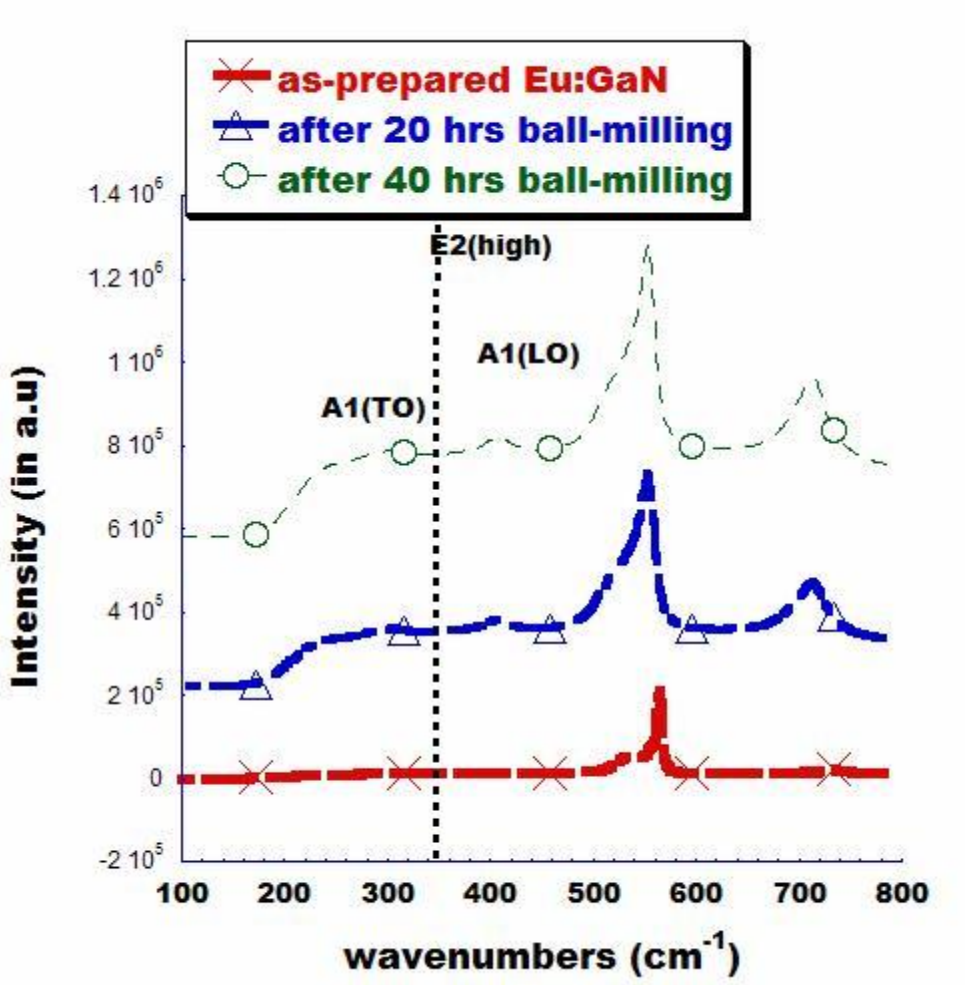

Figure 4.4 Raman spectra of Eu:GaN before and after ball-milling shows red-shifts in the E2(high) and A1(LO) positions, which are used to infer semiconducting properties and stresses in the sample, respectively.

Table 4.1: Measured strains and Eu incorporation in as-prepared and ball-milled Eu:GaN powders. The phonon frequency shift in all powders is reported with respect to pure GaN.

	particle size (nm)	**E2(high) Raman shift (cm^{-1})**	**A1(LO) Raman shift (cm^{-1})**	**strain along a-axis(%)**	**strain along c-axis (%)**	**c/a ratio**
as-prepared Eu:GaN	2000-5000	0.8	0.8	0.09	0.13	1.628
after 20 hrs ball-milling	50-70	-12.9	-24.8	0.2	-0.15	1.621
after 40 hrs ball-milling	30-50	-14.7	-27.3	0.3	-0.3	1.617

$$\varepsilon = (1 - bc)\left(1 - \frac{2v\sigma}{E}\right) - 1 \qquad 4.3.1$$

$$b = \frac{1}{3N}\left(1 - (s/h)^3\right) \qquad 4.3.2$$

In the Kisielowski's equations, ε is the strain along an axis, b is the expansion (or contraction) coefficient, s is the radius of the solute atom, h is the radius of the host atom, N is the concentration of the host matrix, C is the concentration of the point defects (in this case the number of dopant atoms), υ is the Poisson's ratio, σ is the stress along the axis and E is the Young's modulus.

We determined that after 20 hours and 40 hours of ball-milling, the tensile strains in the a direction were 0.2% and 0.3% respectively, while the compressive strains in the c direction were 0.15% and 0.3% respectively (see Table 4.1). To calculate these values we took into consideration the fact that the incorporation of Eu atoms into GaN leads to the expansion of both the a and c lattice constants in Eu:GaN (relative to undoped GaN). The strains associated with Eu dopant incorporation have previously been reported to be 0.09% and 0.13% respectively.[14,15] So in reporting the strain induced in the lattice due to the ball-milling process, we took these reported values into consideration to isolate the effects of doping and ball-milling respectively. It is reasonable to do so, since the strain values reported for Eu incorporation alone uses the same Kisielowski's formula. Both the earlier report and we arrive at the same value for the Eu dopant concentration as well (~0.5 at%).[16]

In our study, we observe that the lattice constant ratio ($_{c/a}$) decreases with increasing ball-milling time, while the volume of a unit-cell of as-prepared Eu:GaN and ball-milled Eu:GaN remains constant. The constant volume indicates that the concentration of Eu atoms remains the same after nanosizing. The change in the c/a ratio indicates increasing biaxial strain with increasing ball-milling time. The c-axis is under compressive strain, while the a-axis is under tensile strain in a ball-milled GaN powder sample. The unit cell volume is found to be the same for each of these

powders. This is indicative of the fact that the ball-milling process might not be resulting in migration of Eu atoms from the GaN lattice during ball-milling.

The electron concentration of the GaN particles is known to influence the A1 (LO) phonon mode.[17] Initially the FWHM of the A1 peak increases with increasing electron concentration. However, beyond an electron concentration of around (~10^{19} cm^{-3}) the peak disappears completely. The as-prepared powder has a distinct A1 (LO) peak at 734.8 cm^{-1}, which is very similar to that of unstrained Eu:GaN, indicating an electron concentration of <$1x10^{17}cm^{-3}$.[16,17] However, ball-milling Eu:GaN for 20 and 40 hours shifts the A1(LO) peak to 710.8 and 708.3 cm^{-1}, respectively. These observed shifts suggest that these powders continue to have semiconducting properties, with electron concentrations below 10^{17} cm^{-3}.[15] The reason for the anomalously large red-shift[4] in the A1(LO) peak in the ball-milled powders is currently unknown.

It is desirable to evaluate the suitability of these ball-milled nanosized Eu:GaN particles as a potential laser gain medium. A laser gain medium must be transparent around the frequency of operation. To determine the transmittance of GaN particles in the IR regime, Fourier transform infrared spectroscopy (FTIR) was performed. Nano-GaN powders were embedded in a KBr matrix, formed by mixing 80 mg of KBr, with 2 wt%, 5wt%, 7.5 wt% and 10 wt% of either as-prepared or ball-milled Eu:GaN. Ball-milled Eu:GaN displayed a greater transmission at all weight percentages, including a tenfold improvement at 2 wt% (Figure 4.5a and b). We attribute the higher transmittances to reduced scattering, resulting from the smaller GaN particles present in the pellets made from ball-milled powders.

Figure 4.5 (a) Comparison of the IR transmittance of a KBr pellet with nano-Eu:GaN and as-prepared Eu:GaN (b) Dependence of peak IR transmittance (at 1600 cm^{-1}) upon Eu incorporation into ball-milled Eu:GaN.

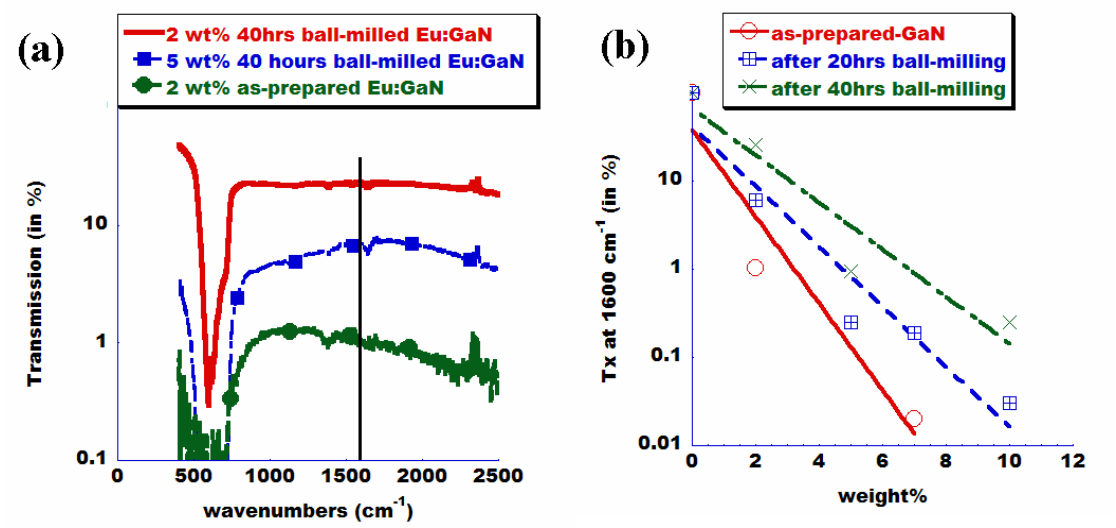

4.4 Conclusions

Synthesizing nanosized GaN particles with a uniform size distribution remains a challenging task. Furthermore, achieving proper concentrations of rare earth dopant ions in a controllable and inexpensive manner remains a significant problem. In the

present work, we demonstrated ball-milling to be a low-cost, high-throughput method for reducing micron-sized GaN to nanometer-sized particles. In addition, we used an easily scalable solid-state reaction technique to achieve rare earth (Er) doping in GaN powders. Hence, we have shown that high quality, nanosized, Eu and Er doped GaN which is free from yellow luminescence can be obtained in a cost-effective, easily scalable manner using a top-down ball-milling approach. However, the nanoparticles obtained in this manner suffer from significant agglomeration, possibly due to a large surface to volume ratio. Methods to prevent this agglomeration are being investigated.

Raman studies indicate that the ball-milled particles retain their semiconducting properties. Longer durations of ball-milling lead to greater reductions of particle sizes, and hence increased agglomeration. Both Raman spectroscopy and XRD indicate that the ball-milled particles have tensile and compressive stresses in a and c-directions respectively, due to mechanical deformation induced by the ball-milling process.

We have also demonstrated that ball-milled Eu:GaN powder in a KBr matrix displays a suitable IR transmittance for a possible applications in lasers. These results may prove useful for realizing GaN as a ceramic laser gain medium.

REFERENCES

1. A. Ikesue, Y.L. Aung, T. Taira, T. Kamimura, K. Yoshida and G.L. Messing, Annual Rev. Mater. Res. **36,** 397-429 (2006).

2. N. Kuramoto and H. Taniguchi, J. Mater. Sci. Lett. **3,** 471 (1984).

3. H. Wu, C. B. Poitras, M. Lipson, M. G. Spencer, J. Hunting and F. J. Di Salvo, Appl. Phys. Lett. **88**, 011921 (2006).

4. T. Thomas, MVS Chandrashekhar, C.B. Poitras, J. Shi, J.C. Reiherzer, F.J. DiSalvo, M. Lipson, and M.G. Spencer, Mater. Res. Soc. Symp. Proc. **1111**, 1111-D04-01 (2008).

5. A. G. Evans and R. M. Cannon, Acta Metallurgica **34,** 761 (1986).

6. D. L. Porter, A. G. Evans and A. H. Heuer, Acta Metallurgica. **27**, 1649 (1979).

7. P.H. Citrin, P.A. Northrup, R. Birkhahn, and A.J. Steckl, Appl. Phys. Lett. **76**, 2865 (2000).

8. H.Wu, C.B. Poitras, M. Lipson, M.G. Spencer, J. Hunting and F.J. DiSalvo, Appl. Phys. Lett. **86**, 191918 (2005).

9. C. Suryanarayana, Progress in Materials Science **46**, 1-184 (2001).

10. K. Sakurai and X. Guo, Materials Science and Engineering: A **304-306**, 403 (2001).

11. J. M. Zavada, Rare Earth Impurities in Wide Gap Semiconductors. In *Processing of Wide Band Gap Semiconductors*; S.J. Pearton, ed.; Noyes Publishers/William Andrew Publications: New York, 2000.

12. G. Sun, X. Liu, S.D. Tse, E.E. Brown, U. Hömmerich, S. Trivedi and J.M. Zavada, Mater. Res. Soc. Symp. Proc. **1111**, 1111-D02-08 (2008).

13. C. Kisielowski, J. Kruger, S. Ruvimov, T. Suski, J. W. Ager III, E. Jones, Z. Liliental-Weber, M. Rubin, E. R. Weber, M. D. Bremser and R. F. Davis, Phys. Rev. B **54**, 17745 (1996).

14. J. H. Park and A. J. Steckl, Appl. Phys. Lett **88**, 011111 (2006).

15. A. R. Goni, H. Siegle, K. Syassen, C. Thomsen and J. M. Wagner, Phys. Rev. B **64**, 035205 (2001).

16. J. Shi, M. V. S Chandrashekhar, J. Reiherzer, W. J. Schaff, J. Lu, F. J. Di Salvo and M. G. Spencer, J. Crystal Growth **310**, 452 (2008).

17. M. Kuball, Surf. Interface Anal. **31**, 987 (2001).

CHAPTER 5

LUMINESCENCE MECHANISM, THERMAL QUENCHING AND RADIATION HARDNESS OF Eu:GaN

5.1 Introduction

In chapter 1, we saw that rare earth ions (RE^{n+}) are used as optically active impurities in phosphor materials.[1,2] We also saw that trivalent rare earth ions (RE^{3+}) have narrow emission lines due to 4*f*-4*f* transitions. Many of these transitions lie in the visible region and can be used to obtain colors, which can in turn be used to achieve additive color mixing with very good color rendering properties. It must also be remembered that the 4*f* levels in RE ions split due to the spin-orbit coupling which is important in the theoretical treatment of these multi-electron systems.[1,2] The spin-orbit coupling that gives rise to the splitting of RE energy levels is called *j-j* coupling. The energy levels in the RE ions remain fairly unperturbed in the host matrix. Given these unique properties, RE^{3+}:GaN materials offer an interesting approach for the realization of optoelectronic devices.[3] It is precisely for this reason that the luminescence mechanism and changes in the electronic configuration in active centers of such materials under perturbations is of great fundamental interest.

We also know that among all RE:GaN materials, Eu:GaN has been used most extensively, because of its strong red emission at room temperature.[4-8] Hence, the mechanism involved in the luminescence of RE:GaN materials is a very important fundamental question. In this chapter we will focus on Eu doped GaN for two reasons (a) we have been able to successfully and reproducibly synthesize Eu:GaN powder with luminescence properties comparable to MBE grown samples (b) Eu is currently the most widely used rare earth dopant in GaN.

In order to investigate the luminescence mechanism involved in Eu:GaN, we will examine the materials under various perturbations. The experimental perturbations we will apply to the Eu:GaN system was chosen to be temperature and pressure. The careful investigation of photoluminescence of Eu:GaN under these perturbations are likely to give important insights into the excitation and de-excitation mechanisms involved with Eu ion in GaN matrix. Also quite often, the functional form of the equations governing the pressure and temperature dependence of photoluminescence in these materials can provide insights into the luminescence mechanism in these materials.[5,9] It is reasonable to expect that knowledge of the temperature and pressure dependence of luminescence in Eu:GaN permits the evaluation of its possible use in high pressure or high temperature systems. It is currently known in that GaN is a radiation hard material. Our interest in the engineering applications of GaN and related materials further prompted us to examine the radiation hardness of RE:GaN material grown by the ammonothermal technique.

In this chapter, we will discuss the optical properties of polycrystalline Eu-doped GaN powders (micron-sized) at ambient and elevated hydrostatic pressures. We will also characterize the thermal quenching characteristics at various temperatures and applied pressures. Radiation hardness of this material will be examined using O^+ flux at MeV energies. We will see that Eu:GaN powder developed by the rapid ammonothermal process is a potential phosphor and sensor material in high pressure and radiation environments.

5.2 Experimental details

The as-grown polycrystalline Eu-doped GaN was used for both compositional and luminescence studies. Eu:GaN powders tends to be in the form of chunks when obtained from the reactor. For the purpose of our experiments, we mechanically

powdered these chunks. From our experience we know that we get down can get down to about 1 μm sized particles by such hand grinding using a pestle. It is these particles that we use for the photoluminescence characterizations. For the compositional analysis, mechanical grinding was avoided, to prevent possible contamination from the porcelain pestle and other grinding equipment. Instead, the as-prepared Eu:GaN was pressed into a pellet, made in a stainless steel mold under a cold temperature hydraulic press at 4.8 MPa.

The compositional analysis involved the use of a secondary ion mass spectrometer (SIMS) at Ohio University. In SIMS, the solid surfaces to be studied are bombarded with high energy ion beams. This ion bombardment causes the emission of secondary ions from the surface. These secondary ions are then collected and detected using a mass spectrometer. The details of the ionic species are used to determine the elemental composition of the sample. Since the secondary ions generated are mostly coming off the surface, this technique is mostly used for surface chemical analysis. We decided to use SIMS since it can detect elements that are present even in low concentrations (SIMS sensitivity ~ parts per billion). In this instance, SIMS yielded the concentrations of both the various dopants, and common residual impurities such as C, O, Si and H on the surface of the material.

To determine the details of the RE electronic energy levels and the changes occurring in the occupation of these levels due to photo-excitation, we decided to perform an electron paramagnetic resonance (EPR) measurement on the same pellets. EPR is a highly element-specific technique used to study chemical species that have one or more unpaired electrons. The basic idea involved is very similar to NMR; with the difference being that here it is the electron spins that are excited instead of nuclear spins. EPR measures the Lande's g-factor associated with the electron(s) under consideration. In the EPR setup, a high magnetic field is applied to the ion of interest.

This causes a split in energy levels, with electrons occupying energy levels which can be predicted using the Maxwell Boltzmann statistics. A photon of precise energy tends to be absorbed very significantly by this system. This is used to provide information about the Lande's g factor of the electrons in the ion, which in turn can reveal details like the oxidation state of the ion and electronic configuration of the system under study.

To study changes in the ion under photo-excitation, EPR was done on an illuminated sample. This was done to determine if the electronic occupation in the 4*f* levels of Eu changes during illumination. The EPR measurements were performed using a conventional 9.5 GHz spectrometer, while varying the magnetic field between 500 to 4500 G. The EPR system was equipped with a liquid helium flow system for temperature control.[10]

Two series of photoluminescence (PL) experiments are presented in this chapter. The temperature dependence of PL was measured at ambient pressure, and the pressure dependence of PL was determined at room temperature. For all PL measurements, the Eu:GaN samples were excited using a 11mW He-Cd laser (325 nm). The luminescence was dispersed by a 2.0 m spectrograph (Carl Zeiss, Jena, PGS2) with a first-order resolution of 0.15 Å, and detected by a cooled photomultiplier tube (Hamamatsu, R943-02) working in the photon counting regime.

At ambient pressure, the PL was determined at a series of temperatures over the range 12-300 K respectively. The samples were cooled using a closed-cycle helium refrigerator. The high pressure luminescence measurements (both CL and PL) were performed at the Institute of Experimental Physics in Gdansk University (Poland) by Dr. Wisniewski. The samples consisted of pieces of Eu:GaN which were small enough to fit into a diamond-anvil cell (DAC). The DAC was used to apply hydrostatic pressures up to 7.7 GPa. The pressure was monitored using a standard

ruby fluorescence technique. In this method, one monitors the position of the R-line luminescence of ruby (694.3 nm at ambient pressure), which undergoes a shift in wavelength proportional to the applied pressure.

CL measurements were performed using an electron gun (Electroscan EG5 VSW) maintained at a vacuum level of ~$5x10^{-7}$ Torr. The depth of excitation was varied by varying the accelerating voltage from 450 V to 5kV. The emitted light was collected by a quartz lens on the entrance slit of a spectrograph monochromator (ISA model HR-320) operated in Czerny-Turner configurations with different holographic gratings. The optical signal was detected by a back-illuminated charge-coupled device (CCD) camera (Princeton Instruments, model TEA-CCD-512TK). The CCD camera was sensitized to detect UV radiation by using a UV absorbing, anti-reflective coating. (UV/AR coating). The CL set up was controlled by a computer.[9]

For the high pressure PL characterization of Eu:GaN powder, a small grain of the powder and a piece of ruby chip were placed together in a stainless steel gasket with a bore of 0.2 mm. The cell was then filled in with a mixture of methanol-ethanol (ratio 4:1) as pressure transmitting medium. The pressure was monitored using the standard ruby fluorescence technique described earlier in this section. Sample was excited with He-Cd laser and high pressure PL spectra were measured at room temperature. High pressure photoluminescence of the powder was dispersed by a 2.0 m spectrograph (Carl Zeiss, Jena, PGS2) having a resolution of 0.015 nm in the first order and detected by a cooled photomultiplier tube (Hamamatsu, R943-02) working in photon counting regime.

In another PL experiment, a 450 W Xe lamp was used as the photoluminescence excitation (PLE) source. The excitation light intensity was monitored using an Oriel thermopile detector model 71750. The maximum excitation light intensity was 400 $\mu W/cm^2$ at 370 nm, which was three orders of magnitude less

intense than the He-Cd laser at 325 nm. The PL excitation (PLE) spectrum was not normalized to the pump energy of the excitation source. The PLE spectra were detected by a Digikrom 242 double grating scanning monochrometer with a 0.5 m focal length. In this set up, a set of low self-fluorescent, long-pass optical filters were used to block any extraneous light from entering the detector. A 0.4 m prism monochromator (Carl Zeiss, Jena, SPM2) along with a second identical monochromator was used to spatially resolve the various components of PL emission from the powders. The luminescence spectra was measured by a 0.3 m Acton spectrograph, and analyzed by a Princeton Instrument PI-MAX CCD camera equipped with a UV intensifier, operating in the spectral region 200-950 nm. The luminescence intensity was detected by a photomultiplier (Hamamatsu, R928). The PLE spectra were corrected for the spectral response of the setup.

In order to characterize the radiation hardness of Eu:GaN powders, acid rinsed particles were used. The Eu-doped GaN powder was mixed with KBr in different weight ratios, and compressed into 0.8 mm diameter pellets in a stainless steel mold, using a cold temperature hydraulic press (pressure applied: 3.25 bars). The KBr-GaN:Eu composites were exposed to a beam of 2 MeV O^+ by Dr. D. Ingram at the Edwards Accelerator Laboratory at Ohio University. The dose rates (fluence) on each pellet surface were measured to be between 1.7×10^{12} and 5×10^{13} ions/cm^2. PL measurements were performed on the samples before and after irradiation, using a 325 nm excitation source operating at 300 K. The penetration depth and ion distribution of these 2 MeV O^+ ions in the GaN powder was estimated using SRIM 2003 software.

5.3 Results and Discussion

5.3.a SIMS and EPR data

The SIMS data shown in Figure 5.1 indicates that the Eu:GaN particle surface is contaminated by oxygen, hydrogen and carbon. Most of the oxygen and hydrogen is attributable either to hydroxylation of the surface due to exposure to atmosphere, or to the formation of gallium oxides. This is consistent with the XPS data analyzed in Chapter 3. Silicon is also present at the surface as a contaminant. We believe this comes from the quartz tube in which the GaN powder is synthesized. The Eu concentration at the surface is observed to be about 0.6 at%, which is slightly higher than the 0.5 at % predicted using XRD and Raman spectroscopy in Chapter 4. However, these values can be considered to agree within the limits of experimental error.

In recently published experimental and theoretical studies on RE-doped GaN, two theoretical models have been proposed for the optical and electrical activities of RE ions in this wide band gap semiconductor. The first model assumes changes in the valence of the RE-ion via charge transfer (charge transfer model).[11,12] The development of the charge transfer model for GaN doped with lanthanide ions can be dated back to a paper published in 2006 by P. Dorenbos and his co-workers.[11] In their published work they used knowledge from lanthanide spectroscopy on wide band gap (6–10 eV) inorganic compounds to understand and predict optical and electronic properties of the lanthanides in the III-V semiconductor GaN. The location of the $4f^n$ ground state energy of each divalent and trivalent lanthanide ion relative to the valence and conduction bands in GaN was predicted (see Figure 5.2). They also suggested that the quantum efficiency of associated with the luminescence phenomenon depends on the location of the lanthanide ion relative to the GaN conduction and valence bands. It was also suggested that the lanthanide ion level location controls the electron acceptor

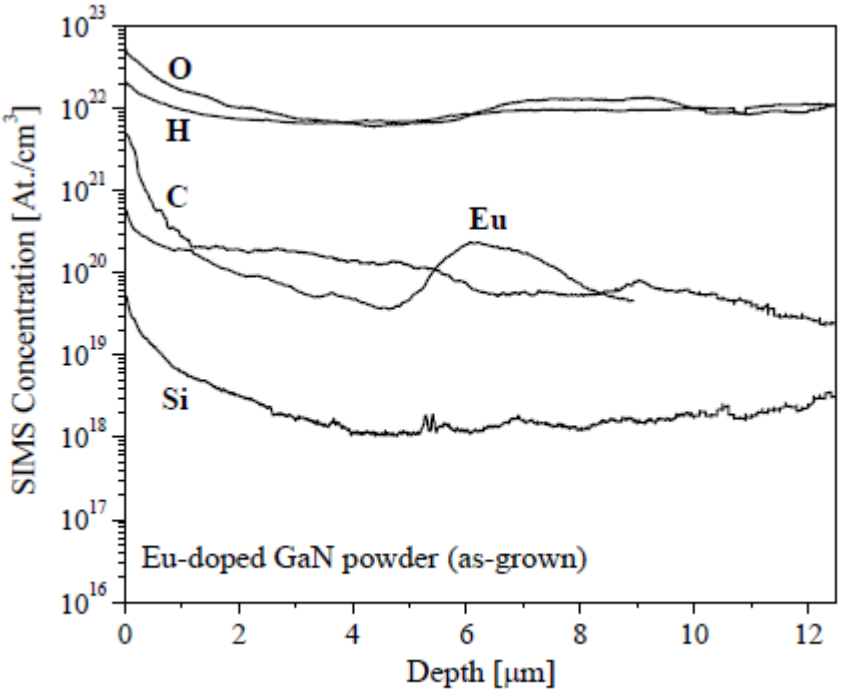

Figure 5.1 SIMS results for as-synthesized Eu-doped GaN. From the SIMS scan, the maximum Eu ion concentration in the powder was estimated at ~0.6 at%.

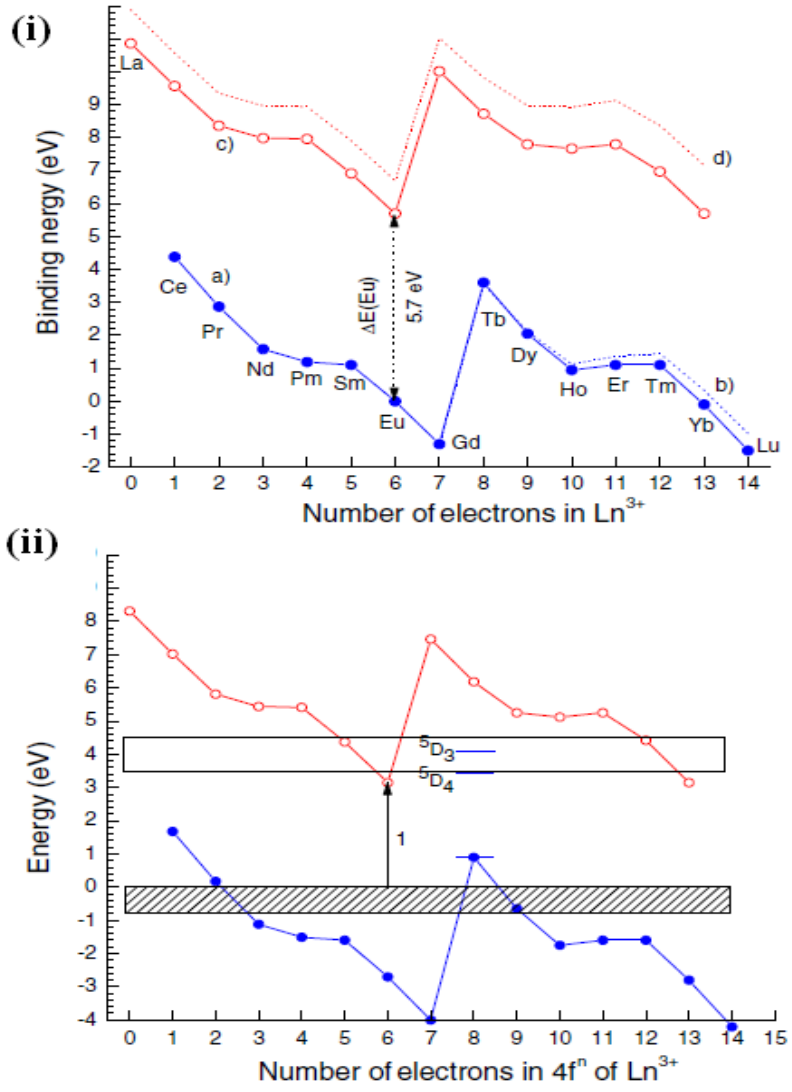

Figure 5.2 (i) Shows the binding energies of 4*f* electron binding energies of (a) trivalent and (c) divalent lanthanide ions in sulfides and bromides (ΔE(Eu) ~5.7 eV). Curves b and d pertain to oxides and fluorides (ΔEu ~6.7 eV). (ii) Proposed location of the lowest $4f^n$ states of divalent and trivalent lanthanides in GaN. The top of valence band is at energy zero, and the GaN exciton is at 3.42 eV. The charge transfer from valence band to Eu^{3+} is indicated by the arrow. (Courtesy: Darenbos)[11,12]

electron donor properties of lanthanide ions. In the charge transfer model proposed by Dorenbos et al, the fact that the 4f-shell of a trivalent lanthanide ion may accept or donate an electron from or to the energy bands of a III–V compound resulting in a $Ln^{3+} \rightarrow Ln^{2+}$ transition or $Ln^{3+} \rightarrow Ln^{4+}$ transition is used to explain luminescence excitation and quenching.

The second theoretical model has its basis on a paper by Lozykowski in 1993.[13] This model used to explain Lanthanide spectroscopy in nitrides is now called Rare earth structured isolvalent (RESI) tap model. The basic idea this model is that Eu ions may act as isoelectronic hole traps in the GaN host. The electron configuration of Ga^{3+} is $1s^2 2s^2 2p^6$, which is isoelectronic with the outer electron configurations of all trivalent RE^{3+}, ie. $5s^2 5p^6$. If the RE^{3+} ions replace metallic cations in the III-nitride host matrix, then they will create structured isovalent traps.[9] Experimental data and crystal-field calculations have confirmed that RE^{3+} ions in GaN occupy relaxed substitutional Ga sites with trigonal C_{3v} crystal symmetry.[14,15] The local lattice distortion due to the substitution of a RE ion is called a rare earth structured impurity (RESI). The RESI is capable of binding excitons due to the short-range potential.[9] In explanations based on this model, the lanthanide ions are treated as iso-electronic impurities. Since lanthanide ions have different size and electro-negativity compared to the cation they substitute for (Ga^{3+} or Al^{3+}), they create a short-range potential that may trap a free charge carrier. Subsequently, the counter charge carrier is trapped forming an exciton bound near or at the lanthanide ion. It is this formation of a localized exciton near or at the RE site that results in energy transfer and subsequent excitation of the 4*f*-shell electrons (isoelectronic trap model).[9]

In this chapter we will examine the presence of charge transfer between GaN and the RE site using EPR data. RE^{n+} ion with odd number of valence electrons will have an EPR signature, while ions with even number of outermost *f* shell electrons

will be EPR silent. Hence EPR was used as the criteria for verifying the presence of charge transfer to the RE ion occurs during the photo-excitation process.

The EPR data in Figure 5.3 show a sharp feature near 3.5 kG. This corresponds to a g-value of 1.95. This is a well-established signature for the presence of shallow donors or conduction electrons in GaN.[16] We believe that this EPR resonance is due to un-compensated Si and O shallow donors. However, the small amplitude of this peak suggests that most of the oxygen is not acting as a simple (group-III) substitutional shallow donor in this material. The same EPR signal was observed in the undoped GaN powder. The weak feature at ~1.6 kG and the stronger signal near 3.4 kG are known to be signatures of quartz. These are attributable to contamination from the quartz Dewar used to contain the sample. Since Eu is known to be stable in both the Eu^{2+} and Eu^{3+} states, EPR was used to test for the possibility of a Eu^{3+} to Eu^{2+} transition under illumination. The EPR of Eu:GaN under dark conditions was compared to its EPR under illumination by a 75 W broad-band Xenon lamp. Our EPR system was capable of detecting 10^{14}-10^{15} spins per cm^3. However, no signal associated with the Eu^{2+} ion was found either in the dark or under photo-illumination.

Additionally, we measured the EPR spectra on Er-doped GaN powder (data not shown) synthesized by the same method as the Eu:GaN. We observed the weak EPR signals characteristic of Er^{3+} ions ($4f^{11}$, EPR active state). However, the EPR spectrum looked similar under dark and illuminated conditions. Given that both Eu- and Er- doped GaN behave this way, this may be generally true for all RE:GaN. Optical excitation causes electronic transitions within the *f* levels, with no resulting change in the RE ion charge.

Our observations suggest that charge transfer (the optical promotion of an electron to the 4*f*-shell system from an outside level) is absent, because if it did occur,

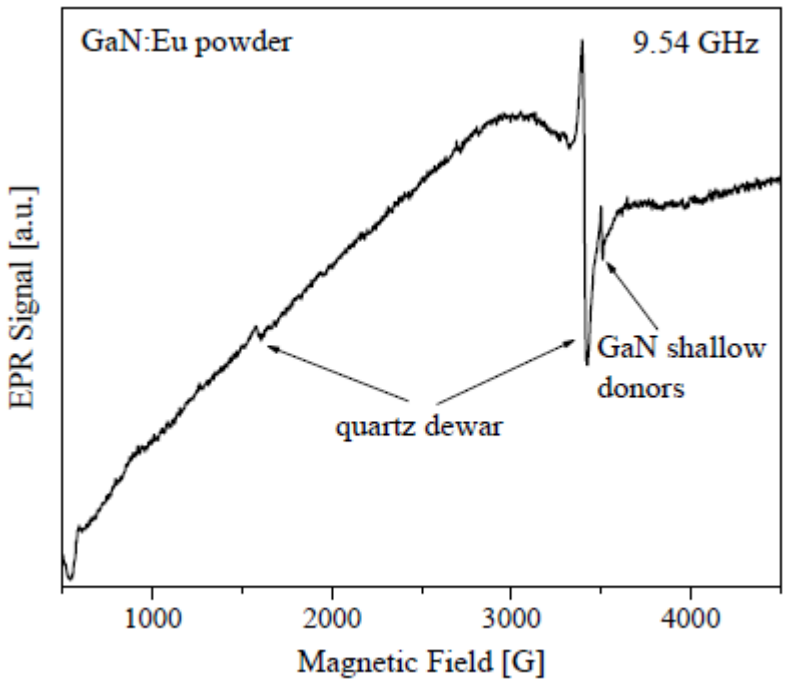

Figure 5.3 A representative EPR spectrum over a wide range of magnetic fields (0.5 kG – 4.5 kG) for the Eu-doped GaN powder at 10 K. EPR was also performed on an undoped GaN powder reference sample, grown using the same technique (data not shown). No features indicative of the presence of Eu^{3+} ($4f^6$, inactive in EPR) or Eu^{2+} ($4f^7$, active in EPR) were observed.

the EPR signal would indicate the presence of Eu ions with an odd number of 4*f* electrons. Hence the charge transfer model has not been verifiable in these RE:GaN systems.

5.3.b Temperature and pressure dependent optical characterization

Figure 5.4 compares the emission lines in the CL and PL spectra. The CL spectra contain many more lines than are observed in PL. This difference may be due to dissimilar dominant excitation mechanisms in the two processes. [17] The additional lines in CL could probably be due to different local bonding geometries associated with Eu^{3+}. The insert in Figure 5.4 shows the temperature dependence of the integrated PL emission intensity (I_{em}). I_{em} is defined as the area under the Eu^{3+} emission lines belonging to the $5D_0 \rightarrow 7F_2$ transition, in the temperature range 13-300 K. I_{em} is nearly constant at low temperatures. However, above 100 K, I_{em} starts to decrease monotonically.

In Figure 5.4 the high-temperature sections of I_{em} shows a rapid decrease in intensity with temperature, which can be fitted to the equation shown in the caption**.** In the equation used parameter ε_{PL} is called the thermal quenching energy. Using a simple curve fit, it was found to be about 80 meV for the Eu^{3+} ion in Eu:GaN. Based on the current understanding of RE ion excitation in RE:GaN, ε_{PL} represents the thermal-activation energy associated with the liberation of a hole from an exciton trapped on an RESI trap. [9,17]

Eu:GaN features can be seen in the PL spectra of Figure 5.5 a, b, and c. In Eu:GaN, Near band edge emission (NBE) is observed at all temperatures. For interpreting our low temperature PL, we used spectra reported by Y. Song et. al (see Figure 5.6). In their 2006 paper,[18] they used Raman and photoluminescence spectroscopies to determine the energies and linewidths of optic phonons, excitons,

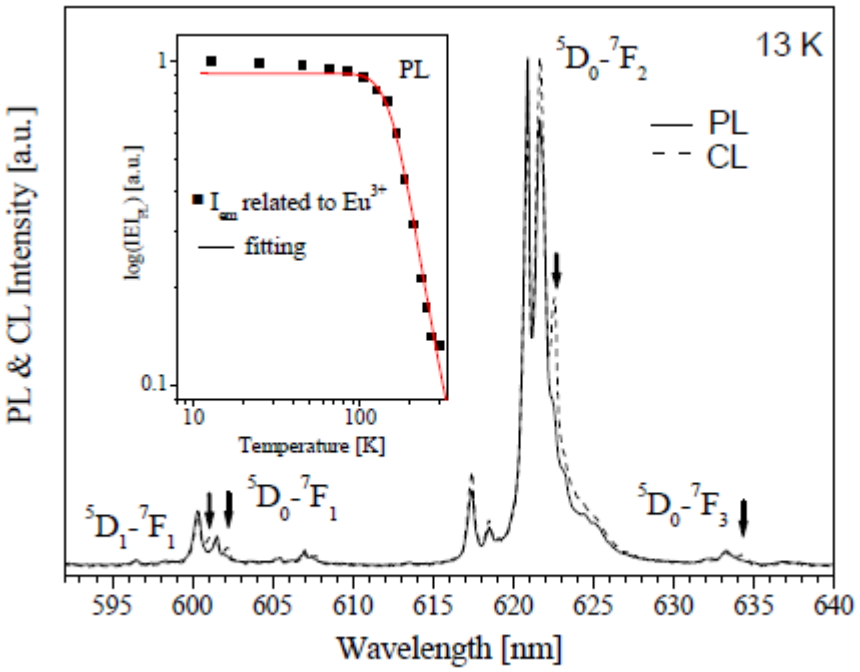

Figure 5.4 High resolution PL (continuous line) and CL (dashed line) spectra of Eu:GaN at 13 K. The PL spectrum was excited with λ_{exc} = 325 nm (He-Cd laser). The CL spectrum was collected using an electron beam with energy of 8 keV and a current density of 0.5 mA/cm^2. The insert shows the temperature dependence of I_{em}, fitted to the equation $I_{em} = A\ (1 + B \exp(-\varepsilon_{PL}/k_bT))^{-1}$, where A and B are fitting parameters, k_b is the Boltzmann constant, and T is absolute temperature, respectively.

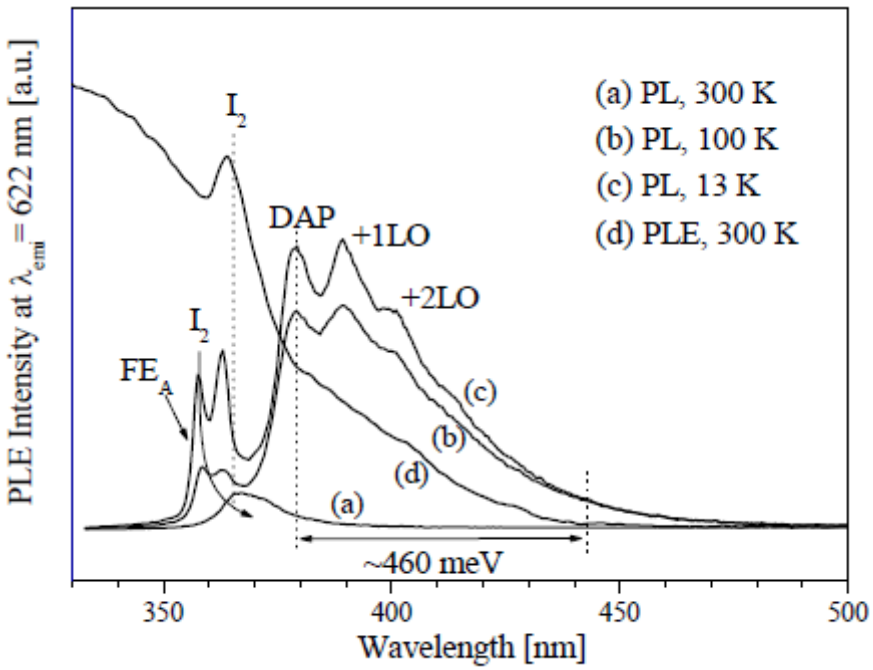

Figure 5.5 PL spectra of Eu:GaN measured at (a) 300 K, (b) 100 K, and (c) 13 K respectively. (d) PLE spectrum of Eu:GaN at room temperature.

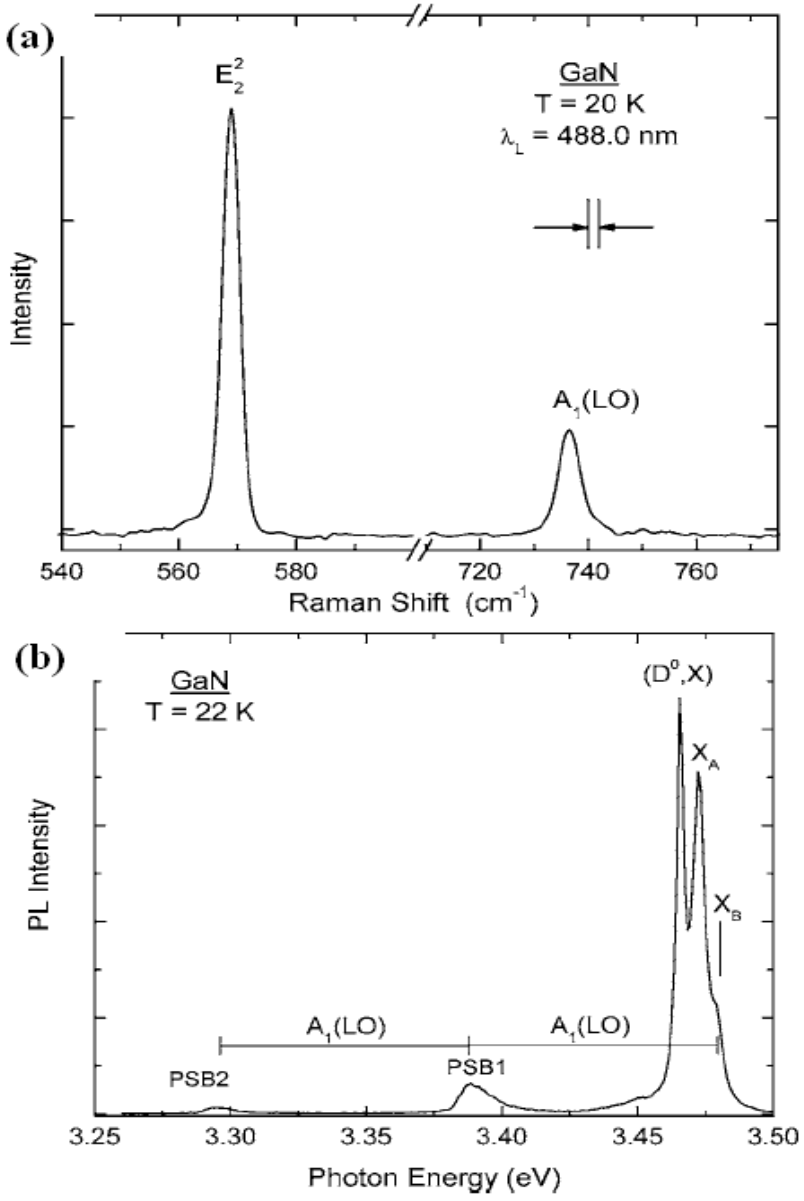

Figure 5.6 (a) Raman spectrum of GaN epitaxial layer at 20 K. (b) Photoluminescence spectra of epitaxial GaN at 22 K. Donor-bound exciton line is labeled (D^o, X), X_A, X_B are free excitons. PSB1 and PSB2 denote A1(LO) phonon sidebands. (Courtesy: D. Y. Song et. al)[18]

and discrete phonon sidebands (PSBs) at cryogenic temperatures. It was shown that temperature dependence of the A1(LO) phonon energy and line-width can be completely described by a two- and three-phonon decay process.

We also identified emission associated with donor-acceptor pairs (DAP) at about 3.27 eV. This is the level associated with an exciton that is bound to the RESI trap hence we will also call it exciton-RESI bound level. The description of the DAP level is in keeping with earlier reports by Paskova et al (see Figure 5.7).[19] In their experiments they found that the PL and CL spectra of intentionally undoped mass-transport (MT) grown GaN showed distinct emission associated with DAP. The intensity of emission associated with DAP varied with significantly with respect to the growth conditions employed. In HVPE grown GaN it is currently believed that a semiclassical potential caused by local strains due to an acceptor like complex/clusters is responsible the DAP levels.

Figure 5.5 also shows the related unresolved excitonic emission peaks of free excitons (*FEA*) and excitons bound to the neutral shallow donors (called I_2 level in the figure) (most likely oxygen) at 3.473 eV. This was identified based on the Donor-binding exciton (DBE) energy level identified in an earlier report (see Figure 5.7). In our samples the precise location of Donor-acceptor pairs (DAP) was found at about ~3.26 eV. The corresponding LO pass bands (PSBs) were seen corresponding to a A1(LO) phonon energy of about 90 meV.[20] As the ambient temperature is increased, the excitonic peak position is red shifted from 357 nm to 366 nm (85 meV). This indicates that as temperature increases, the exciton binding energy decreases. This phenomenon could lead to a less efficient transfer of energy from the bound exciton to the RE at high temperature, resulting in thermal quenching of the luminescence. The curve (d) in Figure 5.4 is the room temperature PLE spectrum monitored at 622 nm. The I_2 line is

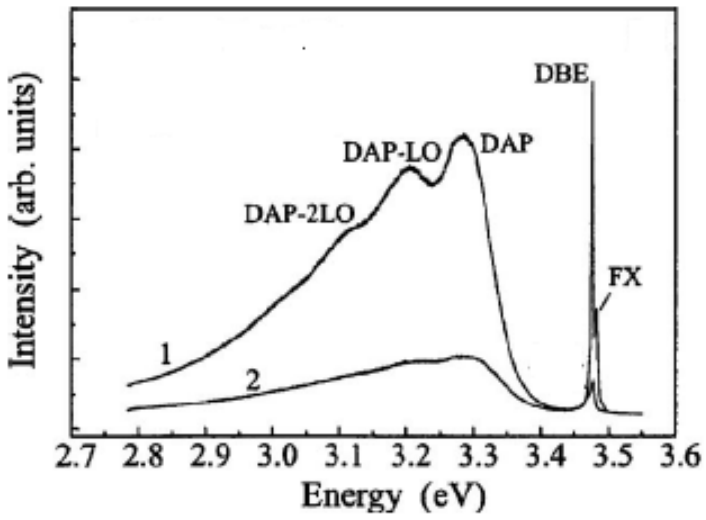

Figure 5.7 Photoluminescence spectra of hydride vapor phase epitaxially (HVPE) grown unintentionally doped GaN. Curve 1 and 2 show two samples of GaN obtained from within the HVPE chamber. The emission associate with the free exciton(FX) is seen clearly only in sample 2. However, the first sample clearly shows emission levels corresponding to donor-acceptor pair (DAP), donor-binding excitons (DBE) and passbands associated with the LO phonons in GaN. (Courtesy: T. Paskova)[19]

associated with the exciton bound to the neutral shallow donors. When the photon energy is just sufficient to excite I_2, weak PL emission is seen.

The spectral overlap between a broad absorption tail seen from 375.7 nm to 442.8 nm and the DAP structure (show as a 460 meV window in Figure 5.4) indicates the participation of intrinsic impurities (and possibly their complexes with defects) in energy transfer processes from the GaN host to the Eu^{3+} center. The width of the absorption tail (~460 meV) is comparable with previous reports in the literature.[21,22] In the present case, the exact nature of the PLE broad band seen in Figure 5.4 may have a more complex origin than a simple DAP recombination and will require further investigation.

5.3.c Pressure dependent photoluminescence in Eu:GaN

The intra-4*f* electrons of the RE ion are shielded from the host valence electrons, making the PL emission lines only weakly dependent on applied pressure. The PL spectra resulting from above band gap excitation of Eu:GaN at 300 K are presented in Figure 5.8. In general, the number of observed Eu^{3+} transition lines does not vary with pressure, but the intensity of each emission changes quite significantly. Each spectrum shows an excitonic emission band in the near UV, and characteristic Eu^{3+} transition lines originating from the $5D_1$ and $5D_0$ levels. The NBE peak intensity changes by a factor of 1.5 when the pressure is increased from ambient to 6.8 GPa, whereas the $5D_0 \rightarrow 7F_2$ peak intensity (at 622 nm) increases ~10 times over the same pressure range. We observed that the Eu^{3+} emission intensity at 6.8 GPa and room temperature was approximately the same as at ambient pressure and 13 K. Also the spectral width of the line at 622 nm changes only slightly with pressure. These minor changes could be due to non-hydrostatic conditions. However, the change in the half-

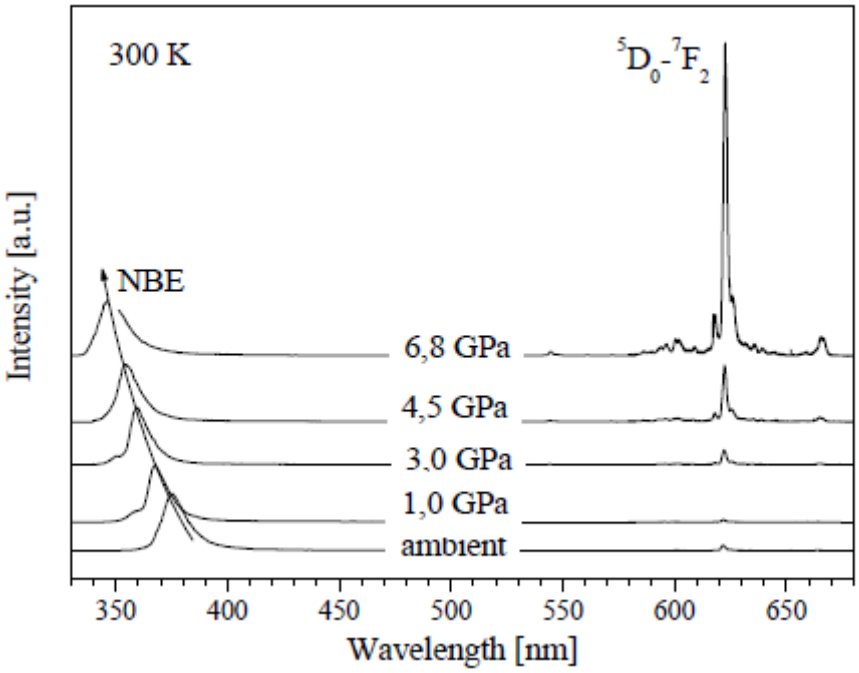

Figure 5.8 Room temperature high pressure PL spectra of Eu:GaN obtained under an excitation of 325 nm.

width of the ruby crystal *R1* line between ambient and 6.8 GaP was only ~2 cm^{-1}, indicating that the non-hydrostatic effects were rather weak.

Although the lines at 622 nm do not show any significant peak position change, we observe a significant blue shift in the I_2/DBE exciton emission band. The estimated shift rate was constant and equal to 44.2 meV/GPa.[23] It is interesting to note that a similar coefficient for the shift of the GaN conduction band minimum under applied hydrostatic pressure has been reported in the literature.[22,23]

At no point are any Eu^{2+} transitions observed. This implies that there is no change in the Eu ion charge under high pressure. In section 5.3.a we saw that there was no change in the Eu ion charge under photoexcitation at ambient pressure. Hence, we expect the luminescence mechanism in RE:GaN to be similar under both ambient and applied pressures. In other words, we expect a bound-exciton model for the excitation of the RE ion to apply, even under applied pressures.

The Eu^{3+} emission intensity increases upon applied pressure, while the NBE emission intensity remains relatively constant. This suggests that the induced compressive stress has modified the mechanism of energy transfer between the RESI trap involving the Eu^{3+} ion and the GaN host. A similar effect has been observed previously for RE doped III-V semiconductors.[11,12]

To understand the mechanism governing the pressure-induced enhancement of the Eu^{3+} emission intensity, we plotted the shifts in the excitonic and $5D_0 \rightarrow 7F_2$ levels with respect to pressure (see Figure 5.9). We also superimposed the PL spectra of the powder at ambient and applied pressures (see Figure 5.10) to examine the peaks individually.

From the fit shown in Figure 5.9, the shift rate of the excitonic band maximum is found to be constant and approximately 44.2 meV/GPa. A similar shift in the coefficient for the change of the conduction band minimum under applied hydrostatic

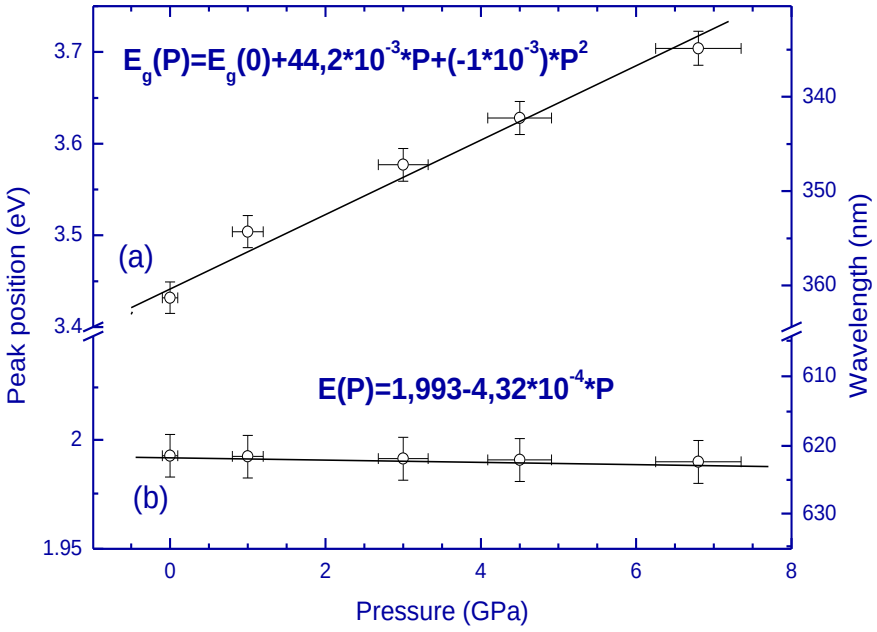

Figure 5.9 Change in the position of (a) the excitonic emission band and (b) the $5D_0 \rightarrow 7F_2$ transition line, with applied pressure. The solid lines are the best fit lines obtained using equation shown in the inset.

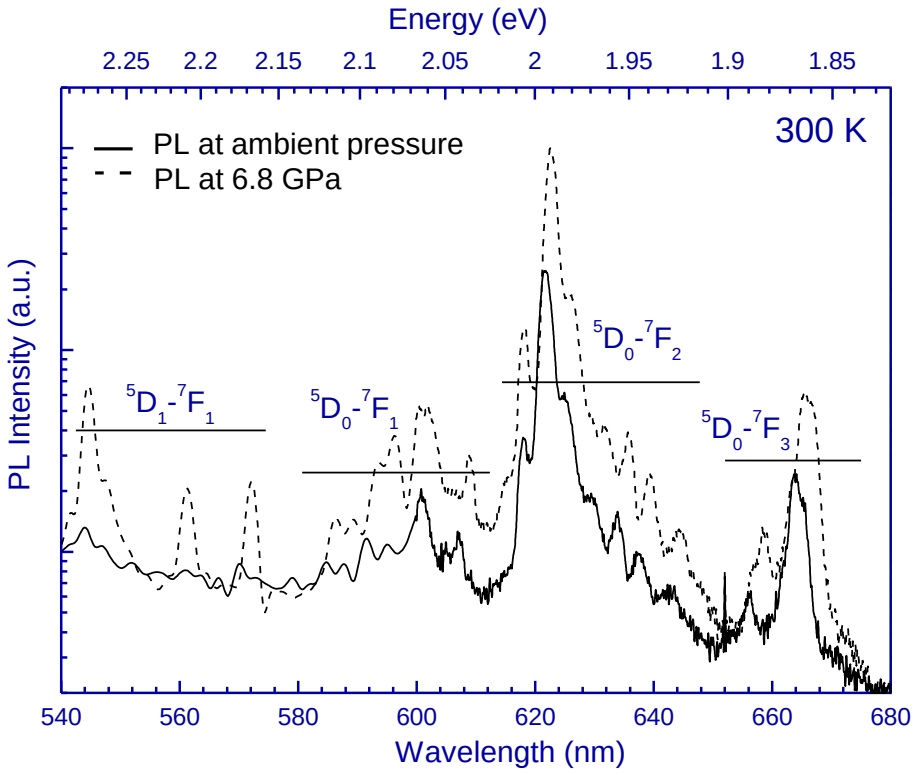

Figure 5.10 Room temperature PL spectra of Eu:GaN powder at ambient pressure (continuous line) and high pressure (6.8 GPa) (dashed line).

pressure has been reported.[22,24,25] In Figure 5.10, several groups of Eu^{3+} emission lines are observed following an above band gap excitation. These transitions are from the $^5D_1$ and $^5D_0$ states toward the ^7F_J ground levels, measured at ambient and under the 6.8 GPa hydrostatic pressure. Figure 5.10 shows that the number of observed transitions from the $^5D_1$ and $^5D_0$ levels remains unchanged. This suggests that there are probably no RE^{n+} centres other than the RE^{3+} which are already optically active. The splitting of the observed Eu^{3+} transition line due to the crystal field effect is similar for both PL spectra in Figure 5.10, suggesting that the symmetry and local atomic structure surrounding the Eu ion remain similar, even when pressure is applied.

Given the experimental results, the high-pressure-induced modifications to the environment around the Eu^{3+} center seems to cause an increase in the localization of bound excitons on the RESI traps, which in turn increases of binding energy of the exciton bound to the RESI (see Figure 5.11). This in turn increases the probability of nonradiative energy transfer from collapsing excitons to the 4*f*-shell system, resulting in the observed increase in the intensity of Eu^{3+} emission with applied pressure.

It was proposed recently that RE^{3+} emission quenching occurs predominantly during the energy-transfer processes between an exciton bound to the RE ion center (an isoelectronic trap) and the 4*f*-shell system, rather than through nonradiative de-excitation of 4*f* transitions.[9] Considering above arguments, we may speculate that the high pressure induced modifications at the Eu^{3+} center prevent a possible undesirable back-transfer of energy from the excited 4*f*-shell system. However, to conclusively prove the exact mechanism of the pressure-induced enhancement of the Eu ion emission intensity, further investigation will be required.

We also studied the thermal quenching of Eu:GaN at various applied pressures over the temperature range 11-300 K (see Figure 5.12). We observed a decrease in

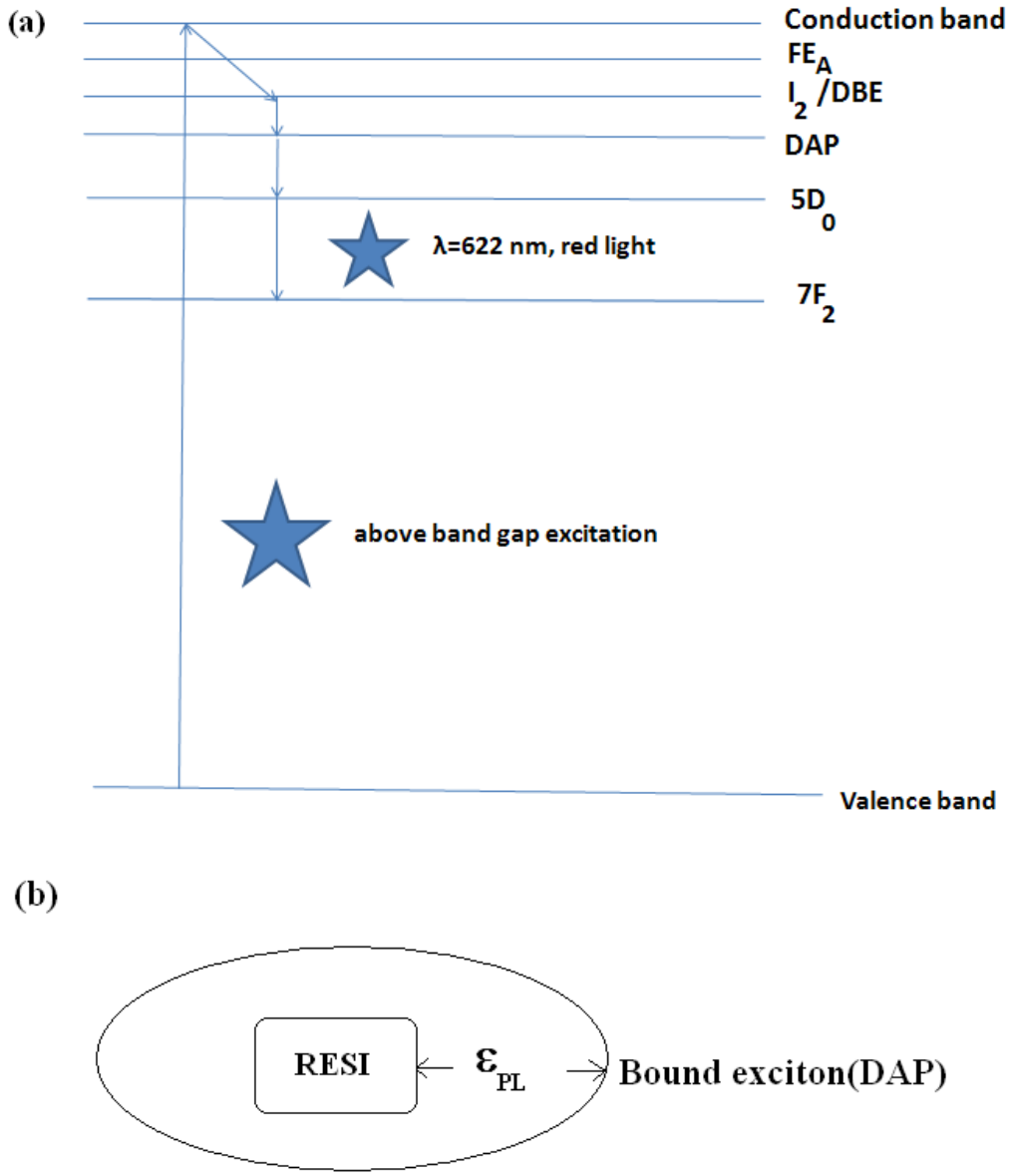

Figure 5.11 (a) Shows the model associated with the energy transfer processes involved in the photoexcitation of Eu^{3+} ion in GaN. The model helps explain the fact that the minimum energy needed for the photoexcitation of Eu^{3+} is determined by the energy level associated with the I_2 exciton. (b) A schematic of the RESI-bound exciton model. The exciton responsible for excitation of the RE ion is bound to the RESI by about 92 meV (which is also the thermal quenching energy ε_{PL}). ε_{PL} increases with applied pressure by about 6.2meV/GPa. This physical interpretation for the thermal quenching energy explains the increase in PL with applied hydrostatic pressure. It must be noted that to form the state shown in this schematic, an I_2 (donor bound exciton/DBE) must be first excited.

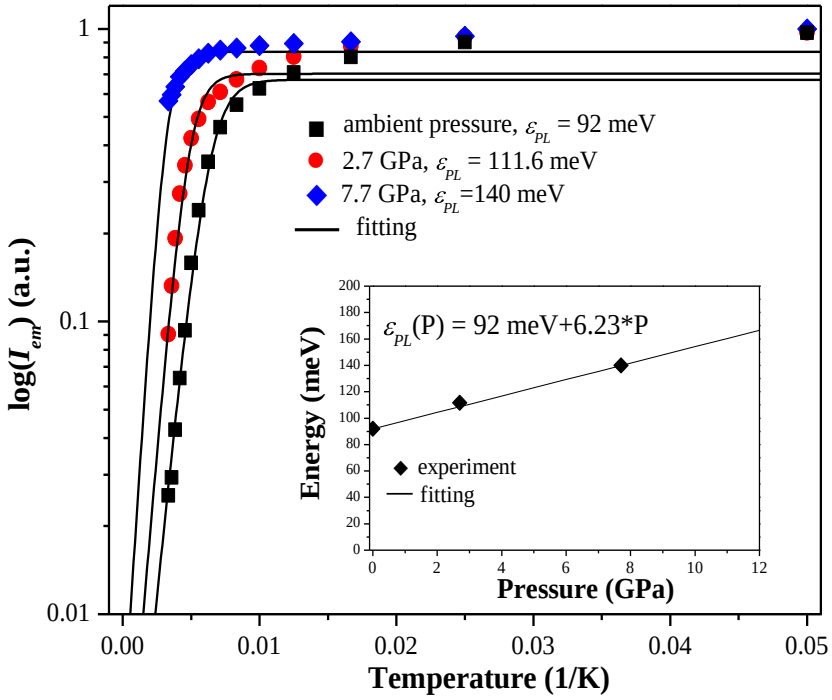

Figure 5.12 Temperature dependence of integrated PL emission intensity (I_{em}) for as-synthesized Eu:GaN powder, measured at different hydrostatic pressures in the temperature range 11 K to 300 K. The solid lines are the least square fittings of I_{em} given by the equation I_{em} =A(1+Bexp(-ε_{PL}/k_BT). The ε_{PL} energies closely approximate only the high temperature sections of the I_{em} curves. The insert projects the evolution of the Eu^{3+} RESI trap exciton binding energy as a function of applied hydrostatic pressure. The solid line is the best fit to the equation shown in the insert.

thermal quenching at higher applied pressures. As the binding energy of the excitons bound to the RE ion site increases with applied pressure, we can expect thermal quenching to occur at higher temperatures. This is consistent with our results from section 5.3.b and this section.

5.3.d Characterization of radiation hardness of Eu:GaN

In the introduction section of this chapter we pointed out that we are interested in the engineering applications of GaN in harsh environments. Currently GaN has found a place in powder electronic devices used in space crafts, radar stations etc. Radiation hardness of wide band gap semiconductors makes it a suitable electronic material for radiation specific application. How would the properties of rare earth doped GaN be affected by radiation? This is the question we will try to partially answer in this section.

In a recent report, the effect of 3 MeV electron irradiation on the photoluminescence properties of Eu-doped GaN was investigated. In this work, Eu was introduced into GaN epitaxial layers grown on sapphire substrates by ion implantation. The peak concentration of implanted Eu was found to be a few atomic percent. The electron dose was in the range of 10^{16}–3×10^{17} cm^{-2}. PL was measured in the temperature range of 13–295 K by using a He–Cd laser as the excitation source. PL intensity corresponding to the transition of $5D_0 \rightarrow 7F_2$ in Eu^{3+} was hardly dependent on the electron fluence. In contrast, the PL intensity of the near-band-edge emission from undoped GaN decreased when increasing the electron fluence.[26]

Likewise in another report, the effect of 380 keV proton irradiation on the photoluminescence (PL) properties was investigated for undoped and Eu-doped GaN. As the proton irradiation exceeds 1×10^{13} cm^{-2}, a drastic decrease of PL intensity of the near band-edge emission of undoped GaN was observed. On the other hand, for Eu-

doped GaN, the PL emission corresponding to the $5D_0 \rightarrow 7F_2$ transition in Eu^{3+} kept the initial PL intensity after the proton irradiation up to 1×10^{14} cm^{-2}.[27]

These results, together with the previous reports on electron irradiation results, suggest that Eu-doped GaN is a strong candidate for light emitting devices in high irradiation environment. If these observations were to be explained base on the RESI model, we would have to conclude that the crystal defects introduced by the irradiation are not preventing RESI-bound excitons from being formed. However it must be noted that defects introduced by radiation would reduce the minority diffusion constants in the GaN matrix. The fact that the exciton formation remains independent of the minority diffusion length seems to suggest that the spatial density of RESI in Eu:GaN matrix is high enough to cause exciton formation independent of minority carrier diffusion length.

As of now, it is believed that the mechanism responsible for this observed destruction of luminescent centers beyond a certain critical fluence is the displacement of Eu^{3+} ions from its equilibrium position on the Ga sublattice to an interstitial or antisite position. Alternately, a Ga or N atom could be moved by the energized particle to an interstitial site near the Eu^{3+} and thus quench luminescence (see Figure 5.13 and 5.14).[28]

In this section, we will investigate the effect of 2MeV O^+ irradiation on the PL properties of Eu-doped GaN powder. O^+ was chosen because of the fact that it is an impurity that is already present in the GaN powder. Besides, it was easier to generate O^+ in the primary ion source in the Edwards Accelerator Laboratory facility. Besides, among all the ions used for GaN irradiation so far, O^+ would be the heaviest and the biggest in size. This would mean that oxygen irradiation could cause more extensive damage to the GaN matrix than the protons, electrons or helium ions reported in the

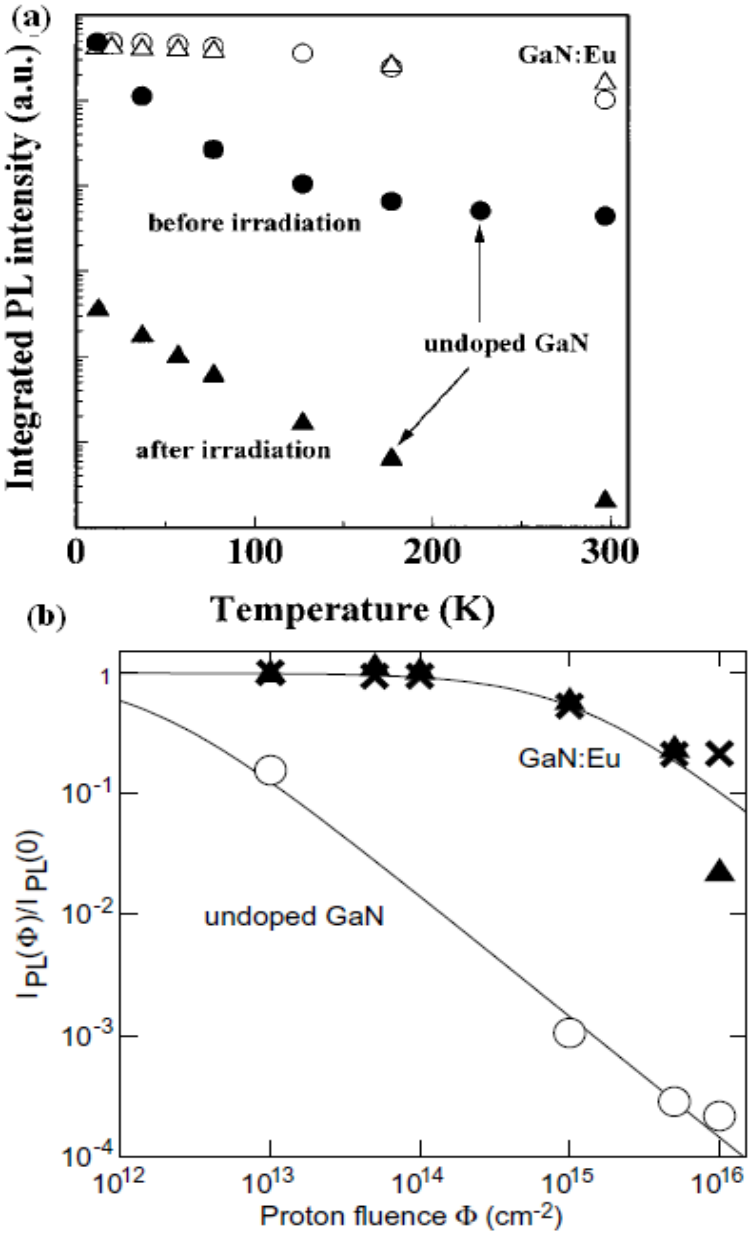

Figure 5.13 (a) Temperature dependence of integrated PL intensity for near-band edge emission of undoped GaN (filled marks) and the $5D_0 \rightarrow 7F_2$ transition of Eu-doped GaN (open marks). Circles and triangles indicate before and after irradiation with electron fluence of 1×10^{17} cm^{-2}. (b) Open circles denote near band-edge emission (NBE) of undoped GaN. Crosses and closed triangles denote $5D_0 \rightarrow 7F_2$ transitions in Eu-doped GaN. [26,27]

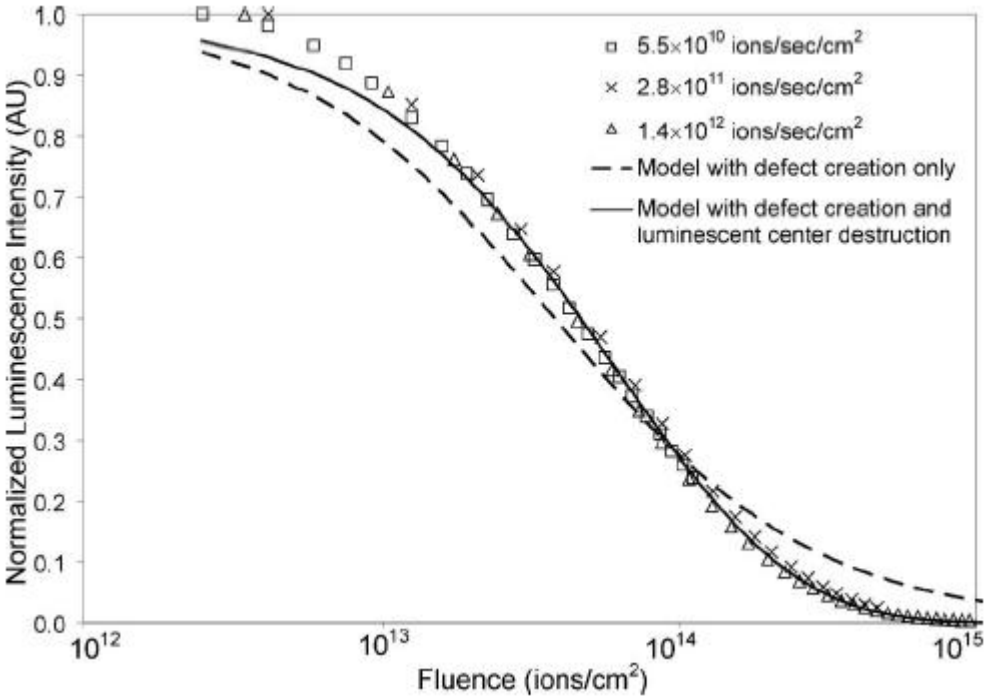

Figure 5.14 Normalized peak (620 nm) ion-induced luminescence of GaN:Eu under irradiation by He^+, plotted as a function of fluence. Dose rates were 5.5×10^{10}, 2.8×10^{11} and 1.4×10^{12} ions*sec^{-1}*cm^{-2}. Results are shown for a constant radiative recombination lifetime model, and for the model used in this experiment wherein the radiative lifetime is exponentially dependent on the fluence. At fluences lower than 2×10^{13}cm^{-2}, where the model agreement is lowest, the rate of nonradiative defect generation may not be constant.

literature so far. It must be recalled that based on the current understanding of luminescence quenching due to ion irradiation of GaN, Eu^{3+} centers can be destroyed either by removing the Eu^{3+} from its equilibrium position on the Ga sublattice, or by the creation of an interstitial defect near the Eu^{3+}center. Based on this model, the ultimate the radiation tolerance of GaN to oxygen ions was estimated.

Oxygen irradiation was used to generate extensive defects in the GaN:Eu powder grains. KBr was selected as a binder for the powder during the irradiation experiment because: (a) combinations of KBr and other alkali halides have shown fairly good long-term stability, (b) degradation of KBr due to radiation exposure is easy to detect visually, because it will usually display a "milky" appearance rather than clear interference colors; (c) KBr has good transparency down to 325 nm.[29]

Using the Beer-Lambert absorption law (also known as the Bouquet' law in some literature), we estimated that the light from the 325 nm excitation will not propagate deeper than ~200 nm in GaN. The maximum estimated penetration range of the oxygen beam into GaN was ~1.7 μm. Figure 5.15 shows the penetration depth of 325 nm photons in GaN (curve (a)) and the oxygen stopping range in GaN (curve (b)). The oxygen stopping range was evaluated using SRIM (Stopping Range of Ions in Matter) software. This software is primarily concerned with the quantitative evaluation of how ions lose energy into matter, and the final distribution of these ions after they stop within the target. The software used established models to predict ion penetration by accounting for the first order effects of the atoms on solids, particularly the electronic excitation of the atoms, the displacement of lattice atoms by energetic collisions (lattice damage), and the production of plasmons and phonons within the solid by the passing ions. However, within the models, no evaluation is made of thermal effects in the solid, especially the redistribution of lattice atoms or implanted ions by thermal or vacancy induced diffusions, and changes in the penetration depth

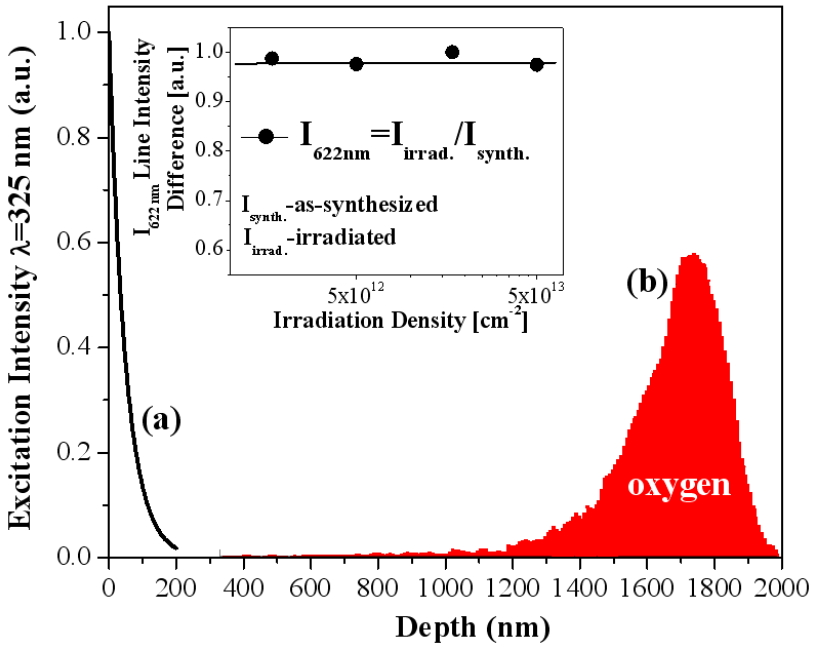

Figure 5.15 (a) Penetration depth of 325 nm excitation in GaN and (b) oxygen stopping range in GaN (solid dropped curve) at 5×10^{13} ions/cm^{-2} fluence. The maximum oxygen concentration, at ~1.7 μm depth, was 1.4×10^{18} cm^{-3}. The curve (a) was generated using equation $I(x)=I_0\exp(-\alpha x)$ where $\alpha=2\times10^5$(cm^{-1}) is GaN absorption coefficient at 325 nm. Both the penetration depth of the 325 nm excitation and the oxygen stopping range should be modified if one considers the average density of the KBr-GaN:Eu composite. The insert shows the dependence of the integrated PL intensity (622 nm) on oxygen fluence, where the PL intensities are normalized to that of the nonirradiated sample.

due to these effects. The latest version of SRIM gives a penetration depth within 5% of experimental data. Hence, SRIM was chosen to predict O^+ penetration in Eu:GaN.

Figure 5.15 shows that most of energetic photons that are used to excite the material penetrate only about 200 nm into the material, while the O+ ions penetrates well into the GaN matrix (1 to 2 μm into the surface). Based on these measurements, we are inclined to think that the incorporated oxygen should not interact with Eu^{3+} in the region of luminescence generation (see Figure 5.15). This is in keeping with the observation that in general, after oxygen irradiation, the PL spectrum did not change. That is the intra 4*f*-shell transition peaks had the same positions and spectral widths before and after irradiation. Also no new Eu^{3+} transitions were observed. The insert in Fig. 5.15 shows the dependence of the integrated PL intensity of the acid-rinsed powder on oxygen irradiation at doses between 1.7×10^{12} and 5×10^{13} cm^{-2}. The PL intensities are normalized to that of the non-irradiated sample. It is seen that the generation of defects does not affect the Eu^{3+} emission in the range of oxygen fluence we studied, confirming the resistance of the Eu:GaN powder to irradiation damage.

The effect of tableting the Eu-doped GaN phosphor with KBr is currently under investigation. At present, we have not completely assessed the possible interactions between Eu:GaN powder and the KBr matrix. The results presented here might be slightly influenced by the tableting procedure employed as well. However, the preliminary results of the irradiation experiments presented here are encouraging, since the KBr-GaN:Eu^{3+} composite was not optimized for luminescence. Optimization of the KBr-Eu:GaN composite and determination of the particle-KBr matrix interactions are both currently being investigated.

5.4 Conclusions

SIMS and EPR study on Eu:GaN powder synthesized using the ammonothermal technique revealed that oxygen and silicon are the main shallow donors. The amount of Eu in the powder determined by SIMS study was similar to the doping percentage determined using other other techniques such as XRD and Raman spectroscopy. EPR spectroscopy of both Eu:GaN and Er:GaN powders were performed under photo-excitation. No discernible change has been observed in the charge state of Eu^{3+} in Eu:GaN under optical excitation. In other words we could not verify the charge transfer model. So we used the RESI bound exciton model to explain the high pressure PL data and thermal quenching observed in our samples.

In high pressure measurements, we observed a 10 times increase in the PL intensity associated with the $5D_0 \rightarrow 7F_2$ emission when 6.8 GPa hydrostatic pressure was applied on a Eu:GaN sample. This *f-f* transition showed no change in spectral location with respect to the applied pressure. However the near band edge emission (NBE) was blue shifted when pressure was applied. Relying on the RESI bound exciton model, we attributed the increased emission intensity of the 622 nm line to the stronger localization of the bound exciton on the RESI trap, induced by the applied pressure. The mechanism of luminescence quenching was investigated in the Eu-doped GaN powder phosphor at different hydrostatic pressures and ambient temperatures. It was found that any Eu^{3+} emission intensity lost to thermal quenching can be restored by applied pressure because the exciton-RESI binding energy increases by with applied pressure.(see Figure 5.11) Luminescence quenching at higher temperatures is attributed to the reduced RESI-exciton binding at higher temperatures. This is reason why the impact of heat can be reversed by application of pressure in Eu:GaN phosphor. At low temperatures in addition to the NBE and *f-f* transitions in Eu:GaN, peaks corresponding the A1(LO) passbands, donor-acceptor pair (DAP) (also called

exciton-RESI bound levels), free excitons (FX) and donor binding excitons (DBE/I_2) were seen. When incident photons have energy level higher than the DBE level, photoluminescence is seen in Eu:GaN. We used this observation to suggest that it is this exciton that is bound to the RESI site.

Furthermore, we studied the degradation of Eu^{3+} emission intensity in a KBr-GaN:Eu composite in response to radiation. 2MeV O^+ irradiation was used to introduce defects into the GaN matrix. O^+ was chosen since it is a relatively massive ion when compared to other particles which have been used to introduce defects into GaN. We found that even after significant irradiation with O^+ ions (fluence ~ 5×10^{13} cm^{-2}), the *f-f* transitions in Eu:GaN powders remain unaffected. This implies that ammonothermally synthesized powders could be a good material for use in radiation intense environments.

REFERENCES

1. W. M. Yen and M. J. Weber. Inorganic Phosphors: Compositions, Preparation and Optical Properties, 1st ed; CRC press: Florida, (2004).

2. R. M. Mach, G. Mueller, M. R. Krames, H. A. Hoppe, F. Stadler, W. Schnick, T. Juestel and P. Schmidt, Phys. Stat. Sol. (a) **202**, 1727 (2005).

3. A. J. Steckl, J. Heikenfeld, D. S. Lee and M. Garter, Mater. Sc. Eng. B **81**, 97 (2001).

4. A. Steckl and J. Zavada, MRS Bull. **24**, 33 (1999).

5. H. Lozykowski, W. Jadwisienczak and I. Brown, Appl. Phys. Lett. **74**, 1129 (1999).

6. C. Poitras, H. Wu, A. Turner, M. Spencer and M. Lipson, Appl. Phys. Lett. **89**, 111912 (2006).

7. A. Steckl, J. Park and J. Zavada, Materials Today, **10**, 20 (2007).

8. R. Dahal, C. Ugolini, J. Y. Lin, H. X. Jiang, J. M. Zavada, Appl. Phys. Lett. **93**, 033502 (2008).

9. H. J. Lozykowski and W. M. Jadwisienczak, Phys. Stat. Sol. (b) **244**, 2109 (2007).

10. E. R. Glaser, W. E. Carlos, G. C. B. Braga, J. A. Freitas Jr, W. J. Moore, B. V. Shanabrook, A. E. Wickenden, D. D. Koleske, R. L. Henry, M. W. Bayerl, M. S. Brandt, H. Obloh, P. Kozodoy, S. P. DenBaars, U. K. Mishra, S. Nakamura, E. Haus, J. S. Speck, J. E. Van Nostrand, T. H. Myers and R. J. Molnar, Mat. Sci. Eng. B **93**, 39 (2002).

11. P. Dorenbos and E. van der Kolk, Appl. Phys. Lett. **89**, 061122 (2006).

12. P. Dorenbos and E. van der Kolk, Opt. Mater. **30**, 1052 (2008).

13. H. J. Lozykowski, Phys. Rev. B **48**, 17758 (1993).

14. J. B. Gruber, B. Zandi, H. J. Lozykowski, W. M Jadwisienczak and I. Brown, J. Appl. Phys. **89**, 7973 (2001).

15. J. B. Gruber, B. Zandi, H. J. Lozykowski, and W. M. Jadwisienczak, J. Appl. Phys. **91**, 2929 (2002).

16. W. E. Carlos, J. A. Freitas, Jr., M. A. Khan, D. T. Olson and J. N. Kuznia, Phys. Rev. B **48**, 17878 (1993).

17. K. Wisniewski, W. Jadwisienczak, T. Thomas and M. Spencer, J. Rare Earth **27**, 667 (2009).

18. D. Y. Song, M. Basavaraj, S. A. Nikishin, M. Holtz, V. Soukhoveev, A. Usikov and V. Dmitriev, J. Appl. Phys. **100**, 113504 (2006).

19. T. Paskova, B. Arnaudov, P. P. Paskov, E. M. Goldys, S. Hautakangas, K. Saarinen, U. Soderwall and B. Monemar, J. of Appl. Phys. **98**, 033508 (2005).

20. H. Morkoc. Handbook of Nitride Semiconductors and Devices, Vol. 1&2; John Wiley-VCH Verlag GmbH & Co.: Germany, 2008.

21. H. Y. Peng, C. W. Lee, H. O. Everitt, D. S. Lee, A. J. Steckl and J. M. Zavada, Appl. Phys. Lett. **86**, 051110 (2005).

22. P. Perlin, I. Gorczyca, N. E. Christensen, I. Grzegory, H. Teisseyre and T. Suski, Phys. Rev. B **45,** 13307 (1992).

23. H. Wu, C. B. Poitras, M. Lipson, M. G. Spencer, J. Hunting and F. J. DiSalvo, Appl. Phys. Lett. **88**, 011921(2006).

24. D.L. Camphausen and G.A.N. Connell, J. Appl. Phys. **42**, 4438 (1971).

25. W. Shan, T. J. Schmidt, R. J. Hauenstein, J. J. Song and B. Goldenberg, Appl. Phys. Lett. **66**, 3492 (1995).

26. Y. Nakanishi, A. Wakahara, H. Okada, A. Yoshida, T. Ohshima, H. Itoh, Appl. Phys. Lett. **81**, 1943 (2002).

27. H. Okada, Y. Nakanishi, A. Wakahra, A. Yoshida, T. Ohshima, Nucl. Instr. and Meth. in Phys. Res. Section B: Beam Interactions with Materials and Atoms **266**, 853 (2008).

28. J. W. Tringe, T. E. Felter, C. E. Talley, J. D. Morse, C. G. Stevens, J. M. Castelaz, C. Wetzel, J. Appl. Phys. **101**, 054902, 2007.

29. J. A. Sampson and D. L. Ederer. Vacuum Ultraviolet Spectroscopy, 1st edition; Academic Press: London, 2000.

CHAPTER 6

LARGE AREA ELECTROPHORETIC DEPOSITION OF GaN POWDER AND CERAMIC GaN: PRELIMINARY RESULTS

6.1 GaN powder: preliminary results

6.1.a Large area deposition of phosphors and the electrophoretic deposition method

Modern applications of phosphor materials include flat screen display technologies such as field effect display (FED) devices, surface conduction electron emitter devices (SED), plasma screens and liquid crystal displays. In these devices, the phosphor materials are excited by using electron emitters based on the principles of field emission (in FED and SED), by generating plasma locally at each sub-pixel (in plasma screens) or by employing a large area photo-excitation source (as in most LCDs). In all these cases, a uniform, controlled, and patterned deposition of the phosphor on a large transparent screen is necessary.[1] In this chapter, we present an electrophoretic deposition (EPD) technique developed for the uniform deposition of GaN on a transparent substrate.

In general, several methods for uniformly depositing thin films exist, such as sputtering and spin casting. The resistive material used in field emission cathodes is usually deposited via a sputtering process. Although sputtering enables adequate control of the thickness and uniformity of the resistive material, it requires specialized personnel and equipment, making it an expensive process for mass scale manufacturing. Hence we decided to explore more cost-effective alternatives for achieving the uniform deposition of GaN.

A technique for spin coating GaN particles on a silicon substrate was developed by Huaqiang Wu. First, the Eu:GaN particles were acid rinsed and then ball-milled for 20 hours. Then, 2 wt.% of GaN particles were dispersed in an aqueous solution containing 0.2 wt% methyl cellulose.[1] Empirically, methyl cellulose has proven necessary to disperse the GaN particles, but the exact mechanism by which methyl cellulose stabilizes the dispersion is not known. This suspension was spin coated onto a 4 inch Si wafer (at 500 rpm), resulting in the distribution of GaN on the Si surface (see Figure 6.1a and b). Unfortunately, with a coverage of less than 1% this spin coating process results in a very non-uniform and low quality deposition of Eu:GaN.

We have seen from our previous Raman studies that the Eu:GaN powder remains semiconducting even when it is nanosized. We can take advantage of this basic observation to develop a technique for uniformly depositing GaN nanoparticles on a conducting substrate.

Electrophoretic deposition (EPD) is a useful technique for the deposition of materials on any electrically conductive, semiconductor or metal surface. Electrophoresis is an electro-kinetic phenomenon, which means it is related to the dynamics of particle motion under electric fields. In most EPD experiments, the applied electric fields are spatially uniform. Particles suspended in a dispersion medium usually develop a surface charge. This surface charge prevents the aggregation of the particles. However, under some circumstances the surface charges may reduce resulting in a phenomenon called flocculation in colloidal chemistry. Surface charges on colloidal particles are responsible for the migration of these particles relative to the stationary dispersant fluid, under the influence of the electric field.

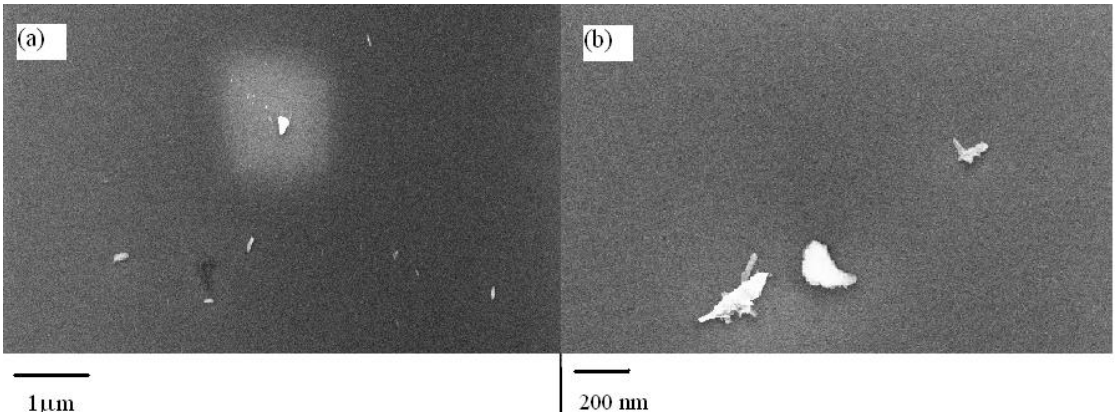

Figure 6.1 Scanning electron micrograph (SEM) of Eu:GaN particles spin coated on a Si wafer. The spin coating was performed using an aqueous methyl cellulose solution (0.1 wt%) as the dispersant.

To achieve a spatially uniform deposition the particles must remain in suspension throughout the process, so that gravitational forces have a minimal impact, relative to the electric forces, on the particle motion. Good deposition for a variety of ceramic and clay systems has been reported to occur for particle sizes in the range of 1–20μm.[2] Furthermore, the density of cracks in a film deposited from a suspension consisting of relatively smaller particles is much less than that of a film deposited from a suspension containing larger particles.[3] Finally, given the nanoscopic sizes of the nano RE:GaN particles, there is a lot of flexibility in the shapes and sizes of the substrates on which these particles may be electrophoretically deposited. All of these factors imply that nanosized RE:GaN particles could be good candidates for an EPD process on a conducting surface. In this chapter, we will present the results of our EPD depositions of acid-rinsed Eu:GaN and nano Eu:GaN on a suitably chosen conducting substrate.

6.1.b Electrophoretic deposition: theory and experimental considerations

Electrophoresis is currently used for a variety of applications including electroplating, dye coating, and ceramic-metal composites (cermets). The success of an electrophoretic deposition is influenced by many experimental parameters, including the applied voltage, the conductivity of the substrate, and the chemical composition of the dispersant.

It is well documented that for a constant applied voltage, the deposited mass increases linearly with deposition time, although eventually the deposition becomes slower and finally stops.[4] 25-100 V/cm is the range of electric fields over which uniform deposition can generally be expected to occur.[4] Electric fields above 100 V/cm are considered high for EPD applications, and usually result in non-uniform deposition due to instabilities near the electrode, and the inability of the particles to

densely close pack because of the very fast deposition rate.[4,5] As a general suggestion, for n-propanol and related dispersants, one must stay below 100 V/cm to ensure a good quality deposition.[5] The concentration of particles should be kept sufficiently large to ensure that the deposition rate remains constant over time, for a given applied voltage.[6]

The conductivity of the surface to be coated is another crucial parameter that determines the quality of the EPD. In two separate independent experiments with different substrates, the lower conductivity substrate displayed a slower deposition rate, and a less uniform deposited layer.[7,8] Hence a highly conducting substrate would be the natural choice on which to deposit GaN particles.

The choice of dispersant is likewise critical for the success of EPD. The primary criteria for determining a suitable dispersant are a high dielectric constant, low conductivity, low viscosity, and a low ionic content.[9,10] A fairly high dielectric constant is necessary to prevent the flocculation of the particles. Similarly, the concentrations of any ionic impurities, including water, must be controlled carefully. An overabundance of ionic species in the dispersant can minimize the thickness of the diffuse layer, which in turn enhances the viscous drag on the particles, and consequently reduces their electrophoretic mobility.[11] For example, in many recipes for the electrophoretic deposition of insulating particles, water and ethanol are used as dispersants. These work very well due to the high dielectric constant of the mixture. Any ionic additives to this alcohol-water mixture modify both the conductivity of the suspension and the mobility of the particles.[12]

One final consideration in the experimental design of electrophoretic deposition setup is the stability of the suspension used. Empirically it is known that unstable suspensions when left undisturbed for some time will result in a dense strongly adhering deposit of particles at the bottom of the container. Such

agglomerations of particles are not observed if the suspension is stable. Hence when the suspension is allowed to stand undisturbed for several hours, a visible lack of agglomerations at the bottom of the container is indicative of the stability of a suspension. To guide experimental practice, a suitable composition for electrophoretic bath dispersion may be developed based on the theoretical principles of colloidal stability.

Colloidal particles held in a suspension (such as the dispersion medium in an EPD bath) are usually surrounded by a layer of fluid, called the diffuse layer, which counters the surface charge of the particles. The movement of the colloidal particles under an electric field is determined by two components: an electrostatic force experienced by a particle due to its surface charge, and an electrostatic retardation force acting in the opposite direction due to the diffuse layer which carries the opposite charge. The electrostatic retardation force is not applied directly to the particle itself, but to the diffuse layer that surrounds the particle. However, part of the electrostatic retardation force gets transferred to the particle, due to viscous interactions between the diffuse layer and the particle.[13] This analysis of the electro-kinetic motion of colloidal particles in a dispersant is based on the hypothesis that the motion is governed primarily by a rigid particle surface interacting with the fluid diffuse layer. It is called the "Double Layer" model, because the "rigid" particle surface and the neighboring diffuse layer are considered to be the two layers most important in the description of the colloidal dynamics. [13,14]

The most common double layer model uses three different potentials to describe the electro-kinetics of the colloidal particle (see Figure 6.2). The surface of the colloid is characterized by its Surface potential. The first ionic layer covering the particle, which is considered to be rigid, is characterized by the Stern potential. The diffuse layer, the last coating of the particle, is used to define the Zeta potential. The

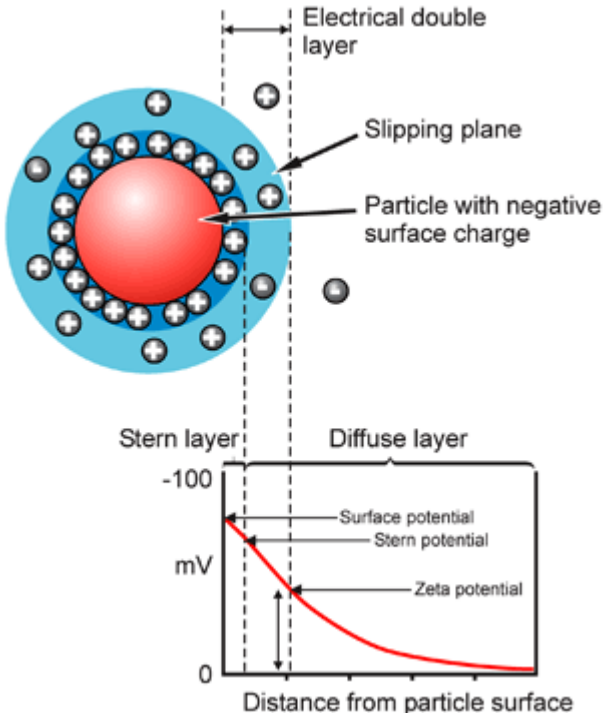

Figure 6.2 The "Double layer" model of a colloid particle with a negative surface charge. This model is characterized by potentials at the surface of the particle (surface potential), at the outside of the first solvation layer (Stern potential), and at the end of the second layer (Zeta potential). Courtesy: Malvern Instruments.

Zeta potential of the particles gives a quantitative measure of the stability of a colloid. It can be seen from Figure 6.2, where the surface charge of the particle is considered to be negative, that the Zeta potential is the potential difference between the bulk dispersant and the supposedly stationary diffuse layer that surrounds the suspended particles. Thus, the Zeta potential is related to the electrophoretic mobility of the particles in the dispersant. The concept of Zeta potential has several applications in the characterization of colloidal particles.

It should be noted that Zeta potential is a very sensitive function of the chemical environment. The Zeta potential may be controlled by means of a variety of charged agents such as acids, bases and salts.[12] The stability of a colloid is related to the Zeta potential of the particles. Typically, Zeta potentials higher than 25 meV indicate a stable colloidal suspension. If Zeta the potential is reduced below this limit, particles tend to flocculate. Thus, the addition of even minor quantities of ionic species can dramatically change the stability of a colloidal suspension. Deposition from a suspension with a low Zeta potential is known to result in agglomerates on the surface.[15] For all these reasons, the stability of an electrophoretic bath dispersion can be tested and improved through knowledge of the Zeta potential of the particles.

6.1.c Colloidal suspension characterization using dynamic light scattering

For the characterization of our dispersions, we used a Malvern Nano-ZS instrument for dynamic light scattering experiments. A schematic of the instrument is shown in Figure 6.3. It uses Zeta potential measurements to determine the size distribution of the suspended particles. The rheological properties of the dispersant and refractive index of the colloidal particles are given as inputs. Then, a laser light scattering process is employed to determine the velocity distribution of the particles in the suspension, using the Doppler Effect. The photodetector picks up a signal

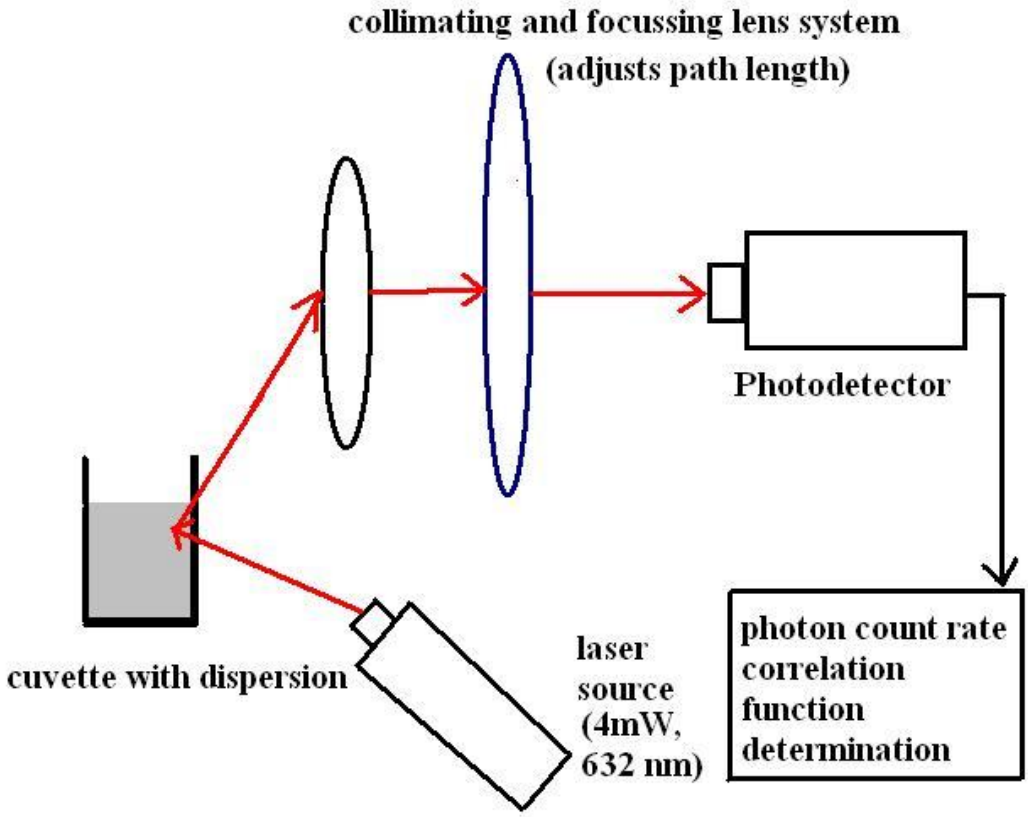

Figure 6.3 Schematic of the optical set up used for the dynamic light scattering experiments for particle size determination.

corresponding to the elastic scattering of incident laser light from the particles in the dispersion. Variations in the light intensity over small periods of time (~millisec) are used by the software to calculate the particle size distribution.

6.1.d Electrophoretic deposition process for GaN

An electrophoretic (EP) apparatus (see Figure 6.4) was made for the deposition of GaN and RE:GaN nanoparticles, which were synthesized using the ball-milling technique. The electrodes are separated from one another by about 0.8 cm. The whole apparatus is enclosed in a glass vessel. The electrodes are held in place by a teflon (polytetrafluoroethene) framework. Teflon was chosen as the framework material because of its chemical inertness under the experimental conditions employed.

A 1 inch^2 quartz glass coated with 600 nm of fluorine doped tin oxide (sheet resistance R_s: 8 ohms/square) was chosen for the cathode. Fluorine doped tin oxide (FTO) is called conversion coating, since this coating makes the glass surface conducting. FTO has excellent adhesion properties on glass. FTO coated glass also has the advantage of being chemically stable in alcohols and aqueous solutions. An SEM of the FTO surface is shown in Figure 6.5. The very sharp features of FTO particles are due to the crystallinity of the material. Despite this sharpness, a very uniform deposition of the FTO particles is observed, resulting in a complete coverage of the glass surface. This is a necessary condition for ensuring uniform deposition of GaN on the glass surface. The FTO coated glass used in this experiment was purchased from Hartford Glass Company.

The anode was a 1 square inch stainless steel plate, which remained uncorroded in the chemical environment of the EP bath. It was observed that copper plates corroded very quickly when used as the anode; hence copper was avoided in all the electric connections in the EP suspension. Considering the sensitivity of

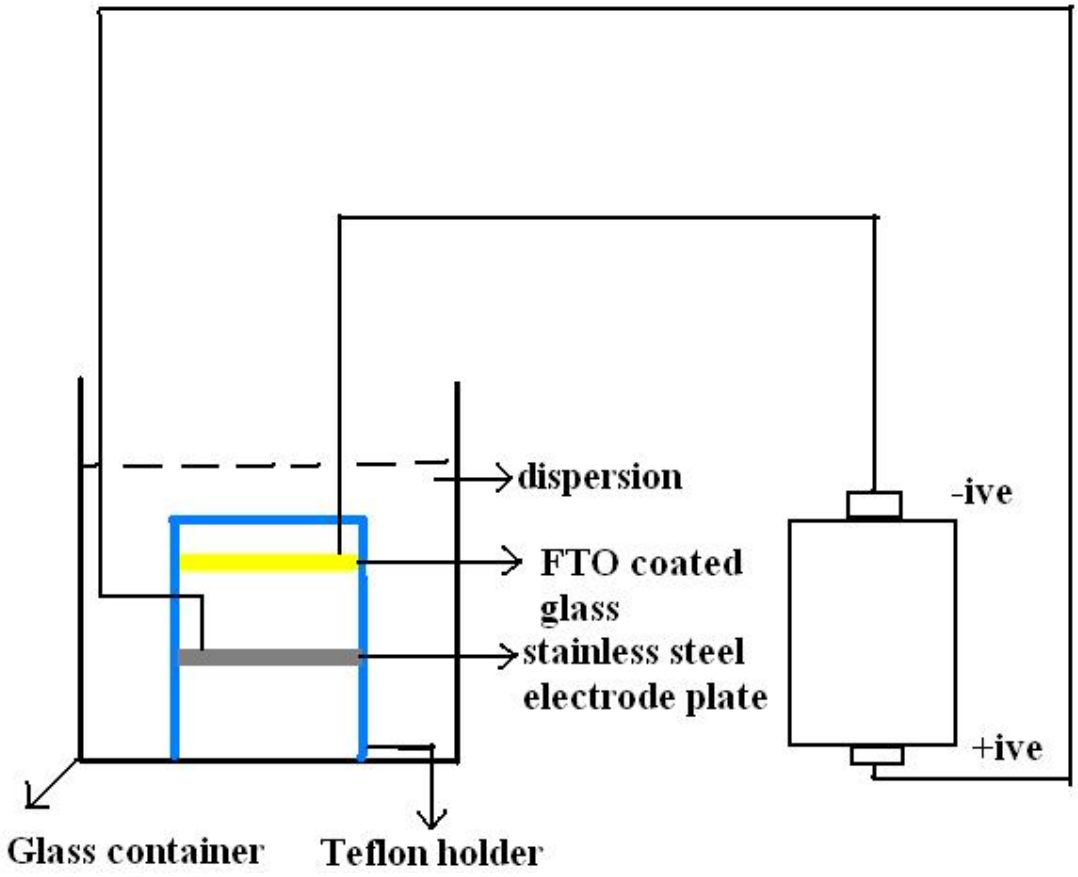

Figure 6.4 Electrophoretic deposition apparatus designed for GaN particle deposition. A programmable power supply was used to apply an electric field between the two electrodes, which were separated by 0.8 cm.

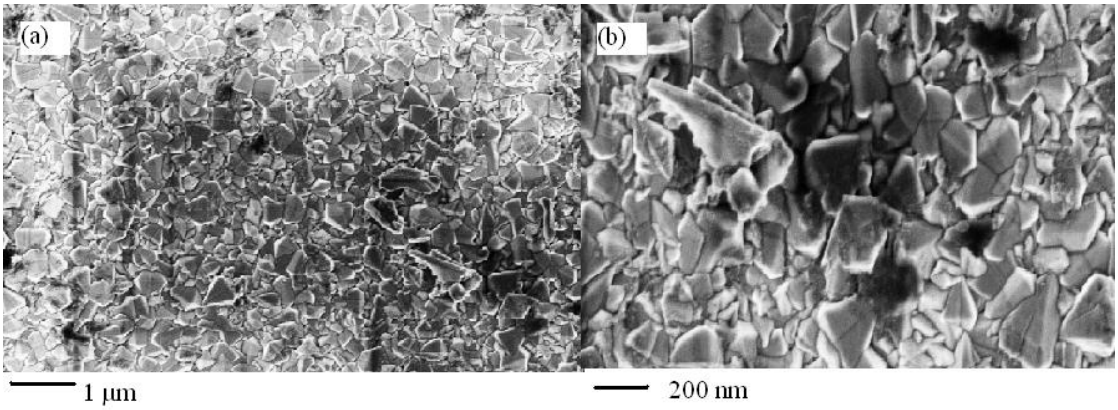

Figure 6.5 SEM of fluorine-doped tin oxide (FTO) coated on silica glass. (a) shows that the FTO covers the glass perfectly, creating a conducting substrate for EPD (b) shows that the FTO particles are sub-100 nm, hence providing a very uniform and smooth coating on the silica glass. This ensures an adequate conductivity and surface smoothness for a high-quality deposition of GaN particles using electrophoresis.

electrophoretic deposition to the various impurities that might be present in the powder, two precautions were exercised (a) the powders used for EPD were stored in a clean environment and (b) all powders were cleaned in de-ionized water prior to use in the electrophoretic bath.[5]

Because of the high dielectric constants of water and ethanol, a mixture of water and ethanol was chosen as the dispersion medium (see section 6.1.b). Dynamic light scattering (DLS) measurements of the powders in the ethanol-water dispersion (see Figure 6.6.b) revealed a bimodal particle size distribution in the NH_3 annealed powder, while the other two samples (air annealed powder, and powder obtained from nanoscission) show monomodal distributions. An SEM analysis of the samples (see Figure 6.6.a) suggests that the average particle sizes in the powders are much smaller than those measured by the DLS measurements. This suggests a significant aggregation of the GaN nanoparticles in the ethanol-water dispersion. As discussed above, one way to combat the problem of particle aggregation is to increase the Zeta potential of the dispersion. It is well-known that the Zeta potential varies very significantly with the addition of ionic solutes. Hence, to raise the Zeta potential, $Mg(NO_3)_2$ was added to the electrophoretic bath dispersion,.

GaN has a density of about 6.15 $g*cm^{-3}$, which is significantly higher than the density of either water (1 $g*cm^{-3}$) or ethyl alcohol (0.789 $g*cm^{-3}$). This means that to prepare a dispersion of GaN particles, a surfactant is needed. Glycerol was chosen for this purpose. Due to its 3 hydoxyl groups, glycerol is expected to form a continuous medium with ethanol and water. The surface of the GaN particles is significantly coated with oxide (<3 nm).[16] Ga_2O_3 has its point of zero charge at a pH of about ~9,[17] which suggests that the oxide-terminated GaN particles should have an affinity for hydroxyl moieties. This implies that glycerol should adhere significantly to the GaN surface. Hence, the addition of glycerol is expected to stabilize the GaN dispersion.

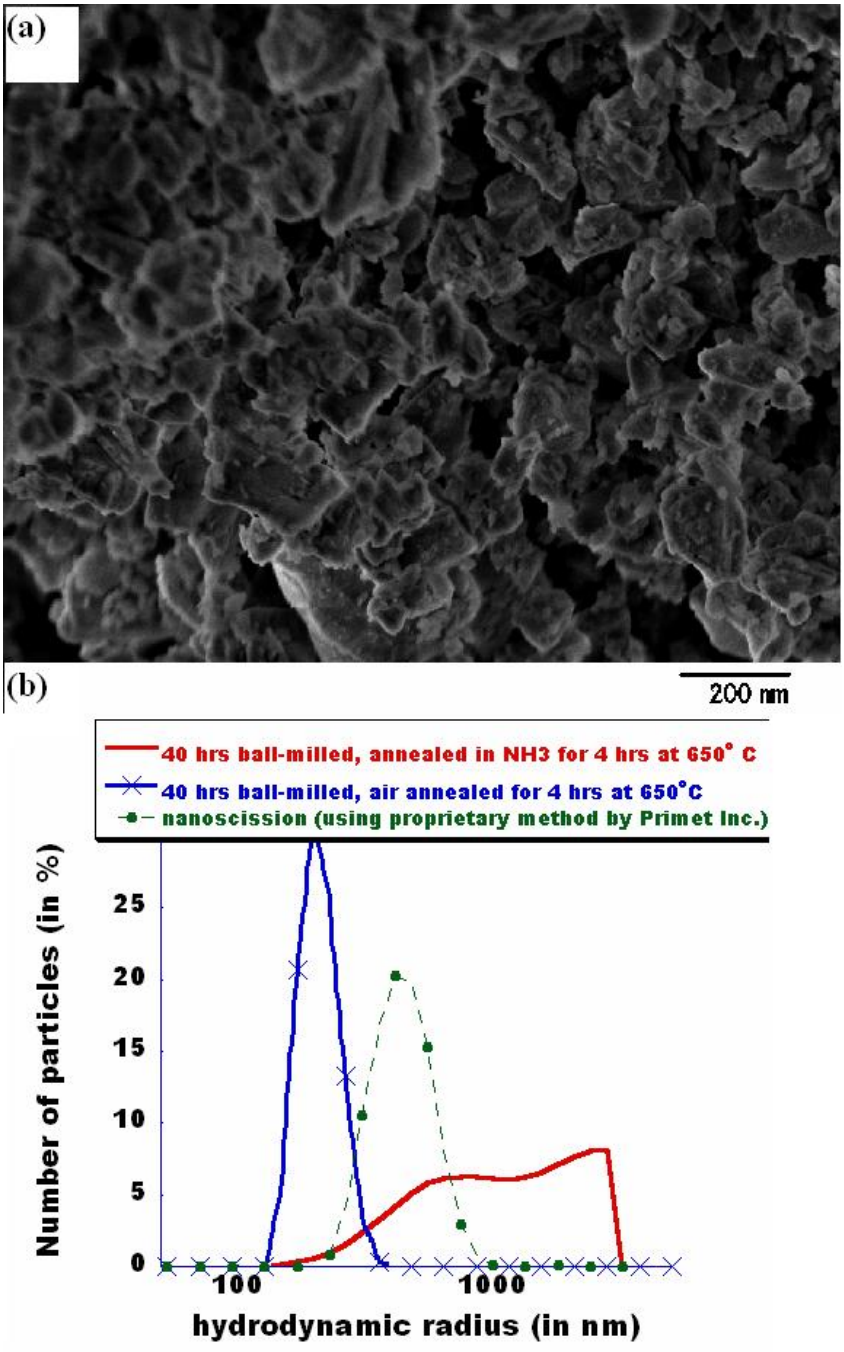

Figure 6.6 (a) SEM image of the as-prepared (unannealed) ball-milled GaN powder. (b) The particle size distribution of various samples, based on dynamic light scattering measurements.

This was empirically verified, as the addition of glycerol did indeed improve the stability of dispersion significantly. Using all these considerations, we developed an electrophoretic bath dispersion whose composition was: 20 ml deionized water, 20 ml ethanol, 10 ml glycerol, 2 mg $Mg(NO_3)_2$, and 2 grams GaN.

The object to be coated was chosen to be one of the electrodes, and a set of counter-electrodes were used to complete the circuit. The applied electric field was maintained at a value of 85 V/cm, and the current density was observed to be 1.4 mA/cm^2. Experiments were always limited to durations over which the current density could be kept constant. After deposition, the surface was rinsed to remove the remaining bath solution. The final step was a 12 hour baking process at 80^oC, to remove any remaining water and organic contaminants from the GaN layer. This process is commonly known as curing.

An SEM image of the electrophoretically deposited nano Eu:GaN is shown in Figure 6.7. The particles of Eu:GaN are observed to be sub-30 nm. The predominance of sub-30 nm particles in the EPD deposited film demonstrates the size selectivity of the particles that are deposited using this process. The networks in which the nanoparticles appear to be held are due to the glycerol used in the electrophoretic bath. The presence of glycerol in the deposit does not interfere with the optical properties of the particles. The deposited GaN can be permanently fixed to the FTO substrate by depositing 600 nm of SiO_2 on top of the GaN layer, using plasma enhanced chemical vapor deposition (PECVD). Figure 6.8 shows red light emission from GaN which was deposited on FTO coated glass, and fixed with PECVD-deposited SiO_2. This is a visual demonstration of the bright red luminescence following the optical excitation of the nano Eu:GaN in the deposit. The high quality of luminescence from these sub-30 nm particles in the deposit suggests that this technique could have promising applications in optical technologies.

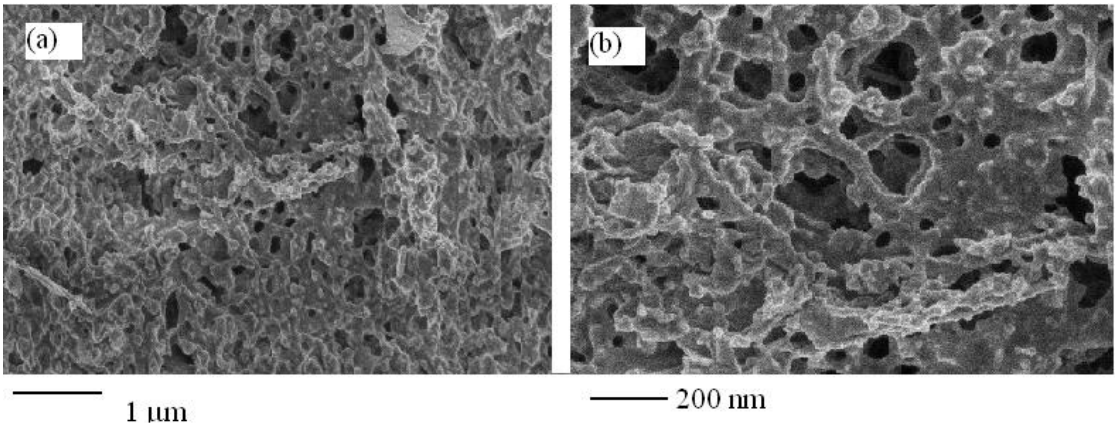

Figure 6.7 (a and b) SEM of nanosized Eu:GaN electrophoretically deposited on FTO coated silica glass. Eletrophoretic deposition was performed for a duration of 4 minutes, during which the electric field and current density were held constant. We observe that the particles cover the substrate very uniformly. The tiny particles (approximately 20-30 nm) seen in the network are the nano-sized Eu:GaN particles. The GaN particles are held together by a very diffuse network of the binder material, which in this case is glycerol. The water initially present in the binder network was removed using a 24 hour oven bake at 80^{o}C.

Figure 6.8 A bright-red uniform emission from nanosized Eu:GaN powder deposited on FTO coated silica glass using electrophoretic deposition, as described in section 6.2. The excitation source used for this demonstration was a simple UV-lamp.

It was observed that the quality of deposit remained the same even when the EPD of GaN was carried out on FTO which had been coated with a layer of 630 nm of SiO_2. This implies that it is possible to embed the GaN particles in an insulating environment, while maintaining the optical properties of Eu:GaN. This process could be useful in waveguide applications where nano-Eu:GaN may be employed.

Occasionally, very large particles get deposited, as shown in Figure 6.9(a). The micron sized particle in the picture shows surface features which suggest possible step flow growth. Well-defined steps are seen on the surface of the particle, suggesting that this particle survived the ball-milling process and is similar to an as-prepared particle. Close inspection of Figure 6.9 (b) suggests that nanoscopically continuous patches of GaN particles exist, with cracks at the interfaces of such patches. These cracks are a consequence of the bake-out step. However, since the powder deposition is overwhelmingly continuous at the sub-micron scale, this technique could still prove promising for making nanoscopic optical devices. Further research is needed to develop optical devices based on EPD deposited Eu:GaN particles.

6.2 Ceramic GaN: preliminary results

Earlier in this thesis, we discussed the significant challenges which must be overcome to grow pure GaN single crystals. The primary issues are the unavailability of a good substrate, the lack of scalability of the MOCVD and MBE processes used for bulk and thin film GaN synthesis, and consequently, the high cost.[18] In this context, one may think of using GaN powder to fabricate ceramic rods for use in optical materials. For example, a ceramic Eu:GaN rod could be used as a laser gain medium. The purity and crystallinity of the powders could be preserved during the ceramicizing processes through the use of appropriate sintering techniques.

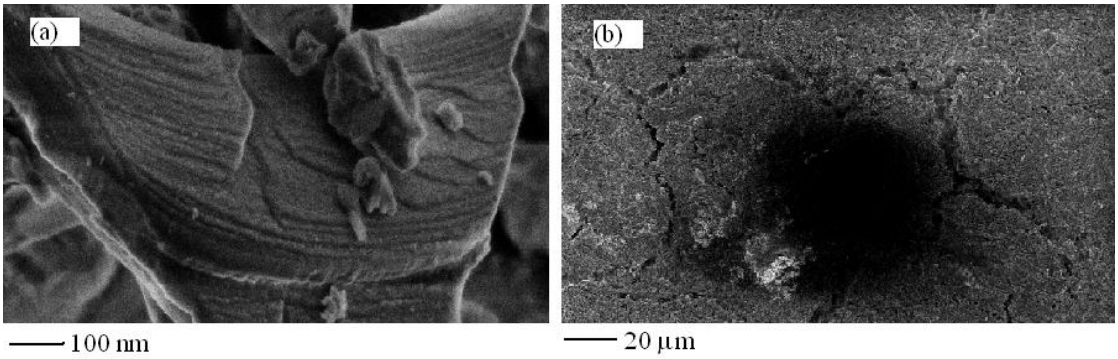

Figure 6.9 (a) SEM picture of a rare micron-sized Eu:GaN particle on the nano Eu:GaN deposited surface. The crystal surface shows structures which reveal the possible step flow growth of the particle. (b) SEM of the electrophoretically deposited surface at low magnification showing cracks. This suggests that the EPD technique results in a fairly uniform deposition at the sub-micron scale, but on the micron scale cracks are present. Hence, these cracks are not expected to interfere with device performance if the device dimensions are in the nanoscale regime.

Currently, one widely used sintering method for the manufacture of ceramics is hot pressing. Hot pressing is mainly used to fabricate hard and brittle ceramic materials, via a high-pressure, low-strain metallurgical process. The simultaneous application of heat and pressure allows for relatively easy control of the porosity in the resulting ceramic rods. The act of reducing porosity in a sample, thereby making it denser, is called densification. Hot pressing is a highly effective, precisely controllable means for densifying a powder at a high enough temperature to induce sintering and creep processes.[19]

Developing an appropriate sintering technique for a given material involves optimizing the temperature and pressure to simultaneously achieve high densification, and suitable grain growth and adhesion. Densification works through particle rearrangement and plastic flow at the particle contacts. In the hot pressing process, atoms may indeed move from the bulk of the crystal to the pores, filling up the pores and increasing densification. However, sintering can also result in significant motion of atoms across grain boundaries. If many atoms simply move from the surface of one grain to another grain, there may be no change in porosity. However, in this situation, the average grain size is likely to grow. Since smaller particles have a relatively higher radius of curvature than larger particles, the atoms in smaller grains tend to have a higher chemical potential. This results in smaller grains losing atoms to larger grains, and shrinking during the sintering process. This is a well-recorded phenomenon called Ostwald ripening.

In our attempt to make ceramic GaN, we used pure as-prepared GaN powder with no additive or filler material. The loose powder (ie. the pre-compacted material), was heated in a high temperature graphite mold that allows inductive or resistive heating up to temperatures of 2400°C. The sintering was performed by Dr. John Lucek of Diamond Innovations. The precise details of the hot pressing equipment and

process were not disclosed because of proprietary restrictions. However, we were told that the instrument used was an ultra-high pressure hot pressing machine. The percentage densification of the pellet was measured using an optical dilatometer.

The resulting ceramic exhibits a very interesting morphology. Figure 6.10.a shows an SEM of ceramic GaN, showing fusion of the GaN particles and the presence of cubic facets. The bulk crystal structure both before and after ceramicization was found to be the Wurtzite phase. A high degree of densification, due to closure of pores is evident in this picture. Figure 6.10.b shows clear evidence of fusion along the edges of the particles as a result of the densification process. We see that the sharp edges observed in the particles are not seen in the sintered ceramic. This is attributed to particle growth occurring through the Ostwald ripening process.

The GaN pellet thus formed emits in the visible, although unfortunately with none of the sharp lines which are characteristic of the constituent powder. So far, we have not yielded a GaN rod that has any sharp emissions (see Figure 6.11). Much development is needed for converting our powder material to ceramic GaN while maintaining its optical properties. Ongoing efforts with Diamond Innovations are aimed at refining the sintering process to achieve transparent GaN ceramics with sharp emission spectra.

There have been reports of successful attempts at achieving transparent polycrystalline ceramic material from powder in oxide materials.[19,20] The transparency of these materials was found to be a significant function of the porosity of the sample. Both the calculated and experimental results in those materials suggest that transparency can be significantly improved by reducing porosity.[19] We believe that our acid-rinse technique (see Chapter 3) for the purification and optical enhancement of GaN, and the realization of nano-GaN for hot pressing, are significant steps in realizing fully densified transparent GaN ceramics with optical characteristics

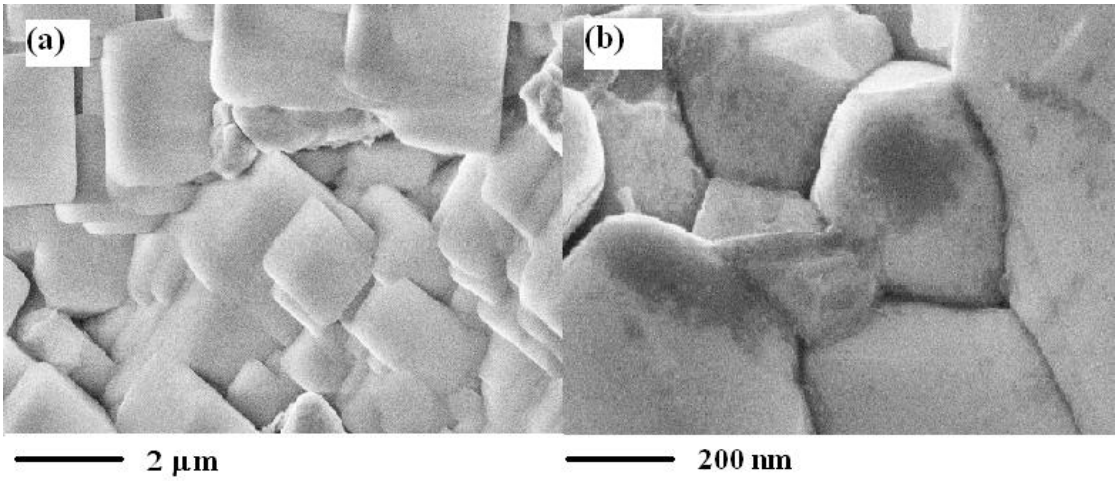

Figure 6.10 (a) SEM of ceramic GaN showing the fusion of GaN particles and the presence of cubic facets. A high degree of densification, due to the closure of pores is observed in this picture. (b) SEM showing clear evidence of fusion along the edges of the particles.

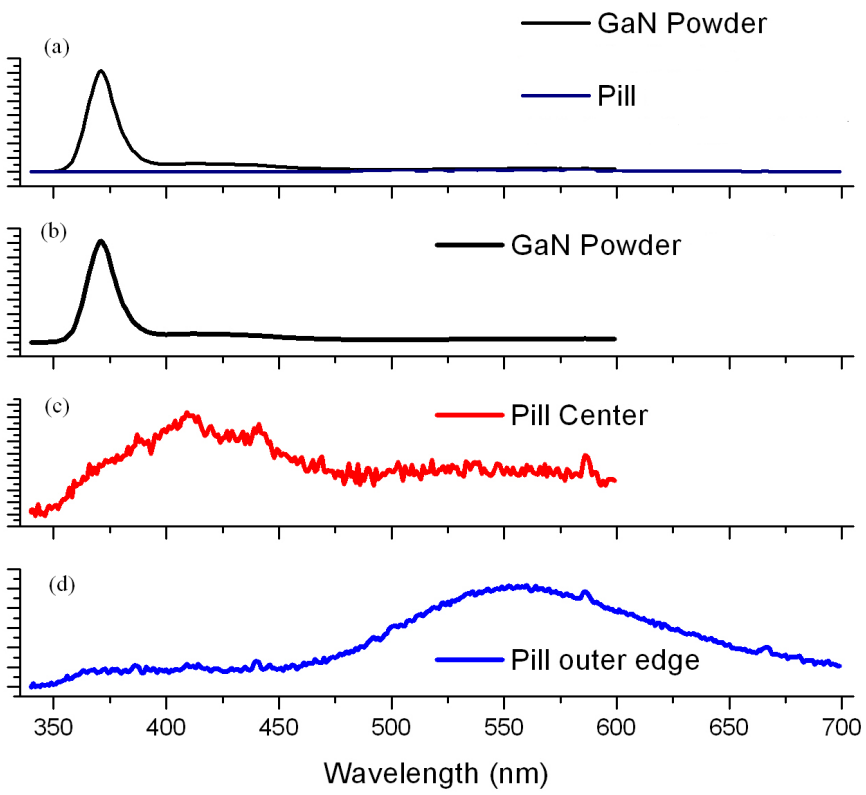

Figure 6.11 (a) Photoluminescence spectra of GaN powder and ceramic GaN plotted on the same scale shows the loss of photoluminescence intensity in the ceramic material when compared to the powder. (b) Shows the 360 nm band edge emission in the GaN powder. This band edge emission is expected to become sharper in the ceramic material with proper handling and surface treatment of the GaN particles. (c) and (d) The PL characteristics are different in different parts of the GaN pellet. We attribute it to the local inhomogenities within the pellet. Achieving a uniform morphology of the pellet is critical for achieving uniform optical properties in the ceramic material.

comparable to the as-prepared powders. Further steps will entail (a) determining the proper surface treatment of GaN particles before hot pressing, (b) handling the particles in a way that contaminants do not enter the pellet, (c) fine tuning the pressure and temperature conditions of the hot pressing, to further reduce the porosity in ceramic GaN while maintaining a uniform morphology throughout the pellet, and (d) investigating the possible use of filler materials to control the porosity in ceramic GaN.

6.3 Conclusions

Large area deposition of ammonothermally grown GaN particles was achieved using an electrophoretic technique. This method was also used to achieve GaN nanoparticle deposition on a SiO_2 coated, conductive substrate. This technique and its variants can therefore be useful for the low cost, rapid, large area deposition of GaN and related materials on various substrates for optoelectronic and display technologies. In short, we have demonstrated methods to perform rare earth doping of GaN, followed by uniform large area deposition of these nanoparticles.

In this chapter, we have also presented preliminary results on the high pressure sintering of GaN powders into ceramic rods. However, the rods produced thus far are not transparent and lack uniform optical properties. Further efforts are needed to make GaN rods synthesized via this method transparent and usable for optoelectronic applications.

REFERENCES

1. H. Wu. Bulk Gallium Nitride crystal growth and characterizations and high purity Gallium Nitride powder synthesis and applications. Ph. D. Dissertation, Cornell University, Ithaca, 2006.

2. S. N. Heavens. Electrophoretic deposition as a processing route for ceramics. In *Advanced ceramic processing and technology*; J. G. P. Binner, Ed.; Noyes Publications: New Jersey, 1990; Vol. 1; p. 255.

3. N. Sato, M. Kwachi, K. Noto, N. Yoshimoto and M. Yoshizawa, Physica C **357-360**, 1019 (2001).

4. R. N. Basu, C. A. Randall and M. J. Mayo, J. Am. Ceram. Soc. **84**, 33 (2001).

5. L. Besra and M. Liu, Prog. Mater. Sc. **52(1)**, 1 (2007).

6. L. Vandeperre, O. V. D. Biest and W. J. Clegg, Key Eng. Mater. **127-131**, 567 (1997).

7. F. Chen and M. Liu, J. Eur. Ceram. Soc. **21**, 127 (2001).

8. Z. Peng and M. Liu, J. Am. Ceram. Soc. **84**, 283 (2004).

9. B. Ferrari and R. Moreno, Mater. Lett. **28**, 353 (1996).

10. B. Ferrari and R. Moreno, J. Eur. Ceram. Soc **17**, 549 (1997).

11. R. W. Powers. J. Electrochem. Soc. **122**, 490 (1975).

12. M. Zarbov, I. Schuster and L. Gal-Or, J. Mater. Sc. **39**, 813 (2004).

13. M. Smoluchowski, Bull. Intl. Acad. Sci. Cracovie, **184** (1903).

14. J. Lyklema. Fundamentals of Interface and Colloid Science, vol.2; Elsevier Ltd.: London, 1995.

15. H. G. Krueger, A. Knote, U. Schindler, H. Kern and A. R. Boccaccini, J. Mater. Sci **39**, 839 (2004).

16. T. Thomas, X. Guo, MVS Chandrashekhar, C. B. Poitras, W. Schaff, M. Dreibelbis, H. Reiherzer, K. Li, F. J. DiSalvo, M. Lipson and M. G. Spencer, J. Crystal Growth **311**, 4402 (2009).

17. M. Kosmulski, J. Colloid and Interface Science, **238(1)**, 225 (2001).

18. R. F. Davis, A. M. Roskowski, E. A. Preble, J. S. Speck, B. Heying, J. A. Freitas, Jr., E. R. Glaser and W. E. Carlos, Proc. of the IEEE **90**, 993 (2002).

19. J. G. J. Peelen and R. Metselaar, J. Appl. Phys. **45**, 216 (1974).

20. K. Tsukuma, I. Yamashita and T. Kusunose, J. Am. Ceram. Soc. **91**, 813 (2008).

CHAPTER 7

CONCLUSION

In this thesis, I have tried to place our research on GaN-based phosphors in the context of developments in optical emission technology through the last four decades. In the introductory chapter, I presented detailed discussions on the excitation and de-excitation mechanisms in phosphor materials, and the various criteria that are considered when engineering new phosphor materials. We saw that an ideal phosphor material has minimal Stokes loss. This analysis has prompted us to examine rare earth doped nitrides as possible phosphor and laser gain materials. We discussed the importance of the chromaticity diagram in phosphor research, emphasizing the need to optically characterize every new material using its emission spectrum and locating its coordinates in the color space. A combination of all these physico-chemical and technological considerations was introduced in chapter 1. In the subsequent chapters, frequent references were made to these topics in discussions about viable phosphors and laser gain materials.

Based on a thermodynamic model for the formation of nitride materials, we justified the design of the ammonothermal reactor that was introduced in Chapter 2. This thermodynamic analysis provided insights into the methods used in this thesis for nitride synthesis. We looked at the ammonothermal method of GaN powder synthesis. The crucial role of bismuth in this process for the complete conversion of Ga to GaN was explained based on the wetting properties of Bi and the interfacial properties of the alloy mixture at the operating temperatures. Combining Knudsen's analysis, experimental crystal growth and characterization of the resulting materials, we demonstrated that the ammonothermal powder growth process is primarily a liquid

phase phenomenon; although there is some evidence of a minor contribution of a vapor phase process. Since Eu has a low vapor pressure at operating temperatures of the synthesis reaction, Eu incorporation into the GaN matrix is believed to be a primarily liquid phase phenomenon as well.

Eu:GaN powder synthesized using the ammonothermal method was found to be dark. The darkness is clearly an impediment in the use of these powders in optical applications, such as in laser gain media or as an efficient phosphor. In chapter 3, we presented a simple chemical etch process which achieved a significant enhancement (~300%) of the luminescence intensity of Eu:GaN powders. The acid-rinsed powders were also visually lighter. Using data from X-ray diffraction and X-ray photoelectron spectroscopy, we showed that the improvement in the PL is primarily due to the removal of dark Eu-containing compounds from the powder.

In chapter 4, we saw that synthesizing nanosized GaN particles with a uniform size distribution remains a challenging task. Furthermore, achieving the proper concentrations of rare earth dopant ions in a controllable and inexpensive manner remains a significant problem. In this chapter, we demonstrated a ball-mill assisted top-down method for obtaining nanoparticles from as-prepared micron-sized powders. In addition, we discussed an easily scalable solid-state reaction technique to achieve rare earth (Er) doping in GaN powders. We observed superior luminescence in Er/Yb:GaN co-doped systems when the reaction was carried out in an atmosphere with equal mol% of NH_3 and air. Further research is needed to determine the reason for the superior performance of the co-doped system, and to understand the interactions of Yb and Er ions with the lattice and with one another. Hence, we have shown that high quality, nanosized, Eu and Er doped GaN powder with desirable optical emission characteristics can be obtained in a cost-effective and easily scalable manner. However, based on both scanning electron microscopy and dynamic light

scattering studies, we found that these nanoparticles suffer from significant agglomeration, possibly due to a large surface to volume ratio. Longer durations of ball-milling lead to greater reductions of particle size, and hence increased agglomeration. Raman studies indicate that the ball-milled particles retain their semiconducting properties. Both Raman spectroscopy and XRD indicate that the ball-milled particles have tensile and compressive stresses in the a- and c-directions respectively, due to mechanical deformation induced by the ball-milling process. To put Eu:GaN into use for optical applications, we investigated its behavior in a KBr pellet. We demonstrated that ball-milled Eu:GaN powder in a KBr matrix displays suitable IR transmittance, making it a possible laser gain medium.

My work with Prof. Wojciech Jadwicienczak is presented in great detail in chapter 5. Through secondary ion mass spectrometry (SIMS) and electron paramagnetic resonance (EPR) studies on ammonothermally synthesized Eu:GaN, we discovered that oxygen and silicon are the main shallow donors in the material. The amount of Eu in the powder determined by SIMS was similar to the doping percentage determined using other techniques, such as XRD and Raman spectroscopy. To test the charge transfer model proposed as the RE^{n+} ion excitation mechanism in RE:GaN, EPR spectroscopy of both Eu:GaN and Er:GaN powders was performed under photo-excitation. No discernible change was observed in the charge state of the Eu^{3+} in Eu:GaN under optical excitation. These data do not support the charge transfer model. Hence we preferred to use the rare earth structured isovalent (RESI) impurity bound exciton model to explain the high pressure photoluminescence (PL) data and thermal quenching observed in our samples.

We observed a factor of 10 increase in the PL intensity associated with the $5D_0 \rightarrow 7F_2$ emission when 6.8 GPa hydrostatic pressure was applied on a Eu:GaN sample. This f-f transition showed no change in its spectral location with respect to the

applied pressure. However, the near band edge emission (NBE) was blue shifted when pressure was applied. Relying on the RESI bound exciton model, we attributed the increased emission intensity of the 622 nm line to the stronger localization of the bound exciton on the RESI trap, induced by the applied pressure.

We also investigated the mechanism of luminescence quenching in the Eu-doped GaN powder at different hydrostatic pressures and ambient temperatures. It was found that any Eu^{3+} emission intensity lost to thermal quenching can be restored by applying pressure. Using the results from high pressure, low temperature PL, we think that the reversal of the thermal quenching occurs because the exciton-RESI binding energy increases by about 6meV/GPa. Luminescence quenching at higher temperatures is attributed to the reduced RESI-exciton binding. This is the reason why the impact of heat can be reversed by application of pressure in Eu:GaN phosphor.

At low temperatures, in addition to the NBE and *f-f* transitions in Eu:GaN, peaks corresponding the A1(LO) passbands, donor-acceptor pair (DAP) levels, free excitons (FX) and donor bound excitons (DBE/I_2) were observed in these ammonothernally grown powders. When incident photons have an energy higher than the DBE level, photoluminescence is seen in Eu:GaN. This observation suggests that the I_2 exciton is bound to the RESI site.

Furthermore, we studied the degradation of the Eu^{3+} emission intensity in a KBr-GaN:Eu composite in response to radiation. 2MeV O^+ irradiation was used to introduce defects into the GaN matrix. These experiments were carried out at the Edwards Accelerator Laboratory of Ohio University. O^+ was chosen since it is a relatively massive ion, and hence can be used to introduce a relatively large defect density into GaN. We found that even after significant irradiation with O^+ ions (fluence ~ 5×10^{13} cm^{-2}), the *f-f* transitions in Eu:GaN powders remained unaffected.

This implies that ammonothermally synthesized powders could be a good material for use in radiation intense environments.

In Chapter 6, we demonstrated large area deposition of ammonothermally grown GaN particles using an electrophoretic technique. This method was also used to achieve GaN nanoparticle deposition on a SiO_2 coated conductive substrate (fluorine doped tin oxide coated glass). This technique and its variants can hence be useful for the low cost, rapid, large area deposition of GaN and related materials on various substrates for optoelectronic and display technologies. Given that we succeeded in uniformly incorporating Eu:GaN on SiO_2 on FTO-coated glass, we anticipate that this method could be useful for diverse applications. We have also presented preliminary results on the high pressure sintering of GaN powders into ceramic rods. However, the resulting rods are not transparent, and lack uniform optical properties. Further efforts are needed to make GaN rods synthesized using this method transparent and usable for optoelectronic applications.

The aim of this dissertation was manifold: (a) to better understand the ammonothermal growth process (b) to achieve nanosized GaN powder with optical properties comparable to bulk GaN (c) to develop solid state reaction methods to synthesize RE:GaN powder (d) to develop an improved understanding of the luminescence mechanism in RE:GaN (e) to develop models to predict and explain the luminescence properties of RE:GaN as a function of temperature and pressure and (f) to develop large area uniform deposition techniques for micron- and nano-sized GaN particles. By achieving most of these goals, we believe that the work we have presented will find future applications in the development of laser and light emitting device technologies based on GaN powders.

We understand that much more research is needed to develop optical technologies based on GaN powder. We wish to continue this work in collaboration

with Prof. Wojciech at Ohio University, Diamond Innovations, and Boston Applied Technologies Inc. to achieve transparent ceramics based on hot pressed GaN powder.

I conclude by saying that I believe our efforts have furthered our knowledge of GaN as a materials system. The results presented here are of interest for people working in solid state physics, solid state chemistry, optical physics, and materials technology. We have tried to probe and understand the RE:GaN system in a variety of ways. In this thesis, we have presented results on GaN that give an understanding of the material from the perspectives of synthetic chemistry, surface chemistry, materials physics, and colloidal science. We believe that much remains to be explored in this system, including further study of the precise luminescence mechanisms involved in RE:GaN, development of light emitting devices based on GaN powder and development of methods to achieve a transparent nitride laser rod using ammonothermally grown powders. Clearly we have resolved some significant questions; but we also realize that we end this dissertation with numerous unanswered questions about GaN in particular, and the world around us in general.